National Institute for Public Health
and the Environment
*Ministry of Health, Welfare and Sport*

# Uncertainty in calculated **nitrogen deposition** from individual sources

RIVM report 2025-0081
H.A.M. Sterk et al.

# Uncertainty in calculated nitrogen deposition from individual sources

RIVM report 2025-0081

# Colophon



DOI 10.21945/RIVM-2025-0081

H.A.M. Sterk (author), RIVM
R. Hoogerbrugge (author), RIVM
C.M.J. Jacobs (author), RIVM
A. Vos (author) RIVM), RIVM
W.A.J. van Pul (author), RIVM
R.J. Wichink Kruit (author), RIVM

Contact:
H.A.M. Sterk
Centre MIL
Marina.sterk@rivm.nl

This study was commissioned by the Dutch Ministry of Agriculture, Fisheries, Food Security and Nature in the context of Project 36: Program Nitrogen & Nature.

Published by:
**National Institute for Public Health and the Environment, RIVM**
PO Box 1 | 3720 BA Bilthoven
The Netherlands
www.rivm.nl/en

# Synopsis


## Uncertainty in calculated nitrogen deposition from individual sources

For policy decisions, it is important to know how much the emissions of a company or activity contribute to the amount of nitrogen deposition on the ground in nature areas. Models calculate this contribution. These models use parameters in order to calculate how nitrogen spreads through the air and how much is deposited. However, there are uncertainties in these parameters which influence the uncertainties in the model's outcomes.

RIVM has studied with a sensitivity analysis the impact of uncertainties in the twelve most important parameters on the uncertainty in the calculated deposition for a livestock farm, an industrial stack and a motorway. It is important to note that the sensitivities examined in the model are not the same as the uncertainty. However, this method does ensure that the sensitivity analyses provide a good indication of the extent and nature of that uncertainty. In this study, only the uncertainty in the model calculation was considered. The uncertainty in the magnitude of the emission is not taken into account.

Prior to the study, the uncertainty in the calculated deposition was expected to increase with distance from the source. This study has shown that the uncertainty declines in the first 50-150 kilometres from the source, depending on the source type, and subsequently increases. It has also confirmed that the deposition velocity has the largest impact on the uncertainty in the calculated deposition. The deposition velocity indicates how easily the emitted substance is transported from the atmosphere to the surface. The impact of uncertainties in the deposition velocity on the calculated deposition is larger closer to the source, and smaller further away from the source.

RIVM has also compared its model results to the results of other models from the Netherlands and abroad. Each model calculates deposition differently. Using these results, the uncertainty in the calculated deposition is estimated as well. This estimate is comparable to the uncertainty determined by the sensitivity analysis. It means that RIVM is likely not missing any important causes of uncertainties in its model.


Keywords: uncertainties, modelling, spread, deposition, nitrogen, OPS

# Publiekssamenvatting

## Onzekerheid in de berekende stikstofdepositie van een individuele bron

Voor beleidskeuzes is het belangrijk om te weten hoeveel de uitstoot van een bedrijf of activiteit bijdraagt aan de hoeveelheid stikstof die op de bodem neerslaat (depositie). De bijdrage wordt met rekenmodellen berekend. Deze modellen gebruiken parameters om zo goed mogelijk te berekenen hoe stikstof zich via de lucht verspreidt en hoe groot de depositie is. Maar deze parameters hebben onzekerheden, die ook invloed hebben op de onzekerheden van de uitkomsten van het model.

Het RIVM onderzocht met een gevoeligheidsanalyse wat het effect van onzekerheden in de twaalf belangrijkste parameters is op de onzekerheid in de berekende depositie. Het RIVM deed dat voor een stal van een landbouwbedrijf, een schoorsteen van een industriebedrijf en een snelweg. Belangrijk hierbij is dat de onderzochte gevoeligheden in het model niet gelijk zijn aan de onzekerheid. Deze methode zorgt er wel voor dat de gevoeligheidsbepalingen een goede indicatie geven van de omvang en aard van die onzekerheid. Er is alleen gekeken naar de onzekerheid in de modelberekening, niet naar de onzekerheid in de grootte van de uitstoot.

Vóór het onderzoek was de verwachting: hoe verder weg van de bron, hoe groter de onzekerheid in de berekende depositie. Dit onderzoek laat zien dat deze onzekerheid kleiner wordt in de eerste 50 tot 150 kilometer vanaf de bron (afhankelijk van het type bron), en pas daarna toeneemt. Verder bevestigt dit onderzoek de verwachting dat de onzekerheid in de berekende depositie het meest wordt bepaald door de snelheid van de depositie. De depositiesnelheid geeft aan hoe snel een uitgestoten stof via de lucht op de bodem komt. Vooral dicht bij de bron is het effect van onzekerheden in de depositiesnelheid op de berekende depositie groot. Verder weg van de bron is het effect kleiner.

Het RIVM heeft ook gekeken naar de resultaten van andere rekenmodellen uit Nederland en het buitenland. Elk model berekent de depositie op zijn eigen manier. Met deze uitkomsten is de onzekerheid in de berekende stikstofdepositie ook geschat. Deze schatting is vergelijkbaar met de onzekerheid die met de gevoeligheidsanalyse is bepaald. Dat betekent dat het RIVM waarschijnlijk geen belangrijke oorzaken van onzekerheden in het rekenmodel over het hoofd ziet.

Kernwoorden: onzekerheden, modellering, verspreiding, depositie, stikstof, OPS

# Contents

# 1 Samenvatting

## 1.1 Inleiding

De berekeningen van stikstofdepositie worden gebruikt als belangrijke indicator voor de mogelijke verslechtering van de natuur. De stikstofdepositie in Nederland is afkomstig van veel verschillende bronnen. Zowel in Nederland zelf, als uit het buitenland.

Om effectief maatregelen te kunnen nemen om de stikstofdepositie op gevoelige natuur te verminderen, is het belangrijk om te weten waar de stikstof vandaan komt. Ook is het relevant om te weten wat de bijdrage is van individuele bronnen. Deze informatie is nodig om te kunnen inschatten wat het effect is van een specifieke maatregel. Of om een beslissing over een vergunningaanvraag te kunnen nemen.

Een berekening is altijd een benadering van de werkelijke situatie. Dat betekent dat de berekende depositie binnen een bepaalde bandbreedte kan afwijken van de werkelijke depositie. Depositieberekeningen zijn complex, en veel parameters en andere factoren kunnen invloed hebben op de uitkomst. De wetenschappelijke term voor deze afwijking is de onzekerheid.

Het is belangrijk om de onzekerheid in de berekening voor de individuele bron te weten. Daarom wordt in dit rapport de onzekerheid voor een aantal relevante bronnen in Nederland onderzocht.

*Verschillende methoden om onzekerheid te bepalen*
Er zijn verschillende methoden om de onzekerheid in de berekende stikstofdepositie van een individuele bron te bepalen. Deze methoden zijn dezelfde als de methoden die bij luchtkwaliteitsmodellen worden gebruikt (zoals in EEA, 2011).

De meest directe manier is door de berekening te vergelijken met depositiemetingen. Maar goede, betrouwbare en nauwkeurige metingen van de totale stikstofdepositie zijn erg ingewikkeld en duur. Dit komt doordat er verschillende stikstofcomponenten zijn die niet met één instrument gemeten kunnen worden en doordat de stikstofcomponenten zowel met regen als direct vanuit de lucht op het oppervlak kunnen neerslaan. Er zijn tot op heden geen meetcampagnes uitgevoerd die een compleet inzicht geven in de totale stikstofdepositie op verschillende afstanden van een bron. Deze directe manier om de onzekerheid in de berekende stikstofdepositie van een individuele bron te bepalen, is momenteel dan ook niet mogelijk.

Een andere manier om inzicht te krijgen in de onzekerheid in de berekende stikstofdepositie van een individuele bron is door modelberekeningen van verschillende modellen met elkaar te vergelijken. De spreiding van de verschillende modeluitkomsten geeft dan inzicht in hoe onzeker de berekende stikstofdepositie is. Deze manier is toegepast in Kooi et al. (2025a). De resultaten van dat onderzoek zullen in deze rapportage worden meegenomen.

Tot slot kan onderzocht worden hoe gevoelig het rekenmodel zelf is voor onzekerheden in de modelparameters, zoals bijvoorbeeld de verticale spreiding van een pluim of de snelheid waarmee een stof via droge depositie op het oppervlak neerslaat. De onzekerheden in de modelparameters werken door in de uitkomsten van het model. Door een inschatting te maken van de onzekerheid in de modelparameters kan nagegaan worden hoe gevoelig de uitkomsten van het model zijn voor deze onzekerheden. De spreiding van de uitkomsten (hoe groot de verschillen zijn) geeft een indruk van de modelonzekerheid op verschillende afstanden van de bron. Deze aanpak zegt in eerste instantie alleen iets over de gevoeligheid van het model zelf, en niet over onzekerheden door de invoergegevens, zoals de emissies of het landgebruik, die daar nog bovenop komen. Daarom kan de aanpak mogelijk tot een onderschatting van de onzekerheid leiden (Abbott et al., 2003). Deze manier om de onzekerheid in de berekende stikstofdepositie van een individuele bron te bepalen, is in deze rapportage verder onderzocht.

Aan het eind plaatsen we de resultaten van dit gevoeligheidsonderzoek in perspectief met andere onzekerheidsonderzoeken.

## 1.2 Doel en methode

De totale stikstofdepositie in een jaar wordt zo nauwkeurig mogelijk berekend met het OPS-model (Sauter et al., 2023). Hiervoor wordt de Lange Termijn versie (OPS-LT) gebruikt.

Een rekenmodel is een benadering van de werkelijkheid. Dat betekent dat de uitkomst altijd een mate van onzekerheid kent. Zo leiden onzekerheden in de invoergegevens, zoals de emissies of het landgebruik, tot onzekerheden in de berekening van de stikstofdepositie. Maar ook het OPS-model zelf gebruikt een groot aantal modelparameters om de stikstofdepositie te bepalen. Onzekerheden in die modelparameters kunnen ook leiden tot onzekerheid in de berekende stikstofdepositie.

*Doel*
Het doel van dit onderzoek is om de gevoeligheid van het OPS-model voor de onzekerheid in de belangrijkste modelparameters inzichtelijk te maken. Daarmee kunnen we iets zeggen over de onzekerheid in de depositieberekeningen op grotere afstanden tot 400 km van de bron. We focussen hier op variatie in de parameters binnen OPS en niet op variatie van de invoergegevens, zoals de emissiesterkte of het landgebruik, waarvan het evident is dat die ook een belangrijke bijdrage aan de onzekerheid in de berekende stikstofdepositie leveren. Het onderzoek richt zich dus op de onzekerheid van het OPS-model en niet op de onzekerheid van de invoer van het model.

*Onderzochte bronnen*
Dit onderzoek beschrijft de verspreiding van de uitstoot van drie kenmerkende bronnen in Nederland: ammoniak uit een stal, stikstofoxiden uit een schoorsteen (van een industriële bron op 50 meter hoogte) en stikstofoxiden van een stuk snelweg (van wegverkeer over een afstand van 65 kilometer).

*Methode*
De gevoeligheid van OPS voor onzekerheden in de modelparameters wordt onderzocht voor de totale depositie en de concentratie van de uitgestoten component. De gevoeligheid van de concentratie is onderzocht omdat deze meestal eenvoudiger te begrijpen is en behulpzaam kan zijn bij de interpretatie van het effect op de depositie. De methode om de gevoeligheden binnen het OPS-model te onderzoeken bestaat uit de volgende onderdelen:

1. Selectie van de *parameters* waarvan wordt ingeschat dat zij een belangrijke bijdrage aan de onzekerheid leveren.
2. Schatting van de vooraf bekende *onzekerheid in de geselecteerde parameters*.
3. Uitvoering van *OPS-berekeningen* waarin de geselecteerde *afzonderlijke parameters* zijn gevarieerd binnen de bandbreedte van de onzekerheid van die parameter.
4. Bepaling van de *gevoeligheid* van de OPS-berekeningen voor de onzekerheden in de geselecteerde afzonderlijke parameters.
5. Uitvoering van *OPS-berekeningen* waarin de geselecteerde *parameters tegelijkertijd* zijn gevarieerd binnen de bandbreedte van de onzekerheden van alle parameters.
6. Bepaling van de *gevoeligheid* van de OPS-berekeningen voor de *combinatie van onzekerheden* in alle geselecteerde parameters samen.
7. Het resultaat van de combinatie is vervolgens nader onderzocht om te bepalen welke parameters, en welke combinatie van parameters, de *grootste bijdrage aan de gevoeligheid van de OPS-berekeningen* leveren.
8. Van de parameters met de grootste bijdrage aan de totale gevoeligheid worden de individuele resultaten getoond. Dit helpt om de resultaten voor de totale onzekerheid te interpreteren.

Een aantal van deze onderdelen worden hieronder verder toegelicht.

*Ad 1) Selectie van parameters*
Figuur 1.1 geeft de geselecteerde parameters schematisch weer. Het betreft de:

- initiële pluimstijging van de bron ($\Delta h$);
- mate waarin de pluim in verticale richting verspreid is ($\sigma_z$)*;*
- hoogte van de menglaag ($z_i$);
- snelheid waarmee de component chemisch wordt omgezet ($k_{chem}$);
- snelheid ($v_d$) waarmee de component via droge depositie op het oppervlak deponeert;
- snelheid waarmee de component opgenomen en verwijderd wordt door de neerslagdruppels onder de wolk via het uitwasproces ($\Lambda_w$) enerzijds, of in de wolk via het uitregenproces ($\Lambda_r$) anderzijds;
- weersomstandigheden (*Meteo*);
- variatie in de emissiesterkte in de tijd (dagverloop). Voorbeelden hiervan zijn een ochtend- en avondspits bij verkeersemissies en temperatuurafhankelijkheid bij stalemissies (*dv*).

Het OPS-model berekent zowel de verspreiding van de primaire component als die van de reactieproducten, ook wel secundaire

componenten genoemd. Voor deze secundaire componenten (die via chemische omzetting uit de primaire componenten in het model worden gevormd) geldt dat de variabelen voor droge depositiesnelheid, het uitwassen en het uitregenen onafhankelijk van de parameters voor de primair uitgestoten stoffen gevarieerd zijn.

In totaal zijn zodoende twaalf parameters gevarieerd.

*Figuur 1.1 Schematisch overzicht van de gevarieerde parameters.*

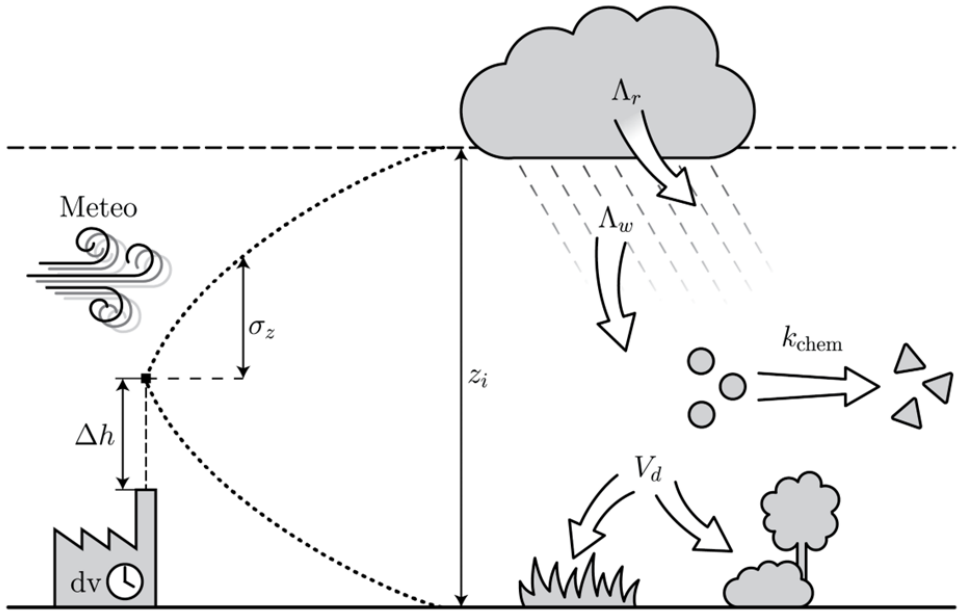


*Ad 2) Schatting vooraf bekende onzekerheid van parameters*
De onzekerheid van de parameters is geschat op basis van literatuuronderzoek, soms aangevuld met een analyse van meetgegevens ($v_d$, $k_{chem}$) of gegevens uit een onafhankelijk weermodel ($z_i$). De onzekerheid in de meeste parameters is lognormaal verdeeld met een standaardafwijking tussen 20 en 40 procent. De droge depositiesnelheid ($v_d$) is minder goed bekend. Daarvoor is uitgegaan van een lognormale verdeling met een standaarddeviatie van 70 procent.

De onzekerheid in de gebruikte weersomstandigheden (Meteo) is niet in een simpele parameter te vatten. In de OPS-berekeningen is Nederland opgedeeld in zes regio's die met name verschillen wat betreft windgedrag. Deze onzekerheid is gesimuleerd door de verschillen in de resultaten van de weersomstandigheden van representatieve KNMI-meetstations uit de zes regio's te vergelijken. Voor de referentieberekening is de gemiddelde representatieve meteorologie voor heel Nederland gebruikt.

*Ad 3) Uitvoering van de OPS-berekeningen*
Bij het uitvoeren van de OPS-berekeningen wordt een virtuele bron in het centrum van het land geplaatst. Van deze bron worden vervolgens de totale depositiebijdrage in een jaar en de concentratie berekend op verschillende afstanden tussen 1 tot 400 kilometer van de bron, en in

twaalf windrichtingen. Deze locaties heten in het model receptoren. Alleen de resultaten boven land en binnenwateren worden gebruikt.

## 1.3 Gecombineerde gevoeligheid voor alle onderzochte parameters

Om de gevoeligheid in te schatten van de met het OPS-model berekende depositie en concentratie voor de onzekerheden in de modelparameters is een Monte Carlo-analyse uitgevoerd. Hiervoor zijn vijfduizend berekeningen met OPS gedaan. De gekozen waarden voor de parameters vallen statistisch binnen de onzekerheid die elke parameter heeft. Per receptor wordt de variatiecoëfficiënt (CV) berekend. Dit is de standaardafwijking van de vijfduizend modelberekeningen gedeeld door de referentiewaarde. Voor elke afstand van de bron zijn er op die manier twaalf CV's berekend, één per windrichting.

*Toelichting op figuren*
Hieronder worden voor elke bron de resultaten van de analyse beschreven aan de hand van twee figuren:

A. een figuur met de *gevoeligheid* in de berekeningen van de concentratie en de depositie voor de onzekerheden in de twaalf parameters als functie van de afstand van de bron (Figuur 1.2, Figuur 1.4 en Figuur 1.6).
B. een figuur met een analyse van de *bijdrage* van de onzekerheden in de verschillende parameters en parametercombinaties aan de gevoeligheid van de berekeningen als functie van de afstand van de bron (Figuur 1.3, Figuur 1.5 en Figuur 1.7).

Ad A) De gekleurde lijnen in de figuur geven de mediaan weer van de CV's in de verschillende windrichtingen op bepaalde afstanden van de bron. De kleurvlakken geven de spreiding van de CV's in de verschillende windrichtingen weer. Hiervoor wordt de Mediaan van Absolute Deviaties (MAD) gebruikt. Er is voor mediaan en MAD gekozen omdat er, in tegenstelling tot de variaties per individuele parameter, af en toe extreme resultaten voorkomen die het gemiddelde te veel beïnvloeden. Hiermee ontstaat een vertekend beeld van de gevoeligheid.

Ad B) Hoe de (combinaties van) parameters bijdragen aan de gevoeligheid is onderzocht via zogenoemde Sobol'-indices. Dit is een techniek om de bijdrage aan de variantie uit te splitsen. Onzekerheden in modelparameters hebben ook gecombineerde effecten. Daarom zijn ook de combinaties van parameters meegenomen. In totaal laten de figuren de 11 belangrijkste (combinaties van) parameters zien. Deze is gemaakt op basis van de grootste bijdragen aan de gevoeligheid voor alle drie de bronnen. De linker figuur toont telkens de bijdrage van de onzekerheden in de (combinaties van) parameters aan de gevoeligheid van de modellering van de concentratie. De rechter figuur laat de bijdragen aan de gevoeligheid in totale depositie zien. De categorie "other" bevat de overige (combinaties van) parameters.

### *1.3.1 Uitstoot van ammoniak uit stal*

Figuur 1.2 toont de middelste (mediaan) van de CV-waarden over de verschillende windrichtingen op bepaalde afstanden van de bron, voor de ammoniakconcentratie (rode lijn) en voor de totale depositie $NH_x$

(blauwe lijn). De totale depositie $NH_x$ is de som van de droge en natte depositie van ammoniak ($NH_3$) en ammonium ($NH_4^+$).

Voor de uitstoot van ammoniak uit de stal zijn de relatieve verschillen in de depositieberekeningen het kleinste op een afstand tussen 50 en 100 kilometer van de bron. De spreiding is hier minder dan 25 procent. Dicht bij de bron (op 1 km) is deze spreiding ruim 60 procent.

De spreiding in berekende concentraties is dicht bij de bron kleiner dan de spreiding in de berekende depositie. Ver van de bron is de spreiding in de concentratieberekeningen juist groter dan die in depositieberekeningen.

*Figuur 1.2 Berekende gevoeligheid (als variatiecoëfficiënt) in de $NH_3$-concentratie en de totale $NH_x$-depositie als functie van de afstand, voor een stal met ammoniakemissie. Dit is de gevoeligheid in de berekeningen van de concentratie en de depositie voor de gecombineerde onzekerheid in de twaalf beschreven parameters. De gekleurde lijnen tonen de mediane gevoeligheid, dat is de middelste waarde van de CV's in alle windrichtingen. De gekleurde vlakken laten de spreiding van de CV's over de twaalf windrichtingen zien als één en twee maal de MAD (zie hoofdtekst). De afstand vanaf de bron is weergegeven op een logaritmische schaal.*

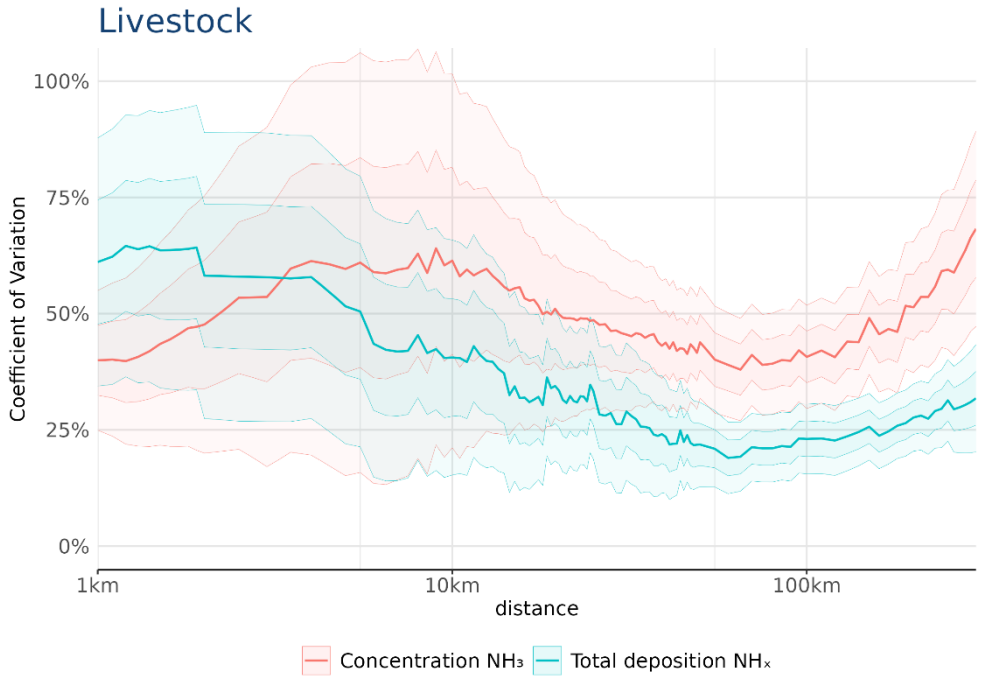


Figuur 1.3 geeft een overzicht van de bijdragen van de onzekerheden in elf belangrijkste (combinaties van) parameters aan de gevoeligheid van de modellering van de concentratie en depositie van ammoniak vanuit een stal. Deze 11 parameters dragen voor 50 tot 75 procent bij aan de gevoeligheid.

Voor de ammoniakconcentratie (linker plaatje), is op korte afstand van de bron de parameter verticale spreiding van de pluim het belangrijkst. De gevoeligheid voor de verticale spreiding wordt snel minder als de

afstand groter wordt. Op grote afstanden levert de droge depositiesnelheid de grootste bijdrage. Andere belangrijke parameters zijn de meteorologie, de hoogte van de menglaag en, met name op grote afstand, de chemische omzetting. Sommige interacties blijken meer impact te hebben dan andere, individuele parameters.

Voor de totale $NH_x$-depositie (rechter plaatje) is te zien dat ook op *korte* afstand de gevoeligheid voor droge depositiesnelheid het grootste is. Rond de 50-100 km is de gevoeligheid kleiner. Dat komt door het effect dat concentratie en depositie op elkaar hebben. Zo zorgt een toename in droge depositiesnelheid voor een toename in depositie dicht bij de bron. Daardoor is de concentratie lager op grotere afstanden. Dit vermindert daar de depositie en kan uiteindelijk zelfs resulteren in een lagere depositie ondanks de hogere depositiesnelheid. Voorbij dit omslagpunt ('crossover'-punt) neemt de gevoeligheid weer toe. Dicht bij de bron is ook de verticale spreiding belangrijk. Figuur 1.3 laat zien dat de gevoeligheid voor verticale spreiding afneemt tot rond de 5 km en bij grotere afstanden weer iets belangrijker wordt. Net als bij de concentratieberekeningen hebben meteorologie en menglaaghoogte een relatief grote invloed op de gevoeligheid van de depositieberekeningen. De relatieve impact van chemische omzetting is kleiner.

*Figuur 1.3 Uitsplitsing van de 11 grootste bijdragen van de parameters, en parameter combinaties, aan de onzekerheid als functie van de afstand voor ammoniak uit de stal. Het linker plaatje laat het resultaat voor de $NH_3$-concentratie zien en het rechter plaatje dat voor de totale $NH_x$-depositie.*

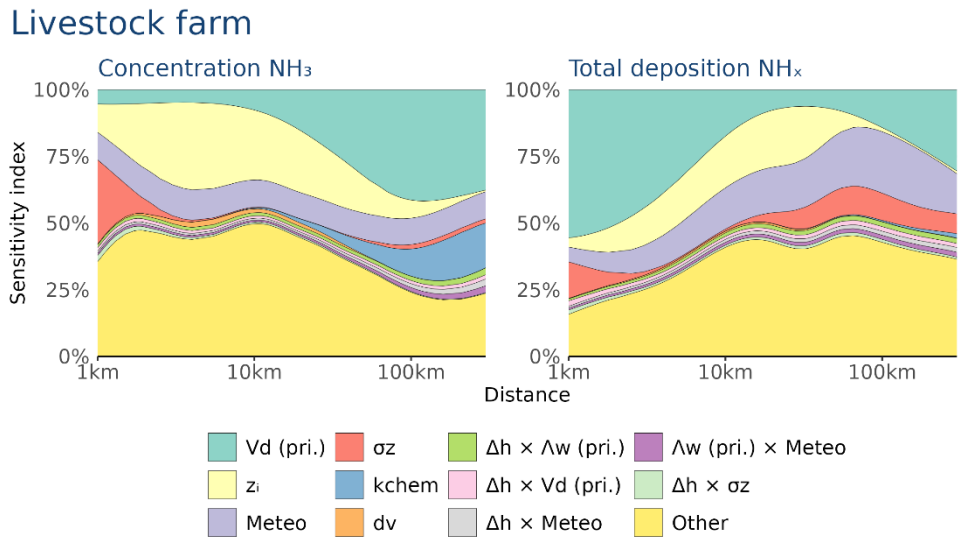


### 1.3.2 *Uitstoot van een industriële bron*

De gevoeligheidsanalyse is voor dezelfde parameters uitgevoerd voor een industriële bron met een schoorsteen van 50 meter hoogte. Voor deze bron worden de concentratie ($NO_x$) en totale depositie van stikstofoxiden ($NO_y$) onderzocht. Figuur 1.4 toont de gevoeligheid als functie van de afstand.

Voor de concentratie is dicht bij de bron de gevoeligheid voor onzekerheid in de parameters minder dan 20 procent. De gevoeligheid

neemt tot 20 kilometer afstand tot de bron toe tot ongeveer 50 procent en neemt vervolgens weer af bij grotere afstanden.

Voor depositie is de gevoeligheid voor de onzekerheid in de parameters rond 70-75 procent bij afstanden tot ongeveer 20 km van de bron. Op grotere afstanden, boven de 100 km, neemt de gevoeligheid af tot 25-30 procent.

*Figuur 1.4 Berekende gevoeligheid (als variatiecoëfficiënt) in de $NO_x$-concentratie en de totale $NO_y$-depositie als functie van de afstand, voor een industriële bron met $NO_x$-emissie. Dit is de gevoeligheid in de berekeningen van de concentratie en de depositie voor de gecombineerde onzekerheid in de twaalf beschreven parameters. De gekleurde lijnen tonen de mediane gevoeligheid, dat is de middelste waarde van de CV's in alle windrichtingen. De gekleurde vlakken laten de spreiding van de CV's over de twaalf windrichtingen zien als één en twee maal de MAD (zie hoofdtekst). De afstand vanaf de bron is weergegeven op een logaritmische schaal.*

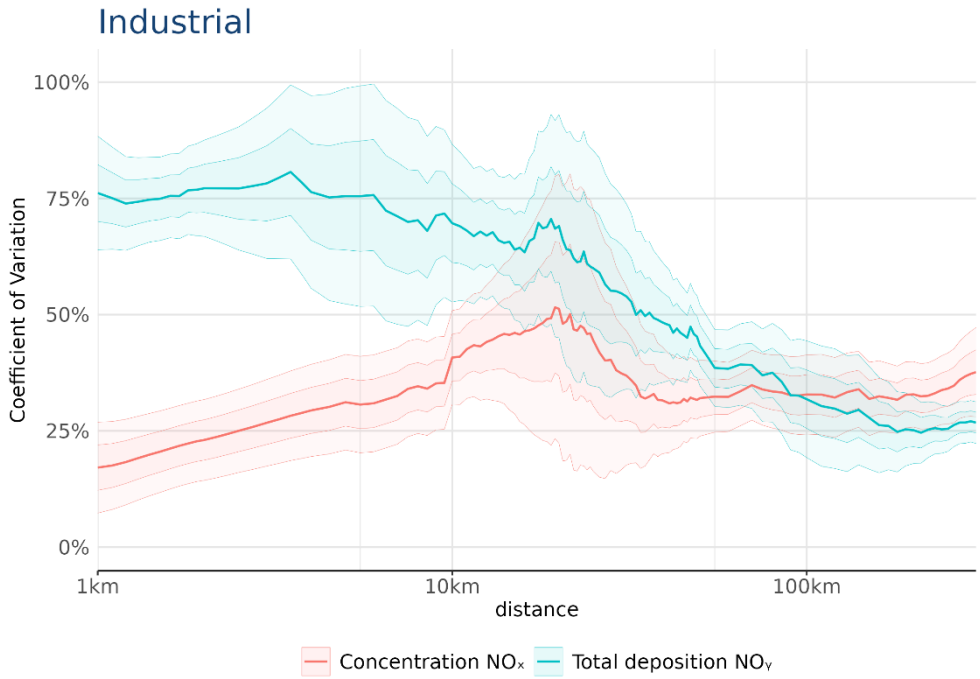


Uit Figuur 1.5 blijkt dat voor de concentratie (linker plaatje) dicht bij de bron vooral de verticale spreiding, de meteorologische omstandigheden en de menglaaghoogte zorgen voor spreiding in de modelberekeningen. Op grote afstand neemt de gevoeligheid voor chemische omzettingssnelheid toe. De droge depositiesnelheid draagt bij de uitstoot van stikstofoxiden uit brontype schoorsteen minder bij aan de onzekerheid in de concentratie dan bij ammoniak uit de stal. Dit was te verwachten omdat de droge depositiesnelheid van stikstofoxiden veel lager is dan die van ammoniak.

De gevoeligheid van $NO_y$-depositie (rechter plaatje) wordt dicht bij de bron gedomineerd door de droge depositiesnelheid. Op grote afstand van de bron neemt de gevoeligheid van de depositie voor de droge depositiesnelheid sterk af, en wordt de gevoeligheid voor de

meteorologie, de menglaaghoogte en de chemische omzetting relatief belangrijker.

*Figuur 1.5 Uitsplitsing van de elf grootste bijdragen van de parameters, en parameter combinaties, aan de onzekerheid als functie van de afstand voor $NO_x$ uit een industriële schoorsteen. Het linker plaatje laat het resultaat voor de $NO_x$-concentratie zien en het rechter plaatje dat voor de totale $NO_y$-depositie.*

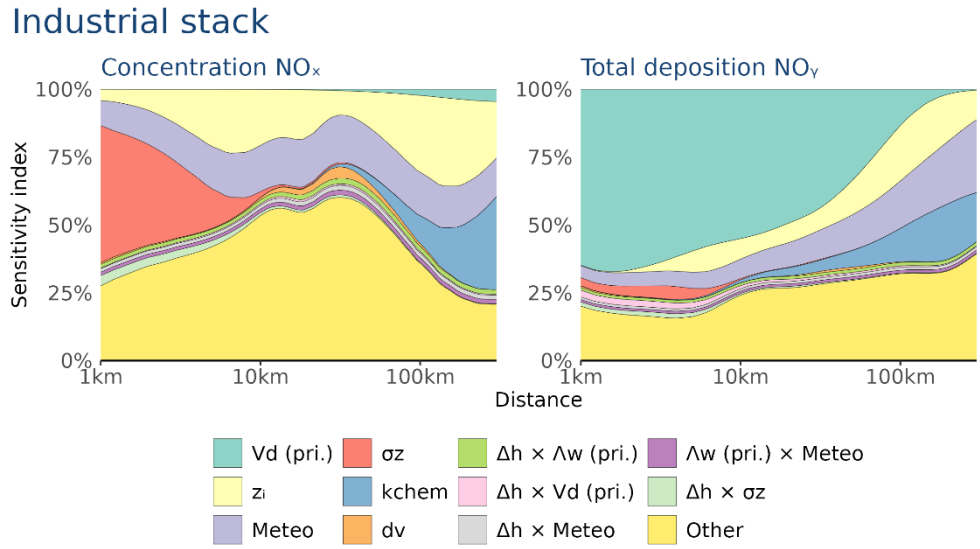


### 1.3.3 *Uitstoot van een snelweg van 65 kilometer*

Het verkeer op de snelweg stoot vooral stikstofoxiden uit. Voor deze bron worden de concentratie en totale depositie van stikstofoxiden onderzocht. Figuur 1.6 toont de gevoeligheid als functie van de afstand.

Op korte afstand van de weg (tot ongeveer 20 km), is de gevoeligheid in de concentratie ongeveer 50 procent. Op grotere afstanden neemt de gevoeligheid af tot 30-35 procent.

De gevoeligheid van de depositie voor de variaties in de parameters is dicht bij de bron ruim 80 procent. Verder van de bron neemt de gevoeligheid sterk af tot ongeveer 25 procent voor afstanden verder dan 100 km. Voor berekeningen in AERIUS, bijvoorbeeld voor vergunningverlening, wordt voor wegverkeer OPS alleen gebruikt bij afstanden groter dan 5 km. Bij kleinere afstanden wordt de Standaard Reken Methode voor snelwegen, SRM-2, gebruikt.

*Figuur 1.6 Berekende gevoeligheid (als variatiecoëfficiënt) in de $NO_x$-concentratie en de totale $NO_y$-depositie als functie van de afstand, voor een snelweg met $NO_x$-emissie. Dit is de gevoeligheid in de berekeningen van de concentratie en de depositie voor de gecombineerde onzekerheid in de twaalf beschreven parameters. De gekleurde lijnen tonen de mediane gevoeligheid, dat is de middelste waarde van de CV's in alle windrichtingen. De gekleurde vlakken laten de spreiding van de CV's over de twaalf windrichtingen zien als één en twee maal de MAD (zie hoofdtekst). De afstand vanaf de bron is weergegeven op een logaritmische schaal.*

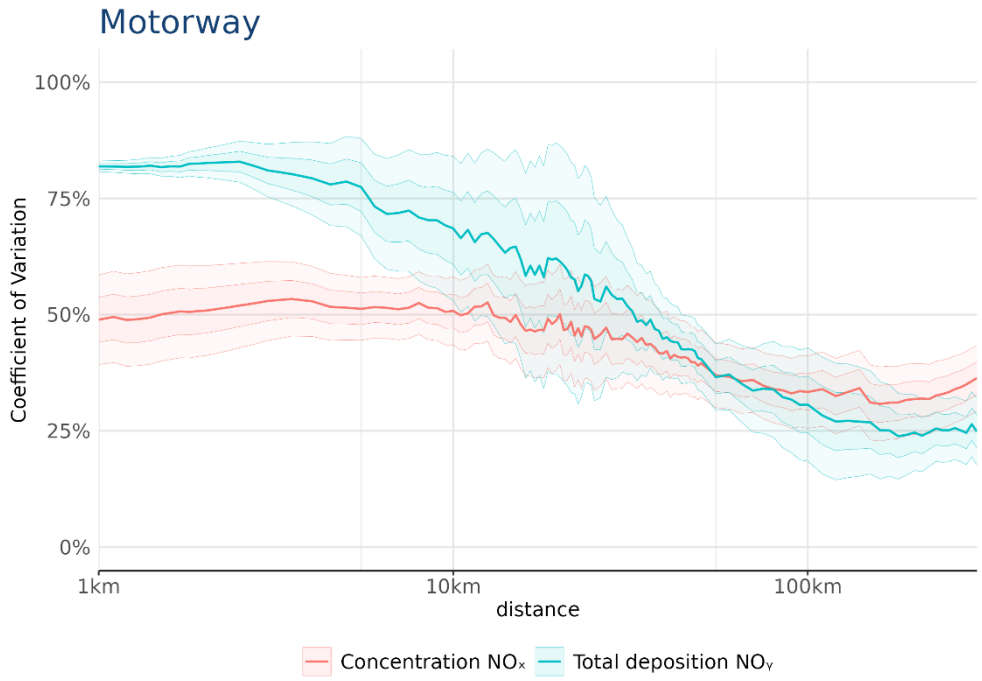


Uit Figuur 1.7 blijkt dat voor concentratie (linker plaatje) de verticale verspreiding het meest bijdraagt aan de gevoeligheid. Daarnaast zijn de menglaaghoogte en de meteorologie belangrijk. Bij deze bron is tot zo'n 50 km afstand de invloed van het dagverloop ook relatief belangrijk. Hierna neemt de invloed van chemische omzetting weer toe.

De gevoeligheid van de totale depositie $NO_y$ (rechter plaatje) wordt dicht bij de bron gedomineerd door de variaties in droge depositiesnelheid. De menglaaghoogte heeft een wat grotere bijdrage vanaf 5 km. Vlak bij de bron geldt dat voor verticale verspreiding. Pas op grotere afstand (meer dan 50 km) wordt onzekerheid in andere parameters relatief belangrijk en is de invloed van droge depositiesnelheid sterk afgenomen. Met name de invloed van chemische omzettingen en meteorologische omstandigheden neemt dan snel toe.

*Figuur 1.7 Uitsplitsing van de elf grootste bijdragen van de parameters, en parametercombinaties, aan de onzekerheid als functie van de afstand voor $NO_x$ van een snelweg. Het linker plaatje laat het resultaat voor de concentratie zien en het rechter plaatje dat voor de totale $NO_y$-depositie.*

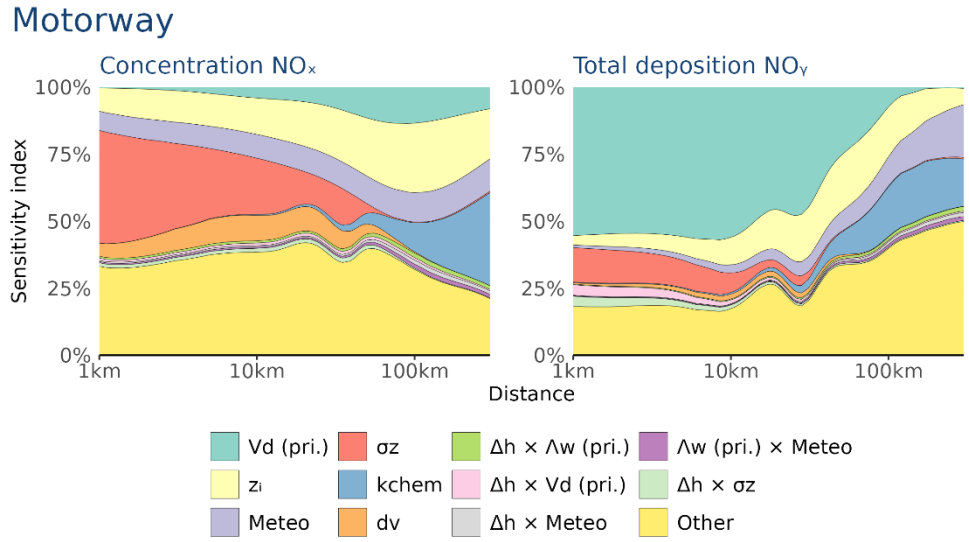


## 1.4 Gevoeligheid voor individuele parameters

Op grond van de in paragraaf 1.3 beschreven analyses komen er vijf parameters naar voren die samen het grootste deel van de gevoeligheid in de berekeningen van de concentratie en de depositie bepalen voor alle drie de brontypes. Dit zijn:

- droge depositiesnelheid van de primaire component;
- verticale spreiding van de pluim;
- menglaaghoogte;
- chemische omzettingssnelheid; en
- meteorologische omstandigheden.

Voor elk van deze parameters hebben we afzonderlijk de gevoeligheid voor de onzekerheden in deze parameter bepaald. Hiervoor hebben we de referentiewaarde van een parameter in de meeste gevallen met een factor vermenigvuldigd. Er zijn telkens 99 runs uitgevoerd waarbij de factor varieert tussen: de referentiewaarde min de onzekerheid in de parameter en de referentiewaarde plus de onzekerheid in de parameter.

De bepaling van de gevoeligheid voor onzekerheden in de individuele parameters ondersteunt de interpretatie van de resultaten van het onderzoek waarin alle parameters tegelijk zijn gevarieerd. Hieronder geven we als voorbeeld de resultaten van de droge depositiesnelheid van de primaire component.

*Voorbeeld: droge depositiesnelheid voor ammoniak uit de stal*
Een belangrijke gevoeligheid is die voor de droge depositiesnelheid van de primaire component. Net als bij de meeste andere parameters is in een modelberekening steeds met dezelfde factor vermenigvuldigd (die in de 99 runs varieert tussen de referentiewaarde min de onzekerheid in de droge depositiesnelheid en de referentiewaarde plus de onzekerheid in de droge depositiesnelheid).

Figuur 1.8 laat de ammoniakconcentratie zien bij verschillende afstanden en verschillende vermenigvuldigingsfactoren voor droge depositiesnelheid van de primaire component (de gekleurde lijnen) voor emissies vanuit de stal. Hierbij is de gemiddelde concentratie genomen van de concentraties in de verschillende windrichtingen. De berekening met de referentiewaarde wordt in geel weergegeven.

*Figuur 1.8 Ammoniakconcentratie als functie van de afstand van de bron, gemiddeld over de twaalf windrichtingen. De gele lijn toont de referentieberekening. De blauwe en rode lijnen laten de resultaten van lagere en respectievelijk hogere waarden van de droge depositiesnelheid van $NH_3$ zien. Het linker plaatje toont de concentratie op een lineaire schaal en het rechter plaatje toont de concentratie op een logaritmische schaal. De afstand is in beide gevallen logaritmisch.*

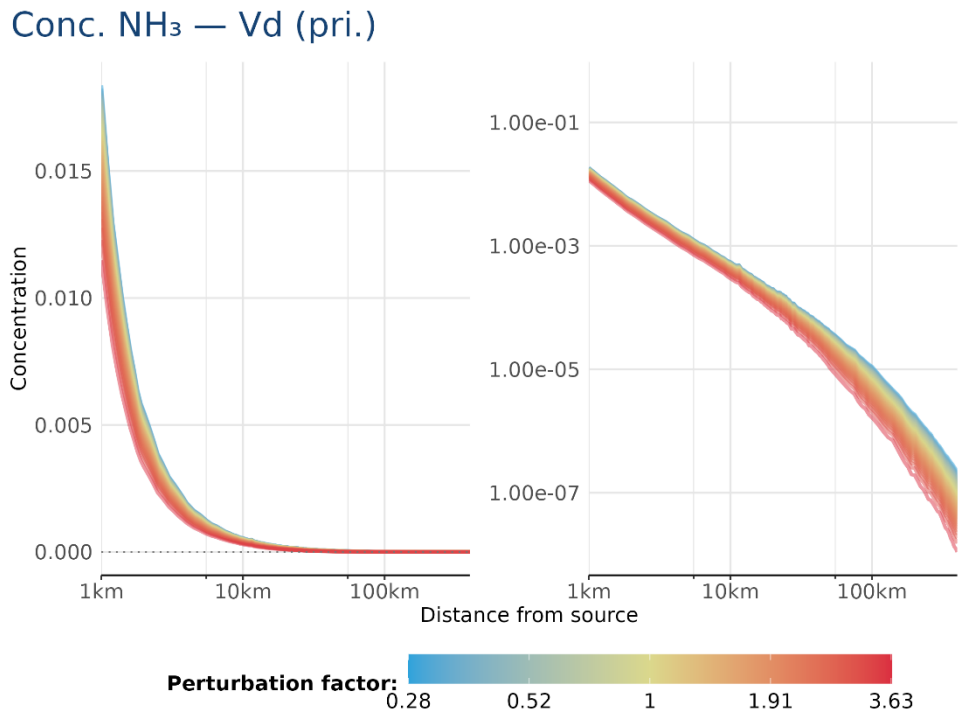


Zoals verwacht, neemt de concentratie sterk af met de afstand van de bron; ongeveer twee ordegroottes binnen de eerste 20 tot 25 kilometer. Verschillen tussen de runs, waarin de droge depositiesnelheid van de primaire component is gevarieerd, zijn duidelijk te zien in de lineaire plot (links). Na 25 kilometer lijken de absolute verschillen te verdwijnen in de lineaire plot, maar worden ze duidelijk zichtbaar in de logaritmische plot (rechts). Dit duidt op een sterk signaal van gevoeligheid of onzekerheid over grotere afstanden.

*Onzekerheden op enige afstand van de bron*
Aangezien het een belangrijk doel van de huidige studie is om de onzekerheid op enige afstand van de bron te bepalen, hebben we besloten ons te richten op relatieve gevoeligheid, ook al kunnen de absolute verschillen klein zijn. Het is daarbij belangrijk op te merken dat er in de praktijk op grotere afstanden vaak veel kleine bijdragen zijn, elk met een eigen onzekerheid, die gezamenlijk de totale concentratie en

depositie kunnen beïnvloeden. Dit maakt de relatieve gevoeligheid voor een individuele bron op grotere afstanden nog steeds relevant, omdat die samen met de andere bronnen op grote afstanden de onzekerheid in de totale stikstofdepositie bepaalt.

*Relatieve gevoeligheid ten opzichte van de referentieberekening*
Figuur 1.9 laat de relatieve verschillen zien in de concentratie, die het gevolg zijn van de variatie in de droge depositiesnelheid van de primaire component, ten opzichte van de concentratie zoals berekend met de referentiewaarde daarvan.

De afwijking is relatief gemaakt door het concentratieverschil op elke receptor te delen door de op die receptor berekende referentie-concentratie. Deze analyse van het effect van (onzekerheden in de) parameters op de berekende concentratie is een belangrijke stap om het model te begrijpen en ook om, in een volgende stap, het effect op de depositie te kunnen duiden.

Figuur 1.9 laat in vier afbeeldingen zien dat een lagere droge depositiesnelheid (blauwe lijnen) overal leidt tot een hogere ammoniakconcentratie. In de andere figuren is steeds het resultaat gemiddeld over de twaalf windrichtingen. Als uitzondering toont Figuur 1.9 vier losse windrichtingen vanaf de bron.

Op grotere afstand wordt het relatieve verschil ten opzichte van de referentieberekening steeds groter. Dit generieke resultaat was te verwachten: als de droge depositiesnelheid lager is, dan is er minder verlies onderweg. En dat leidt tot een hogere concentratie.

Andersom leidt een hogere droge depositiesnelheid tot meer verlies onderweg. Dat zorgt voor een lagere concentratie dan in de referentieberekening. De resultaten verschillen per windrichting. Dat komt onder andere doordat ook het landgebruik en de daarbij behorende droge depositiesnelheden per windrichting verschillen.

*Figuur 1.9 Relatieve verschillen in concentratie $NH_3$ ten opzichte van de referentieberekening, bij verschillende waarden voor de droge depositiesnelheid van $NH_3$, als functie van de afstand van de bron (stal). De figuur toont als voorbeeld de resultaten voor vier windrichtingen vanuit de bron gezien. De kleine windroos rechtsboven in de subplots geeft de betreffende x-as-afstandsrichting aan. De afstand is weergegeven op een logaritmische schaal.*

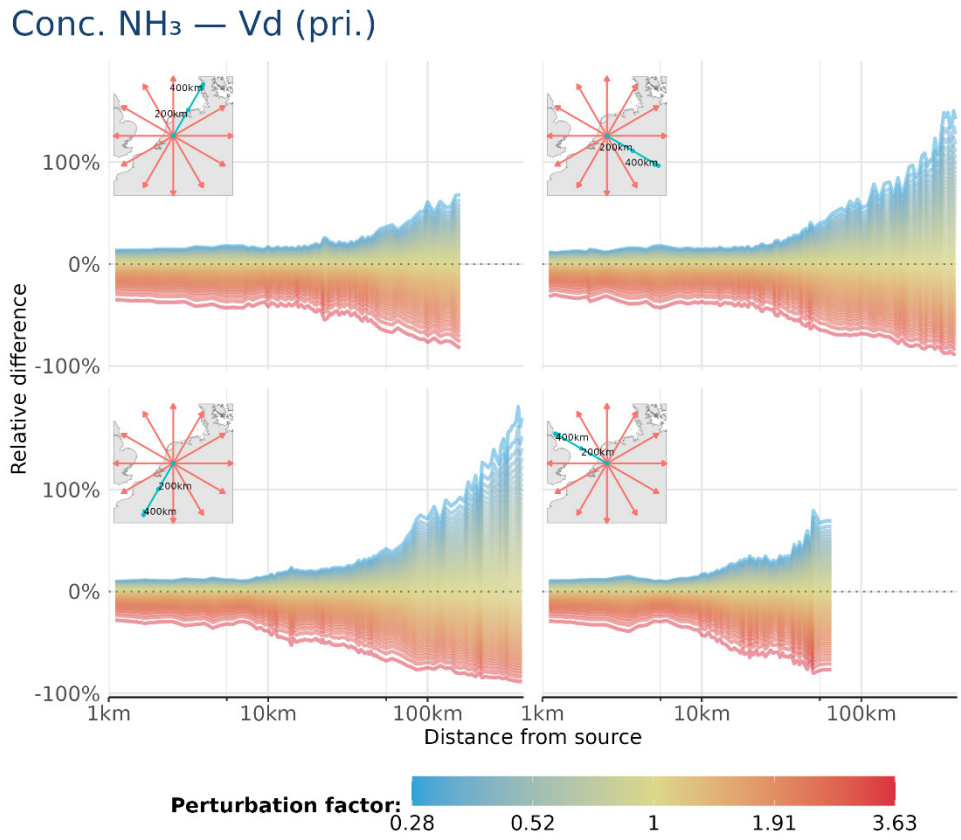


Figuur 1.10 laat voor dezelfde variaties in de droge depositiesnelheid van de primaire component ($v_{d,pri}$) zien wat het effect is op de berekende droge depositie van ammoniak en ammonium ($NH_x$) als functie van de afstand tot de stal.

Het algemene beeld is dat bij hogere droge depositiesnelheid van de primaire component (rode lijnen) de depositie vlak bij de bron hoger is.

Ook dit was te verwachten, omdat de droge depositie het product is van de droge depositiesnelheid en de concentratie. Verder van de bron wordt het verschil met de referentieberekening kleiner. Op grote afstanden van de bron wordt de droge depositie zelfs lager dan die van de referentie. Dit is te verklaren door de eerder genoemde lagere concentratie bij hogere droge depositiesnelheid van de primaire component, $v_{d,pri}$ ten opzichte van de referentie.

Voor de primaire componenten kan de gevoeligheid van de droge depositie voor verandering in droge depositiesnelheid ($v_{d,pri}$) beoordeeld worden aan de hand van de spreiding (positief of negatief) van de resultaten. De spreiding, en dus gevoeligheid, is het grootst op korte en

heel lange afstanden. Tussen de 100 en 200 km is de gevoeligheid juist kleiner. Daar zien we een omslag van positief naar negatief en omgekeerd. Dit soort kruisende gevoeligheden zijn voor meer parameters geconstateerd.

*Figuur 1.10 Relatieve verschil in droge depositie van $NH_x$ ten opzichte van de referentieberekening, bij verschillende waarden voor de droge depositiesnelheid van $NH_3$, als functie van de afstand van de bron (stal). De figuur toont het gemiddelde van twaalf windrichtingen. Afstand is weergegeven op een logaritmische schaal.*

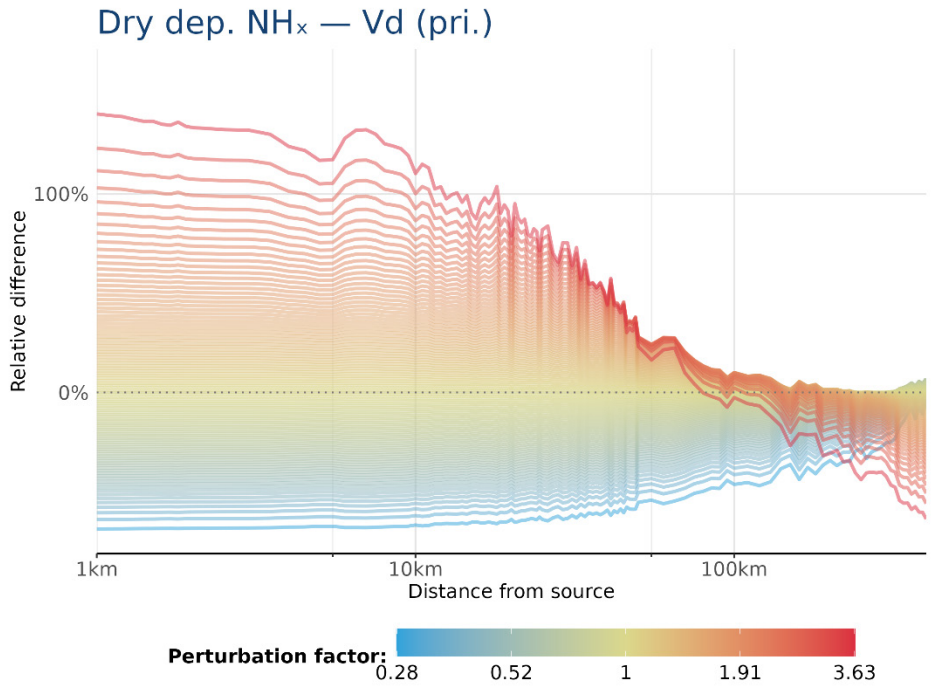


*Kruisende gevoeligheden door terugkoppeleffect*
Figuur 1.11 toont hiervan een voorbeeld. De rode lijnen laten zien hoe groot de relatieve verschillen zijn tussen de totale depositie van de som van ammoniak en ammonium bij een grotere verticale spreiding. Een hogere rode lijn leidt vlak bij de bron tot lagere depositie. En ver van de bron tot een hogere depositie. We zien rond de 10 km een overgang van positieve naar negatieve verschillen met de referentieberekening.

Bovenstaande observaties sluiten aan bij het recente onderzoek naar de onzekerheid in de totale stikstofdepositie waarbij is vastgesteld dat de onzekerheid in depositie van grote gebieden, zoals Nederland, veel kleiner is dan de onzekerheid van een klein gebied. Dit is geïnterpreteerd als een terugkoppeleffect (Hoogerbrugge et al., 2023).

*Figuur 1.11 Relatieve verschil in de totale depositie van $NH_x$ ten opzichte van de referentieberekening bij verschillende waarden voor de verticale spreiding van de pluim, als functie van de afstand van de bron (stal). De figuur toont het gemiddelde van twaalf windrichtingen. Afstand is weergegeven op een logaritmische schaal.*

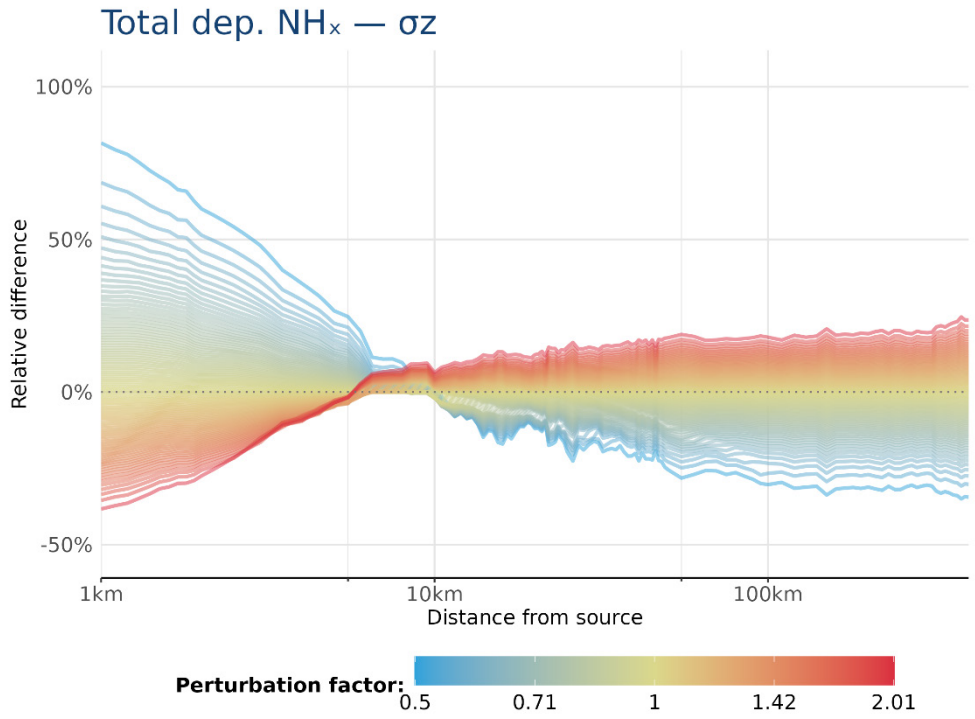


## 1.5 Verkleinen onzekerheden door betere inschatting parameterwaarden

Het OPS-model wordt niet alleen gebruikt voor het berekenen van de bijdrage van een individuele bron. De som van de bijdragen van alle bronnen wordt bijvoorbeeld berekend voor gebruik in de Grootschalige Concentratie- en Depositiekaarten Nederland (GCN/GDN) en voor de monitoring van de stikstofdepositie in Natura 2000-gebieden in het kader van de Wet stikstofreductie en natuurverbetering (Wsn).
Deze totale concentratie en stikstofdepositie kan worden vergeleken met beschikbare concentratie- en depositiemetingen en die vergelijking kan weer worden gebruikt om de onzekerheden in de parameters nader te evalueren.

Het instrument dat voor deze evaluatie wordt ontwikkeld als onderdeel van het Nationaal Kennisprogramma Stikstof (NKS-SAGEN) is de Uncertainty Analysis Tool (UAT).

De verwachting is dat deze evaluatie leidt tot betere schattingen van de (onzekerheden in de) parameters die gebruikt zijn in de gevoeligheidsanalyse. De verwachting is ook dat dit uiteindelijk de onzekerheid in de berekende stikstofdepositie kan verkleinen.

## 1.6 Onzekerheden in de emissies

Hoewel in deze studie vooral naar de onzekerheid in het model zelf is gekeken, is het belangrijk om te beseffen dat de onzekerheid in de invoer (en vooral wat betreft de emissies) ook een groot aandeel zal hebben in de uiteindelijke onzekerheid in de berekende stikstofdepositie.

De onzekerheid in de emissie van een individuele bron hangt sterk af van het soort bron en de component. Indicatief wordt voor relatief goed bekende bronnen deze onzekerheid geschat op een factor 2 voor de jaargemiddelde emissie. Voorbeelden zijn fijnstof en stikstofdioxide ($NO_2$) uit een grote fabriek of snelweg. Voor kleinere bronnen en bronnen met beperkte informatie kan de onzekerheid meer dan een factor 2 zijn. Meer informatie over onzekerheden in emissies staat in de Methoderapporten op Emissieregistratie.nl.

De verwachting is dat onzekerheid in de emissie nauwelijks samenhangt met de onzekerheid in de modelberekening. Dat betekent dat de onzekerheid in de emissie relatief eenvoudig kan worden opgeteld bij de onzekerheid in de modelberekening.

## 1.7 Vergelijking met andere studies

De afgelopen jaren zijn er in Nederland verschillende gevoeligheids- en/of onzekerheidsstudies naar stikstofdepositie uitgevoerd. Hieronder zullen de resultaten van de huidige gevoeligheidsstudie (‘*sensitivity OPS*’) worden vergeleken met de meest relevante studies (in chronologische volgorde):

1) In 2021 maakte het RIVM een eerste inschatting van de onzekerheden in depositiebijdragen van individuele bronnen (Roest et al., 2021).
2) In 2022 publiceerde TNO een gevoeligheidsanalyse met het SRM 3-model Stacks (‘*sensitivity TNO Stacks*’) voor een beperkt aantal parameters (TNO, 2022).
3) In 2023 heeft het RIVM een onzekerheidsanalyse uitgevoerd van de stikstofdepositie op verschillende schaalniveaus in Nederland (Hoogerbrugge et al., 2023). Bij de berekening van de stikstofdepositie zijn de bijdragen van alle bronnen (in binnen- en buitenland) meegenomen. De depositie op elke locatie is dus de som van heel veel bronnen. De onzekerheden zijn berekend op basis van een vergelijking met metingen (‘*uncertainty OPS based on comparison measurements*’). Omdat in deze analyse de focus lag op de totale stikstofdepositie (vooral in natuurgebieden), maakt dat de vergelijking met de onzekerheid in de berekening van de depositiebijdrage van een individuele bron lastig.
4) In 2024 publiceerden Meijer en van Loon (2024) het rapport “Een ondergrens in de berekening van stikstofdepositiebijdragen voor vergunningverlening”, waarin eveneens uitgebreid naar onzekerheden in de depositiebijdrage van individuele bronnen is gekeken.
5) In 2025 publiceerden (Kooi et al., 2025a) een modelvergelijkingsstudie (‘*benchmark*’) uitgevoerd met OPS-LT en zeven andere modellen. De spreiding van de verschillende modeluitkomsten geeft inzicht in hoe onzeker de berekende

stikstofdepositie is. Dit beeld hoeft overigens niet compleet te zijn vanwege overeenkomsten in modelkeuzes.

6) Tot slot voegen we een variant toe van de huidige gevoeligheidsstudie waarbij rekening wordt gehouden met de mogelijkheid dat de schaling van de droge depositiesnelheid afhangt van het landschapstype. In de variant is dus alleen de droge depositiesnelheid van bos gevarieerd (*'sensitivity OPS forest'*).

Figuur 1.12 laat de resultaten van de huidige en vier van de zes geselecteerde studies (studie 2, 3, 5 en 6) zien, voor berekeningen aan een stal.

*Figuur 1.12 Onzekerheden/gevoeligheden in de berekende depositie van $NH_x$ door ammoniakemissie uit een stal. De getoonde studies zijn in de tekst beschreven. De onzekerheid die volgt uit de vergelijking met de metingen kan niet aan een individuele bron en dus een afstand gekoppeld worden en is daarom los van de afstand schaal apart weergegeven.*

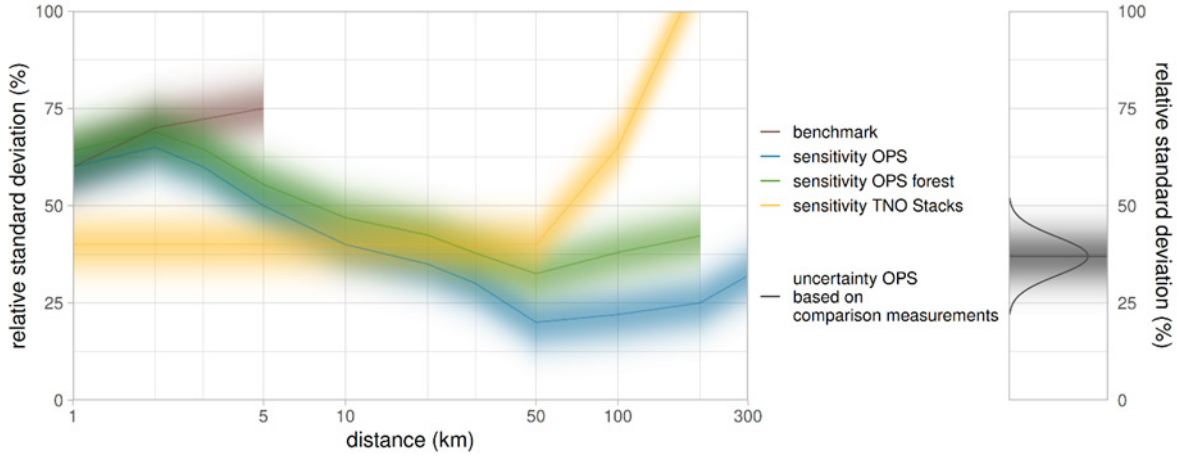


Hieronder zullen de resultaten van de huidige studie in perspectief worden geplaatst met de zes bovengenoemde studies:

Ad 1) In 2021 maakte het RIVM een eerste inschatting van de onzekerheden in de depositiebijdragen van individuele bronnen (Roest et al., 2021). Op lokale schaal werd een onzekerheid ingeschat van een factor 2. Verder van de bron (>25 km) zou de onzekerheid vermoedelijk aanzienlijk groter zijn, met de kanttekening dat die onzekerheid alleen via modelberekeningen kan worden vastgesteld.
Figuur 1.12 geeft de resultaten weer van dergelijke modelonderzoeken. De inschatting van een factor 2 (wat overeenkomt met een CV van 70 procent) dicht bij de bron wordt bevestigd. De verwachting dat onzekerheden boven de 25 km aanzienlijk toenemen, blijkt echter niet correct. Onzekerheden nemen tot 100 km eerder af. Bij heel grote afstanden >100 km nemen de onzekerheden wel toe, maar niet boven de verwachte factor 2. In de luchtkwaliteitsmodellering wordt ernaar gestreefd dat 50 procent van de modelresultaten binnen een factor 2 van de metingen moet liggen. Vertaald naar deze onzekerheidsstudie komt dit ongeveer overeen met een CV van 100 procent. De resultaten in Figuur 1.12 voldoen daar in het algemeen ruim aan. Dit geldt ook

voor de resultaten uit het gevoeligheidsonderzoek voor de industriecasus en de snelwegcasus.

Ad 2) De gevoeligheidsanalyse met TNO *Stacks* laat bij korte afstanden een lagere gevoeligheid zien. Dit komt waarschijnlijk doordat het TNO-onderzoek uitgaat van een kleinere onzekerheid in de droge depositiesnelheid. In deze studie hebben we gezien dat juist dicht bij de bron de gevoeligheid voor de droge depositiesnelheid groot is. Waarschijnlijk wordt de gevoeligheid in TNO Stacks hierdoor lager ingeschat. Bij grotere afstanden, zoals rond 100 km van de bron, is de gevoeligheid van OPS kleiner geworden terwijl de gevoeligheid van TNO Stacks daar juist toeneemt. Het laatste zou kunnen komen doordat het TNO Stacks-onderzoek de verandering van de droge depositiesnelheid voor het beschrijven van de lokale depositie, en de verandering van de droge depositiesnelheid als verliesterm langs de trajectoriën, als twee onafhankelijke parameters beschrijft. Hierdoor is de compensatie, die bij OPS een grote rol speelt, bij TNO Stacks uitgeschakeld. Stacks is in het algemeen minder gericht op de depositie op grote afstanden van bronnen dan OPS.

Ad 3) De gevoeligheid van de depositieberekeningen voor onzekerheden in de parameters levert op grote afstand van een bron ongeveer dezelfde spreiding op als de onzekerheid die uit de *vergelijking met metingen* volgt.
Op het eerste gezicht lijkt dit vreemd; omdat random onzekerheden uitmiddelen wanneer verschillende individuele bronnen bij elkaar opgeteld worden.
Sommige belangrijke bronnen van onzekerheid, zoals de droge depositiesnelheid, zijn echter locatie-afhankelijk. Ze middelen bij optelling daardoor veel minder uit.
Ook speelt bij vergelijking met metingen de onzekerheid in gemeten depositie en in emissiesterkte een belangrijke rol.

Ad 4) In Meijer en van Loon (2024) wordt gesteld dat de onzekerheden die optreden in de depositieberekeningen mogelijk een additionele factor 2-3 of meer toevoegen aan de onzekerheden van de concentratieberekeningen. De huidige gevoeligheidsstudie ondersteunt deze stelling niet, met name verder weg van de bron. Het laat daar zien dat de gevoeligheid in de depositieberekeningen van dezelfde orde van grootte is als de gevoeligheid in de concentratieberekeningen. De gevoeligheid hangt wel af van de component en in mindere mate van het type bron.

Ad 5) In de voorliggende gevoeligheidsstudie zijn dezelfde bronnen gebruikt als in de *benchmarkstudie* (Kooi et al., 2025a). Toch lag de focus in de benchmarkstudie op de directe omgeving van de bron (tot 5 km), terwijl bij de gevoeligheidsstudie ook naar grotere afstanden is gekeken.
De benchmarkstudie geeft in potentie een completer beeld van onzekerheden dan de gevoeligheidsstudies. De benchmarkstudie bevat namelijk ook de verschillen *tussen* modellen.
Een vergelijking van beide studies laat zien dat de spreiding in dezelfde orde van grootte is. Dit suggereert dat er bij de afstand tot 5 km van de bron, geen belangrijke bronnen van onzekerheid ontbreken.

Ad 6) Tot slot wordt in de figuur ook een variant van deze studie getoond waarbij rekening wordt gehouden met verschillen in afwijking van droge depositiesnelheid tussen gras en bos. Bij verschillende afwijkingen voor diverse landschapstypes verzwakt de koppeling tussen de droge depositiesnelheid over de trajectorie en de lokale depositiesnelheid. Daardoor is de compensatie minder effectief. In de figuur zien we rond 100 km een minder sterke daling in de gevoeligheid dan bij de optimale compensatie, met gelijke afwijking voor elk landschapstype.

## 1.8 Discussie

Het doel van dit onderzoek is om te schatten wat de onzekerheid is van een berekende bijdrage van een individuele bron aan de stikstofdepositie.
Het is in de praktijk niet mogelijk om deze schatting te doen door de berekening te vergelijken met metingen. Daarom hebben we voor de belangrijkste modelparameters onderzocht hoe gevoelig de berekeningen zijn voor onzekerheden in deze parameters.

De vergelijking met andere typen onzekerheidsonderzoek laat zien dat de totale gevoeligheid een redelijke indicator is voor de onzekerheid.

In dit onderzoek hebben we de belangrijkste te onderzoeken parameters vooraf geselecteerd. Deze lijst is niet uitputtend. Uitbreiding van de lijst leidt mogelijk tot iets hogere schattingen van de gevoeligheden. Bij de inschatting van de onzekerheden is voor die parameters vaak de spreiding in metingen of modelberekeningen gebruikt.
Omdat we niet weten welke van deze metingen het beste aansluit bij de OPS-berekeningen, is deze spreiding een indicatie voor de onzekerheid in de parameter.

Op basis van deze onzekerheid gebruiken we voor elke modelberekening een parameterwaarde die afwijkt van de standaardwaarde in het model. Deze waarde kan beschouwd worden als een systematische afwijking in de specifieke modelberekening. In het OPS-model zijn de parameters vaak zelf weer variabel in ruimte en tijd. Als een deel van de spreiding in een dergelijke parameter ook een randomcomponent heeft (bijvoorbeeld: menglaaghoogte is soms iets te hoog en soms iets te laag), kan de systematische onzekerheid kleiner zijn. Met andere woorden, de schatting van de gevoeligheid die is verkregen door de afwijking als systematisch in ruimte en tijd te beschouwen zou daardoor ietwat te hoog kunnen zijn.

De vergelijking van de berekeningen met metingen van het MAN (Meetnet Ammoniak Natuurgebieden) geeft inderdaad aan dat de onzekerheden vermoedelijk overschat worden. Op dit moment doen we onderzoek om dit verder te kunnen kwantificeren.
De onderzoeksresultaten laten de onzekerheden zien bij een afstand van 1 tot 400 kilometer ten opzichte van de bron. De opzet van de studie was gericht op afstanden van 20 tot 400 km. Daarom zijn geen parameters meegenomen die waarschijnlijk alleen binnen enkele kilometers van de bron tot verschillen zouden leiden, zoals de invloed van het gebouw van de bron. Daardoor zijn de resultaten bij heel korte

afstanden (minder dan 1 km van de bron) mogelijk niet representatief en worden ze niet getoond. Ook de analyse met de MAN-metingen heeft waarschijnlijk meer toegevoegde waarde bij de grotere afstanden. Het MAN richt zich vooral op natuurgebieden, waarbij de meetlocaties zo veel mogelijk niet bij een lokale bron staan.

In dit onderzoek zijn onzekerheden relatief weergegeven. De absolute bijdrage aan de depositie en de concentraties zijn dicht bij de bron veel groter. En dus ook de impact van de onzekerheid van die bronbijdrage. Verder weg van bronnen gaat het om de optelsom van vele kleine bijdragen met elk een onzekerheid.

De resultaten uit dit onderzoek laten zien dat voor depositie de modelonzekerheden dicht bij de bron vermoedelijk groter zijn dan verder weg.

Dichter bij de bron kan beter onderscheid gemaakt worden tussen de bron en de achtergrond. Ook dan nog is het meten van een concentratiebijdrage alleen mogelijk via een complex en kostbaar onderzoek. Goede, betrouwbare en nauwkeurige metingen van de totale stikstofdepositie zijn nog ingewikkelder en duurder. Dit komt doordat er verschillende stikstofcomponenten zijn die niet met één instrument gemeten kunnen worden en doordat de stikstofcomponenten zowel met regen als direct vanuit de lucht op het oppervlak kunnen neerslaan.

De resultaten van dit onderzoek naar de onzekerheid van de depositiebijdrage kunnen van belang zijn voor analyse van de statistische aspecten van een salderingsbesluit. Bij zo'n besluit wordt de sluiting van één of meer bestaande bronnen gebruikt om een nieuwe bron toe te staan. De kansen op het daadwerkelijk verminderen van de stikstofdepositie zal zowel van het type bron, de locatie van de bron en de locatie van de gevoelige natuur afhangen. Een dergelijke analyse viel buiten de scope van dit onderzoek.

## 1.9 Conclusie

Het gevoeligheidsonderzoek voor onzekerheden in de twaalf geselecteerde parameters is voor depositieberekeningen met OPS uitgevoerd voor drie soorten bronnen (stal, industriële bron en snelweg). Analyse van effecten op concentratie is in dat onderzoek een belangrijke tussenstap. Onzekerheden in berekeningen van concentratie en totale depositie zijn gekwantificeerd, als functie van de afstand vanaf de bron.

Voor ammoniak uit een stal bedraagt de gevoeligheid tot 10 km, uitgedrukt als relatieve standaarddeviatie (variatiecoëfficiënt) in de totale $NH_x$-depositie, ruim 60 procent. Bij afstanden rond 100 km is de gevoeligheid aanzienlijk kleiner (ongeveer 25 procent). Boven de 100 kilometer neemt de gevoeligheid weer toe.

Voor stikstofoxiden uit een industriële bron is de gevoeligheid voor de onzekerheid in de parameters voor totale stikstofdepositie het grootst (70-75 procent) bij kleine afstanden (tot 20 km) van de bron. Ook hier

neemt de gevoeligheid af bij grotere afstanden. Boven de 100 km is de gevoeligheid 25-30 procent.

Voor een snelweg zien we een vergelijkbaar verloop. De gevoeligheid rond de 5 km bedraagt ongeveer 80 procent. Op grotere afstanden van de weg neemt de gevoeligheid af tot ongeveer 25 procent bij afstanden ruim boven de 100 km. Deze gevoeligheden zijn kleiner dan de onzekerheden die vooraf bekend waren (Roest et al., 2021; TNO, 2022; Meijer en van Loon, 2024).

Op grotere afstand van de bron zijn depositieberekeningen relatief minder gevoelig voor onzekerheden in het model dan concentratieberekeningen. Hier speelt compensatie door met name de droge depositie een grote rol. Immers, een veronderstelde grotere droge depositiesnelheid leidt bij de bron tot grotere depositie. Op grotere afstand van de bron neemt de concentratie daardoor sterker af, omdat er gaandeweg meer depositie plaatsvindt. Door deze lagere concentratie is uiteindelijk ook de depositie op grotere afstand lager (en omgekeerd). Dit is het duidelijkst voor de stalberekeningen. Dat komt doordat de droge depositie van ammoniak en ammonium relatief efficiënter is dan de droge depositie van stikstofoxiden. Waardoor het compenserende effect al op kortere afstand optreedt.

## 1.10 Aanbevelingen voor verder onderzoek

Deze studie was met name gericht op onzekerheden op enige afstand van de bron. De volgende aanbevelingen geven mogelijkheden om toekomstig onderzoek te verbeteren.

- De onzekerheid van de droge depositiesnelheid van de primaire component is de belangrijkste factor in de onzekerheid van de totale depositie. Verdere uitsplitsing van deze parameter, over verschillende aspecten van het depositieproces, wordt aanbevolen. Daarbij kan ook overwogen worden om de schaling van de droge depositiesnelheid per landgebruiksklasse te variëren.
- Meteorologische omstandigheden dragen in belangrijke mate bij aan de onzekerheid van concentratie en depositie. Om effecten hiervan in kaart te brengen was een eenvoudige schaling, zoals bij de andere parameters, niet mogelijk door de complexiteit van de meteorologische processen en hun interacties, en de daarmee samenhangende effecten op verschillende modeluitkomsten. Daarom is een regionale categorisatie toegepast. Voor vervolgonderzoek wordt aanbevolen om te onderzoeken of het mogelijk is om de complexe meteorologische processen meer als samenhangende schaalbare variabelen te beschrijven, met name ook voor de ontwikkeling van de Uncertainty Analysis Tool.
- De Uncertainty Analysis Tool, die momenteel in ontwikkeling is, vergelijkt modeluitkomsten op basis van emissies van alle bekende bronnen met de verschillende sets metingen. De tool kan leiden tot meer waarschijnlijke modelparameterinstellingen in combinatie met kleinere parameteronzekerheden. Een eenvoudige eerste poging is in deze studie gedaan ter illustratie. Verder onderzoek en toepassing van de resultaten uit de tool voor modelverbetering is aan te bevelen.

- De onzekerheid in de berekende depositie van individuele bronnen kan relevant zijn voor beleidsbeslissingen. Vooral als de beëindiging van huidige bronnen wordt gebruikt om de emissie van nieuwe bronnen mogelijk te maken. Het is daarom aan te bevelen om bij de berekening van het verschil tussen de oude en de nieuwe situatie ook de correlatie tussen de onzekerheden in beide situaties te beschouwen.
- Dit onderzoek richt zich op grotere afstanden. Onzekerheden dicht bij de bron, zoals gebouweffecten, zijn niet opgenomen in dit onderzoek. Toch zijn de relatieve onzekerheden in de depositiebijdrage dicht bij de bron groter dan op grote afstanden. Voor een eventueel vervolg op het huidige onderzoek is meer aandacht voor onzekerheid dicht bij de bron dan ook aan te bevelen.

# 2 Introduction

## 2.1 Background

The deposition of nitrogen components has been one of the most persistent environmental issues in the Netherlands. Many activities from which nitrogen components are emitted to the air require a permit. This requires, among other things, an assessment of the amount of reactive nitrogen that deposits on nature areas due to the activity. In the law on Nitrogen reduction and Nature recovery (WSN, Wet Stikstofreductie en Natuurherstel, 2021), it is stated that this has to be calculated using AERIUS calculator. This tool is used to evaluate the deposition of the nitrogen components from point sources such as livestock farms and (industrial) stacks, and from line sources such as roads and water ways. For most source types, the OPS-LT model (Operational Priority Substances model, Long-Term version, henceforth simply referred to as OPS) is used. For line sources consisting of moving road traffic, the SRM2 (Standaard RekenMethode 2) is used up to 5 km, while from 5 km onwards, OPS is deployed.
One important concern regarding the assessment of the contribution to the deposition is the uncertainty in its calculation. In this report, we will elaborate on the uncertainty in the contribution made by several types of nitrogen sources to the deposition, which is calculated using OPS.

The OPS model calculates the annual average concentration and deposition up to several hundreds of kilometres from the source. Far from the source, the contribution to the deposition amounts to very low numbers. Since the limit of the amount of deposition that is being considered is only 0.005 mole/ha/yr, many activities had to be assessed for distances up to several hundreds of kilometres from the source. Here, the questions arose whether these low numbers were based on reliable calculations, and whether these values can be attributed to a particular source with any certainty at such great distances. In 2021, the Minister of LNV decided that calculation using AERIUS calculator is mandatory up to 25 km only. Beyond 25 km, the contribution by a source to the nitrogen deposition is part of the background deposition and is no longer part in the permitting procedure. The decision was based on information by RIVM and TNO/Erbrink Stacks Consult. RIVM stated that there are no scientific grounds on the basis of which a maximum cut-off distance can be determined, but that policymakers can choose at which maximum distance the government wishes to stop calculating. RIVM did provide policymakers with a number of suggestions for choosing such a cut-off distance. One possibility is to choose the distance up to which nitrogen emissions from a project can actually be measured. Another possibility is the maximum distance up to which a model has been validated. TNO/Erbrink Stacks Consult also stated that the Gaussian plume models generally have an application distance of 20-25 km, and that validation of these models was only carried out up to 20 km. TNO/Erbrink Stacks Consult carried out an uncertainty analysis with STACKS (a Gaussian plume model) but could not conclude at which distance the uncertainty shows a typical increase. It was recognised that the application distance of Gaussian plume

models for concentration estimates can be extended beyond 25 km by means of trajectory approaches, as is the case in OPS. However, it was argued that the uncertainty in deposition estimates exceeds a factor of 2 beyond 20 km, both with and without implementing trajectories (Duyzer and Erbrink, 2021). Recently, in the ViA15 court case (ABRvS 5 april 2023, ECLI:NL:RVS:2023:1299), it was accepted that the distance of 25 km is a distance limit up to which AERIUS calculator can be used. This was primarily based on the argumentation of Duyzer and Erbrink (2021) that uncertainty beyond 25 km becomes larger than a factor of 2 and model results become too uncertain to deduce reliable conclusions.

Up to now, no thorough analysis has been performed of the uncertainties in the contribution by an individual source to nitrogen deposition as calculated using OPS. In this report, we will elaborate on the uncertainties in the concentrations and depositions of reactive nitrogen compounds, which were calculated using OPS, at distances up to 400 km from the source. We roughly follow the method used by TNO/Erbrink Stacks Consult (Duyzer and Erbrink, 2022), using OPS, which particularly differs from Stacks at great distances from the source (> 25 km) because of the use of trajectories in OPS. In addition, the analyses by Duyzer and Erbrink (2022) are elaborated upon in more detail in the present study. Here, more model parameters are included and a detailed analysis of their contribution to the overall sensitivity is applied. The study presented here investigates the uncertainty within the OPS model itself, focusing on an individual source. This is carried out by means of an analysis of the model's sensitivity to specific parameters and parameter combinations.

Reducing the uncertainties in the modelling of nitrogen deposition is also an important research topic within the NKS-SAGEN project (Dutch knowledge programme on nitrogen – a project on the use of satellite data and ensemble modelling; hereafter simply referred to as the SAGEN project). The results of the current uncertainty analysis for an individual source will eventually also be used in the SAGEN project to construct an Uncertainty Analysis Tool (UAT) for OPS in which all sources in the Netherlands and foreign countries are used. When using all sources, the calculations can be compared to measurements from operational monitoring networks. The aim of the UAT is to reduce the uncertainty in the model parameters. Model parameters settings can be optimised, within realistic boundaries, by minimising the differences between the calculated and measured concentrations and deposition.

Other and complementary approaches are followed within the SAGEN project. In this research programme, simulations from a range of models are compared in two benchmark studies. The first benchmark study focuses on the local scale, up to 5 km from the source. This benchmark study provides a model intercomparison with sensitivity analyses as well as a model validation study for single-source cases. The second benchmark study focuses on the national scale of the Netherlands, using all sources in the Netherlands and Europe. Model outcomes are compared to each other and to measurements. Due to the different spatial scales, the respective benchmark studies include different sets of models in their evaluation. However, OPS is included in both. Recently, the uncertainty of OPS with respect to all sources in the

Netherlands and Europe has also been assessed in a direct comparison to measurements (Hoogerbrugge et al., 2023). The various studies combined will provide more insight into the total uncertainty in the amount of nitrogen deposition in the Netherlands.

## 2.2 Aim of the study

The research question of this study is: what is the uncertainty in the annual nitrogen deposition on a nature area caused by a single source, at greater distances from the source (up to 400 km), computed using OPS. The source types that will be investigated are a livestock farm, an industrial stack and a motorway.

## 2.3 Reading guide

In this study, a sensitivity analysis with the OPS model is performed to obtain insight into the model-specific uncertainty in the annual nitrogen deposition caused by a single source up to several hundreds of kilometres. The remainder of the present chapter provides a brief literature survey on earlier attempts to evaluate the performance of Gaussian plume models against observations. The methodology of the sensitivity analysis in the present study is described in Chapter 3:

- Selection and description of the parameters taken into account, including their uncertainty ranges;
- Scaling procedure for perturbing the various parameters;
- Model version including used data;
- Description of the source types and their characteristics included in this study;
- Analysis method to determine the uncertainty in all parameters combined and pinpoint this to specific parameters (Sobol' Sensitivity Indices), as well as analysis of the impact when varying the parameters one at a time;
- Uncertainty Analysis Tool (UAT): the tool in which the concentration and deposition in the Netherlands is calculated by using the contribution of all sources, which can be compared to measurements. Subsequently, model parameters and model input can be optimised by minimising the differences between the calculated and measured concentrations and deposition.

Results are presented in Chapter 4. The combined uncertainty in all studied parameters based on the Monte Carlo calculations is analysed (Sections 4.1-4.3). The results of the Sobol' Sensitivity Indices reveal that a few parameters are responsible for more than half the uncertainty for the sources and components studied here. Therefore, the sensitivity to these parameters are studied in somewhat more detail in Section 4.4. Section 4.5 discusses possible links between the present sensitivity study and the Uncertainty Analysis Tool. This is followed by general discussion and conclusions in Chapters 5 and 6, respectively.

## 2.4 Brief literature survey of uncertainty in single source dispersion modelling of air pollution

### *2.4.1 Introduction*

Full model evaluation covers many aspects and is complex (Monteiro et al., 2018). There are several approaches to assessing uncertainty in deterministic models in a policy and regulatory context (Uusitalo et al., 2015). Studying uncertainty by comparing model predictions to observations is often considered the most obvious and straightforward one (Fox, 1984; TNO, 2022; Hoogerbrugge et al., 2023), as long as measurement errors can be dealt with (Uusitalo et al., 2015; Hoogerbrugge et al., 2023). However, it is stressed that such a comparison is only one step in a full model evaluation procedure (Monteiro et al., 2018), be it a crucial one. In this section, using scientific reviews as a starting point, we briefly discuss previous efforts to evaluate Gaussian plume models on the basis of comparisons between model results and measurements. To this end, we start with some general considerations regarding such validation efforts (Section 2.4.2). It appears that suitable datasets for evaluation are rare, in particular at distances beyond a few tens of kilometres beyond the source (sections 2.4.3-2.4.5). This is especially so for evaluation of deposition due to single sources. Yet, some general patterns regarding performance of Gaussian plume models used for single sources have emerged (section 2.4.6). Because of the scarcity of datasets for evaluation, other methods – such as the one applied here – may be considered. We briefly list the main options as well (Section 2.4.7).

### *2.4.2 General considerations*

Estimates of contributions from single sources and hence, the estimates of uncertainty in the outcomes for such computations are challenging. Gaussian plume models originally were designed for calculations not too far from the source only. Here, 'not too far' corresponds to travel times during which meteorological conditions can be considered to be stationary, usually taking one hour or less (Seinfeld, 1986; Holmes and Morawska, 2006; Leelőssy et al., 2014; Snoun et al., 2023). For example, at a wind speed of 5 $ms^{-1}$ this corresponds to a travel distance of 18 km. Advanced Gaussian plume models, such as OPS, may have been extended with trajectory approaches. These allow following a plume over greater distances, particularly taking into account changes in wind speed and wind direction (Leelőssy et al., 2014; Sauter et al., 2023). Note that grid-based Eulerian models are typically applied at greater distances (see, for instance, https://atmosphere.copernicus.eu/).

Although Gaussian models can compute contributions from individual sources by design (Leelőssy et al., 2014; Snoun et al., 2023), evaluation of the outcomes against measurements is a difficult task, especially at greater distances from the source. Contributions from single sources to concentration and deposition quickly reduce with distance from the source and become indistinguishable from measured background levels. Furthermore, for regulatory purposes involving single source contributions, Gaussian plume models have typically been applied at distances within their validity range, up to a few tens of kilometres from the source at most (Seinfeld, 1986; Holmes and Morawska, 2006; Leelőssy et al., 2014; Snoun et al., 2023). For these reasons, interest in

single-source contributions at greater distances from the source has been very limited in practice.
The performance of Gaussian plume models cannot be captured in a single parameter or number. There is no single best performance measure or superior evaluation methodology. Hence, different performance measures and methods should be applied to become well-informed on the model quality, and the choice may depend on the specific evaluation purpose (Chang and Hanna, 2004; Bennett et al., 2013). Furthermore, evaluation may be focused on specific aspects of the model (Irwin and Hanna, 2005). In addition, the accuracy of the model predictions depends strongly on the scenario and conditions applied in the study, including the selection of the meteorological database (Hood et al., 2024). Whereas a specific model may perform well in one situation, it may perform much less well in another (see, for instance, Hanna et al., 2001; Kooi et al., 2025b). A general ranking of Gaussian models with regard to performance is also impossible at present (Snoun et al., 2023).

### *2.4.3 Observation-based datasets of concentration for evaluation*

Although the number of observation-based datasets for dispersion model evaluation and validation aimed at single source contributions has been growing, both from field experiments and from wind tunnel experiments, such datasets only allow evaluation at distances up to some tens of kilometres (Perry et al., 2005; Irwin and Hanna, 2005). That is why, while quite a few efforts to validate Gaussian models have been reported (Weber et al., 1982; Miller and Hiverly, 1987; Snoun et al., 2023), such validation reports on single source contributions are available for short distances only, typically up to 20-25 km from a source (Duyzer and Erbrink, 2022).
Advanced Gaussian plume models using a trajectory approach, or so-called puff models, may sometimes be evaluated over greater distances from the source, using studies of accidental releases of radionuclides from nuclear powerplants (e.g. Chernobyl, Fukushima). Such releases can be followed with sufficient reliability over distances beyond 100 km (Leelőssy et al., 2018). However, the latter type of evaluations are often restricted to short periods of time (Miller and Hively, 1987; Leelőssy et al., 2018). Furthermore, in such cases, the required estimate of source strength may introduce considerable uncertainty (Leelőssy et al., 2018). This is a particularly important consideration in view of the sensitivity of dispersion model predictions to emission estimates and source characteristics. The latter include, for example, temporal behaviour of emission strength, plume height and plume rise as driven by efflux temperature and velocity, and source diameter (Miller and Hiverly, 1987; Clegg, 2006; Price et al. 2016). Thus, the question may be raised whether such studies actually assess the quality of the emission estimate, rather than the quality of the dispersion model. As an additional complication, dispersion calculations for such releases may be particularly sensitive to mesoscale atmospheric phenomena needed to drive the dispersion model (Leelőssy et al., 2018) and precipitation (Hood et al., 2024).
Dedicated experiments or observations around continuous sources from tall stacks, such as power plants, could be another option for validation across distances beyond a few tens of kilometres. But again, such experiments usually run over a limited period of time or a number of

relatively short time intervals (Price et al., 2005; Snoun et al., 2023; Kooi et al., 2025b). Using these datasets to evaluate model estimates at longer timescale, one year for instance, as in the operational version of OPS, requires some form of gap filling or imputation. This in itself introduces uncertainty (Uusitalo et al., 2015). It must be concluded that datasets allowing evaluation of model performance for single sources at an annual timescale, as is required for models such as OPS, are quite rare (Kooi et al., 2025b).

### *2.4.4 Observation-based datasets of deposition for evaluation*

Most of the available measurements allow evaluation of concentration only (Perry et al., 2005; Kooi et al., 2025b). Datasets that are suitable for a direct evaluation of dry deposition are comparatively rare, due to the complexity of dry deposition measurements as well as to the modelling included in the measurement method (Walker et al., 2019; Hoogerbrugge et al., 2023). Many studies of dry deposition, which is the most important component of the total nitrogen deposition in the Netherlands (Hoogerbrugge et al., 2023), provide so-called inferential deposition fluxes. In other words, they are based on a model in combination with concentration observations (Flechard et al., 2011; Schrader and Brümmer, 2014). As a result, only a few datasets allow for evaluation of single-source contributions, at short distances and from a clearly distinguishable and well-defined source (Kooi et al., 2025b).
At distances beyond several tens of kilometres from the source, dry deposition due to a single source will be virtually indistinguishable from the background contributions. Similarly, while wet deposition measurements available in national observational networks are often used in model evaluation (e.g. Dore et al., 2015, Van der Swaluw et al., 2021), this quantity is affected by background concentrations over greater distances and considered unsuitable for the evaluation of single-source contributions.

### *2.4.5 Deployment of inert tracers*

Field studies have often been deploying releases of inert tracers such as $SF_6$, sometimes in combination with well-traceable gases such as $SO_2$ (Perry et al., 2005; U.S. EPA, 2023). Obviously, the characteristics of such gaseous species may be quite different from the modelled target substances, in our case, reduced and oxidised nitrogen components. In particular, the chemical conversion rates and characteristics determining dry and wet deposition will differ from those of nitrogen species. Furthermore, inert tracer releases are often aimed at evaluating modelled transport and dispersion characteristics only (e.g. Irwin and Hanna, 2005). It should also be noted that tracer release experiments usually run for very short – and intermittent – periods of time (Perry et al., 2005; Kooi et al., 2025b). Hence, such datasets are generally considered less suitable for full model evaluation studies, including deposition schemes.

### *2.4.6 Performance of Gaussian plume models*

The following, more general, patterns regarding the performance of Gaussian plume models emerge from the available reviews and a limited number of additional papers and reports.
Average annual concentrations within several tens of kilometres from the source can generally be predicted within a factor of 2 to 4, as long

as the terrain is flat (Miller and Hively, 1987). Although this deviation seems large, Chang and Hanna (2004) concluded that a 'good' model is able to produce predictions that are within a factor of 2 from the observations for at least 50% of the time, along with a relative mean bias within ± 30%, and a relative scatter up to about a factor of 2 to 3 (see Chang and Hanna, 2004, for a definition of these measures). Such measures are still being used and are still shown to be appropriate to evaluation of air quality models (e.g. Dore et al., 2015; Yang et al., 2020; Pandey et al., 2023). In this context, one should also realise that estimates of concentration and deposition with contributions from many sources, as in the case of nitrogen species in the Netherlands, are usually comparatively robust, because uncertainties due to single sources tend to cancel out (Duyzer and Erbrink, 2022; Hoogerbrugge et al., 2023).

For *ideal* conditions, *fully conform* Gaussian assumptions – homogeneous terrain and steady state meteorological conditions (one hour or less) and with near-neutral stability conditions – uncertainty is estimated at 10-20% at short distances for ground sources and up to about 10-50% for higher sources (Miller and Hiverly, 1987; Projectgroep Revisie Nationaal Model, 2002). The lower end of the range indicates annual averages, the higher end hourly numbers. Indeed, better performance is obtained with increasing averaging time (Projectgroep Revisie Nationaal Model, 2002; Snoun et al., 2023; Pandey et al., 2023). During sunny conditions with light to moderate wind speed, the uncertainty may increase to 20-50% for low sources and to 30-100% for elevated sources (Projectgroep Revisie Nationaal Model, 2002).

In general, Gaussian models tend to underestimate concentrations when the wind speed is low (Miller and Hiverly, 1987; Leelőssy et al., 2014). Very low wind speed conditions often coincide with extremely stable or unstable conditions (Stull, 1988; Garratt, 1992), which can lead to poor model performance as well (Miller and Hiverly, 1987; Leelőssy et al., 2014; Snoun et al, 2023).

Model performance decreases with increasing complexity of terrain and meteorological conditions, and also at great distances from the source. This is because basic assumptions underlying the Gaussian approach are violated in such conditions (Snoun et al., 2023). Special, more advanced, Gaussian approaches have been developed to deal with such complexity and also include other processes that are not described in simple Gaussian approaches (Leelőssy et al., 2014). Notable examples also applied in OPS are the trajectory approach that allows following the plume over greater distances, while taking into account effects of changing meteorological conditions, and parameterisation of the effect of turbulence in convective boundary layers (Sauter et al., 2023).

In Gaussian models, chemical conversions have usually been dealt with in a simplified way, as is the case for OPS. This becomes apparent when comparing results of Gaussian models to those of more complex grid-based Eulerian models at a national scale, using results from extensive observation networks. While the performance of Gaussian models with regard to concentrations of primary species is comparable to or sometimes better than for the more complex models, their estimates of secondary species are clearly worse (Dore et al., 2015; Van der Swaluw et al., 2017; Van der Swaluw et al., 2021). For single-source contributions, evaluating chemical conversion effects against observational evidence is considered impossible.

### 2.4.7 *Other evaluation methods*

Given the comparatively scarce possibilities to evaluate Gaussian plume models applied at single sources against observations, alternative approaches may be used as well. An overview of model uncertainty assessment in the context of decision support can be found in Uusitalo et al. (2015). Briefly, these authors distinguish:

- *Expert assessment*, using knowledge of experts to assess the quality and uncertainty in model results. Expert judgement may also be applied in combination with sensitivity analysis to assess the uncertainty in model input parameters.
- *Model sensitivity analysis*, in which case probable ranges of model output values are studied by means of an analysis of their response to changed values of model parameters or boundary conditions. There are many different approaches to conduct sensitivity analyses, varying from so-called one-factor-at-a-time analyses to Monte Carlo methods. If parameter uncertainties are specified and deployed by (random) propagation in the model, sensitivity, studies may be considered an uncertainty analysis (Norton, 2015). The method applied in our study and the one described in Abbot (2003) and Duyzer and Erbrink (2022) can be ranked in the category of Monte Carlo methods (see Chapter 3), providing a first estimate of model uncertainty.
- *Model emulation*, using a lower-order approximation of the full model allowing multiple approximate runs with varying parameter settings in a relatively short period of time.
- *Temporal or spatial variability in the deterministic models*, which uses model-predicted variability (spatial, temporal) to estimate variance, and hence uncertainty. This method can only be applied to grid models.
- *Multiple models*, in which uncertainty is assessed by intercomparing model outcomes from various, independent models, run for the same scenario in the same domain. Multiple-model ensembles are included in this category. One of the ways in which such ensembles have typically been used is for the evaluation of predictive uncertainty. Examining a multi-model ensemble is one of the methods applied in Kooi et al. (2025a,b) to study uncertainty in Gaussian plume models at a short distance from a source.
- *Data-based approaches,* which perform a statistical assessment of the uncertainty related to model outputs using large quantities of observations. This approach can also be used to estimate the parameter value probability distributions. It is applied in a complementary study on the development of an Uncertainty Analysis Tool (UAT) briefly touched upon in the present report (see Sections 3.6 and 4.5).

According to Uusitalo et al. (2015, quote), "the most fitting choice is always case-dependent, depending on the available models as well as the decision problem at hand." The methods must be considered complementary to *direct* comparison to observations and represent only one step in a full evaluation chain (Monteiro et al., 2018). They are valuable when observations are unavailable or cannot be used for direct comparison between model outcomes because of, for instance, diverging foci of the observational study and a model experiment.

# 3 Methodology

## 3.1 Description of parameters and uncertainty ranges

### *3.1.1 General*

In the present study, the estimate of uncertainty is based primarily on a model sensitivity analysis. The type of sensitivity study we perform here is an uncertainty assessment akin to a Monte Carlo-type analysis (Uusitalo et al., 2015; Norton, 2015). Default values of preselected model parameters are perturbed as follows. A perturbation factor is drawn randomly from a probability distribution describing the uncertainty in each of the parameters selected for perturbation (see Section 3.1.3). The idea is to choose the distribution in such a way, that the values of model parameters are varied within a predetermined realistic interval width around the default value; see Figure 3.1 for a schematic example. The parameter uncertainties are then propagated to estimate the model uncertainty. To this end, a base run (or reference run) is performed first, using the default values for all parameters. Next, five thousand model runs are performed with randomly perturbed values of each of the selected parameters. The outcomes from all model runs are then statistically analysed (see Section 3.5 for more details).

*Figure 3.1 Schematic example of a probability density function for the lognormal distribution (see Section 3.2.1) describing the uncertainty in a certain parameter. A $\theta$ value of 1 implies no change from the default value, smaller and larger values indicate a decrease and increase of the original parameter value, respectively. The spread determines the 'amount' of uncertainty.*

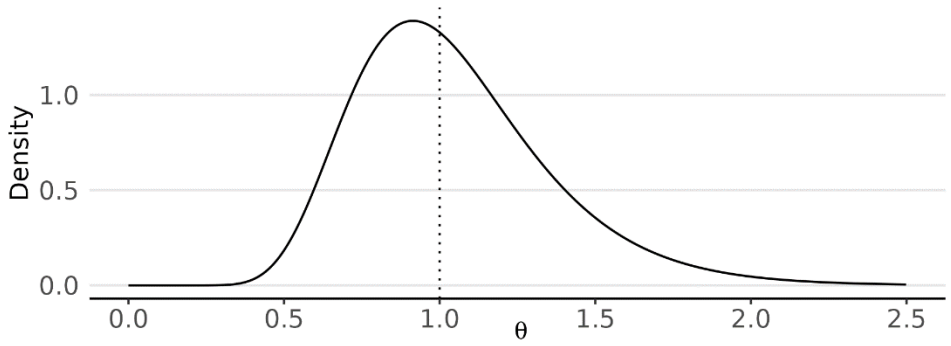


### *3.1.2 Outline of the modelled processes and underpinning of parameter selection*

The selection of parameters to be varied and the definition of their uncertainty distribution is a crucial step in the type of analysis performed here. An understanding of the various processes within the OPS model is required to be able to select a set of parameters that, together, cover the main aspects of model uncertainties. Given the goal of the study, we focus on parameters that are expected to have a major impact at the greater distances in particular. To this end, we first provide a short outline of the processes being modelled, briefly highlighting the role of the model parameters selected for variation in the sensitivity study. The selection was based on a combination of choices substantiated in scientific literature in previous sensitivity

studies, uncertainty analyses, and expert judgement in the context of the OPS modelling system. The description that follows also briefly motivates the selection of specific parameters.

*General aspects*
Figure 3.2 shows a schematic overview of the fate of the various nitrogen compounds in the atmosphere. Two groups of nitrogen compounds may be distinguished, being the oxidised nitrogen ($NO_y$) and the reduced nitrogen ($NH_x$). Both groups contain primary emitted compounds as well as compounds that are formed by atmospheric chemical reactions. Secondary components may be gaseous, or occur in aerosol form (secondary inorganic aerosols, SIA). Regarding *$NO_x$*, the main gaseous species are nitrogen oxides NO, $NO_2$ and $HNO_3$, and in SIA-form nitrate $NO_3^-$. For *$NH_x$*, the main gas is ammonia $NH_3$, and the main SIA is ammonium $NH_4^+$.

*Figure 3.2 Reactive nitrogen in the air. Left: the sources of reduced ($NH_3$, black) and oxidised ($NO_x$, grey) nitrogen used in this study, right: dry (yellow) and wet (blue) deposition.*

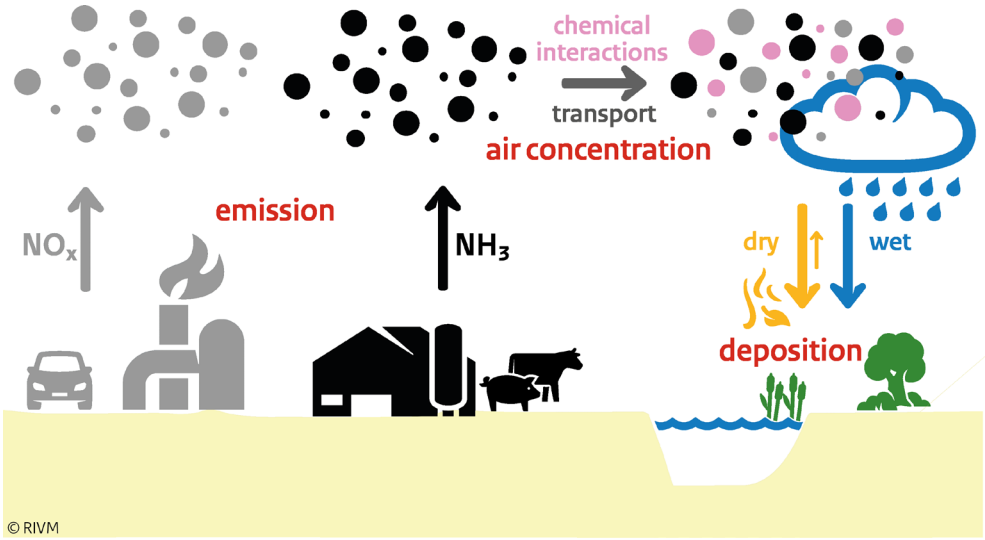


After emission into the air, the compounds are transported away from the source by the wind and dispersed (further diluted) under the influence of atmospheric turbulence. During transport, some of the emitted mass may 'disappear' from the atmosphere by chemical conversion and by deposition. In the context of Gaussian plume models, this 'disappearance' across the trajectory is called depletion. The resulting amount of a compound per unit volume of air is called the concentration.
For our purpose, it is convenient to consider the processes modelled by OPS as being grouped into the aforementioned three main stages of the fate of the compounds in the atmosphere: 1) emission; 2) transport and dispersion; 3) depletion. For each stage, characteristics and parameters are highlighted that are crucial to the modelling results and are subsequently selected for variation in the sensitivity study. The selection is further visualised in Figure 3.3, using the symbols referred to in the text.

Note that the emission strength is uncertain in practice. However in the context of the present study, emission may be considered a well-defined property. Also note that in our case, differences in OPS model outcomes are expected to scale linearly with differences in emission.

*Figure 3.3 A schematic overview of the parameters varied in the sensitivity analysis in OPS, see also Table 3.1. This includes 1. the initial plume rise ($\Delta h$) due to buoyancy (heat) or momentum (exit velocity) in case of the livestock farm and industrial stack; uncertainty in emission height in case of motorway, 2. meteorology (Meteo), 3. dry deposition velocity ($v_d$), 4. scavenging rate for either the below-cloud process washout ($\Lambda_w$) or the in-cloud process rainout ($\Lambda_r$) 5. chemical conversion rate ($k_{chem}$), 6. mixing layer height ($z_i$), 7. diurnal variation (indicated by the clock), and 8. vertical dispersion length ($\sigma_z$).*

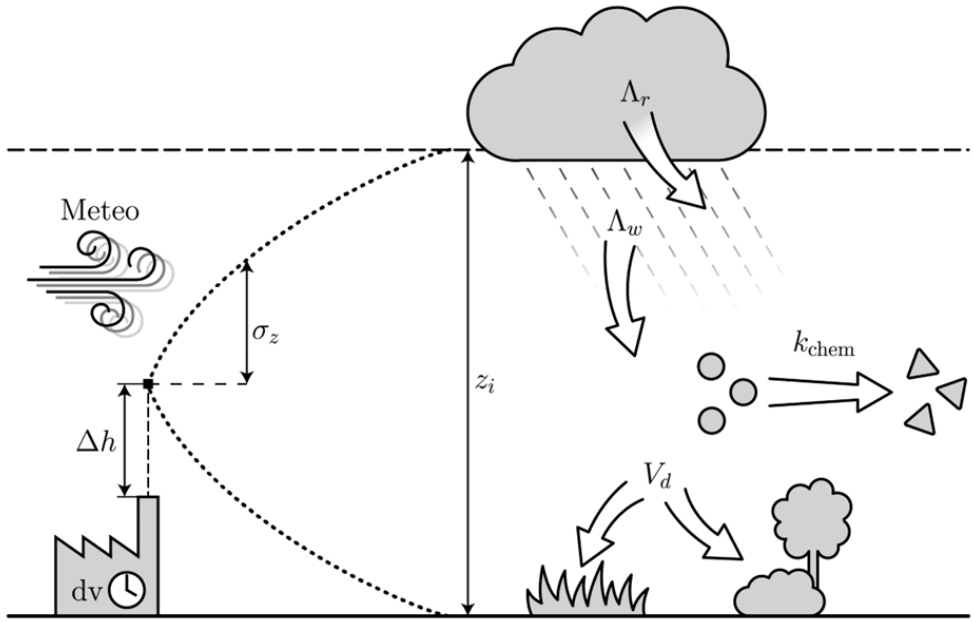


*1. Emission*

When the temperature of an emission exceeds the air temperature, or in the case of a mechanically forced exit velocity, the plume with emitted compounds initially rises relative to the height of the physical source height. This initial ***plume rise*** *($\Delta h$)* due to buoyancy or momentum, respectively, results in an elevated plume centre line. At these higher levels, wind speeds and directions may differ from the ones at the physical source height. This influences the plume dispersion and transport, and the distance from the source where the plume 'touches' the ground may increase. Moreover, the plume may penetrate the top of the mixing layer. As a result, a fraction of the mass may initially be emitted above the ***mixing height*** ($z_i$, sometimes also called 'boundary layer height') and hence has no, or less, influence on concentrations at the surface. This is especially relevant for high sources and/or high plume rise. The ***diurnal variation of the emissions*** (*dv*, symbolised in Figure 3.3 by means of the clock) influences the atmospheric concentrations, since the timing of the emission determines the degree of initial mixing of the plume. For instance, in more convective conditions (typically occurring during daytime in fair-weather summer

conditions), the plume will be more diluted upon emission than in stable conditions (typically occurring during the night) when there is not as much mixing.
All of the aforementioned characteristics and processes relating to emission imply a strong link with the ***weather conditions*** (Meteo). In some cases, this link is quite direct and obvious. For instance, plume rise due to buoyancy depends on air temperature. Variations of ammonia emission are influenced by temperature. In other cases, the link is less obvious. In the case of plume rise, for instance, the amount of material emitted above $z_i$ depends on conditions that determine $z_i$, which are, in turn, secondary meteorological variables (notably momentum transport, heat flux) depending on a set of primary meteorological variables (e.g. wind speed, solar radiation) in combination with land-surface properties (e.g. roughness).

*2. Transport and dispersion*
After emission, the compounds are transported away from the source in the direction of the mean wind. The wind speed strongly affects the volume of air into which a compound is emitted. Indeed, according to the Gaussian Plume Equation, the atmospheric concentration is inversely proportional to wind speed. During transport away from the source, further dilution in the atmosphere takes place due to turbulence. The latter process is described in terms of dispersion parameters, which describe the extent or size of the plume as a function of distance from the source. These are a measure for width and depth of the plume in horizontal (lateral) and vertical direction, respectively. In the operational long-term version of OPS used here, the lateral dispersion parameter is fixed to the width of the wind sector applied, that is, 30° (see also 3.1.3). Furthermore, dispersion along the wind direction can be neglected since its effect may be assumed to be much smaller than from transport by the wind along the wind direction. Hence, only the ***vertical dispersion length*** ($\sigma_z$) is relevant in the context of our sensitivity study. Particularly near the source, this parameter determines the development of the vertical extent of the plume. At greater distances, the plume may become well-mixed across the entire boundary layer. In this case, the vertical extent of the plume is determined by the ***mixing height*** ($z_i$), which can be considered as a vertical dispersion parameter at great distances. Higher values of $\sigma_z$ and $z_i$ imply a larger mixing volume and hence lower concentrations. Both parameters are related to the main mechanism of turbulence generation in the atmosphere and hence to atmospheric stability, as well as to the resulting intensity of the turbulence.
It is obvious that ***weather conditions*** (*Meteo*) fulfil a crucial role during transport and dispersion. This includes the role of primary weather variables, such as wind speed, solar radiation and temperature, as well as related secondary variables such as heat fluxes and friction velocity (momentum transport) and the stability conditions assessed from them. The impact of secondary meteorological variables also implies an intimate link between weather conditions and the characteristics of the Earth's surface. Hence, surface properties will affect the model outcomes as well. Wind speed and direction are used to compute the length and direction of the trajectory paths. Along with other meteorological variables, they determine the primary and secondary meteorological properties of the trajectory. Chemical

conversion rates ($k_{chem}$) and background concentrations are read from background maps at locations along the trajectory paths and averaged per trajectory. Thus, the properties relevant to the source-receptor-trajectory and the receptor itself are also influenced by wind speed and direction. Similarly, land use properties are determined along the paths using land use maps, from which a representative $v_d$ per trajectory is determined. Such primary and secondary properties directly influence transport, as well as dispersion and depletion, between a source and receptor.

3. Depletion

***Chemical conversion*** ($k_{chem}$) in the atmosphere may cause primary material to be converted into secondary material, resulting in a loss of primary species and production of secondary species. Concurrent effects on deposition of primary and secondary components will depend on their respective deposition velocities.

Deposition is the amount of compound taken up by the surface (plants, soil, water) per unit surface area (e.g. $m^2$ or ha) and per unit of time (e.g. a year). This process leads to a loss of primary as well as secondary components. Deposition strongly depends on the atmospheric concentration. Thus, the depletion effect caused by deposition provides an atmospheric negative feedback mechanism: more deposition across the trajectory implies more depletion, leading to lower concentrations, which in turn reduces deposition. Two mechanisms of deposition can be distinguished.

The first is dry deposition, which is sustained by turbulent transport in the atmosphere. Hence, it is influenced by ***meteorological conditions*** (Meteo) and surface properties. The impact of turbulent transport and surface characteristics on the dry deposition is modelled using a so-called ***dry deposition velocity*** ($v_d$). This $v_d$ determines how easily the compounds move through the air towards the Earth's surface and how easily they are subsequently absorbed by soil and plants or water. This depends not only on the physico-chemical properties of the compound, but also on interactions between Meteo, land use, aerodynamic surface roughness, soil and plant properties and plant responses. Parameter $v_d$ not only affects depletion and hence concentration over greater distances. It directly determines the computed dry deposition at a given location as well, including locations near the sources.

The second deposition mechanism is wet deposition, which is the process whereby the compounds are removed by means of precipitation. Here, a distinction is made between washout and rainout. Washout is important near pollutant sources, where there has been no interaction with clouds yet. Second, rainout, also called in-cloud wet scavenging, is related to the uptake of pollutants by precipitation formed within clouds, that is, during cloud formation. In the modelling approach of both processes a so-called ***scavenging rate*** ($\Lambda_w$ for washout, $\Lambda_r$ for rainout) plays a pivotal role. This is strongly related to a compound's solubility and vapor pressure, combined in the Henry coefficient. Larger solubility implies better (and faster) uptake by precipitation and hence more wet deposition and lower concentrations. Precipitation characteristics, such as its probability and intensity, also affect the efficiency of the uptake of the compounds. Hence, Meteo is crucial in this regard as well.

All depletion mechanisms are modelled using a so-called source depletion approach, in which the initial emission is modified in

accordance with the amount of removed mass. To this end, so-called depletion factors are being used, which are based on $k_{chem}$, $v_d$, $\Lambda_w$ and $\Lambda_r$ to a large extent.

### *3.1.3 Selected parameters and uncertainties*

The following Sections 3.1.4 - 3.1.11 provide more detail on the probability density functions of the specific parameter values. We apply the same distributions for reduced as for oxidised nitrogen.
Table 3.1 lists the parameters that were selected for perturbation in the present study and the subsequent error propagation. Also shown are the main sources of uncertainty information and the uncertainty distribution that was based on this information and actually used.
The selection of parameters has been briefly motivated in the previous section, considering the main characteristics of the modelled system of emission, dispersion and transport, and depletion of nitrogen compounds. As such, the selection was mainly based on expert judgement (cf. Duyzer and Erbrink, 2022; see also Uusitalo et al., 2015 for a general discussion of this method).
Practical considerations also influenced the selection. One important example is the lateral dispersion coefficient, which is fixed to 30° in the operational version of OPS applied here. Operational assessments of annual averages for multiple sources are expected to be not that sensitive to this choice, since errors will cancel out when multiple sources and long time periods are involved. However, this might be different for single sources, even when computing annual averages. Yet, we have to consider this a fixed model property of the operational OPS version, rather than a parameter. Changing the approach would require a considerable change of the OPS code as well as of the meteorological preprocessors, notably of METPRO (Sauter et al., 2023), and hence imply a strong deviation from the present model version. For this reason, the sensitivity to this parameter was not tested.
Another important example relates to the use of meteorological conditions. OPS currently applies the same meteorological dataset for construction of trajectories throughout the country. Thus, the trajectory path for a plume exiting a source in the East of the Netherlands is the same as the path for a plume exiting a source in the West. Only slight differences in meteorological statistics due to the differing origins of the paths are obtained. In reality, different trajectories will be followed due to varying wind speeds and directions as well as other meteorological conditions. Testing the sensitivity in OPS to the latter effect would imply a major adjustment in the code and is not included in the present study.
While the focus of the present study is on uncertainty at great distances from the source, some parameters that were expected to have a particularly large initial effect at short distances were chosen as well. This is because their initial effect may be strong enough to contribute significantly to the overall uncertainty at great distances. Such parameters tend to affect the mass balance close to the source. An example is plume rise, which may or may not lead to a significant portion of pollutant mass being ejected above the mixing layer (cf. Price et al., 2016). By contrast, we did not include parameters that are assessed to have a significant effect at short distances only. One example in this category is a parameter used to describe building effects on dispersion near the source. Effects of including buildings on results of

Gaussian Plume Models are examined in more detail in Kooi et al. (2025a).
Some of the selected parameters actually represent a set of parameters or even the outcome of an OPS sub-model rather than an isolated, single, model parameter. For example, mixing height $z_i$ is computed from a parameterisation requiring secondary meteorological variables, which in turn also require a modelling approach (see Sauter et al., 2023, for further information on these approaches). For OPS, this procedure is carried out in the meteorological preprocessor METPRO. For each distance class, the maximum value of $z_i$ encountered across that trajectory is stored in the meteorological statistics used as input in OPS. In the sensitivity analysis performed here, we vary each maximum $z_i$ value read in OPS by multiplication by the same perturbation factor (see Section 3.1.7). Along a similar line, meteorological conditions required to run OPS actually are model input data, rather than a parameter.
The type of sensitivity study chosen here requires good coverage of the entire parameter space for each disturbed parameter. To this end, the uncertainty range per parameter must be sufficiently captured, for all individual parameters as well as for the entire parameter set. Typical probability distributions of parameter values were derived from reports in scientific literature or from freely available large datasets, or a combination of these. In some cases, assessments were based on expert judgement.

*Table 3.1 Summary of model parameters considered in the present sensitivity study and their uncertainty probability distribution. See Section 3.2 for more information on the GeoSD and conversion between normal and lognormal distributions. Note that for $v_d$, $\Lambda_w$ and $\Lambda_r$ parameter values are varied separately for primary and secondary components, but their uncertainty distribution is assumed to be the same.*

| | **Parameter** | **Initial uncertainty information** | **Remarks on method and/or source** | **Resulting probability distribution** |
|---|---|---|---|---|
| 1 | $\Delta h$: plume rise (livestock farm and industrial stack), source height (road source) | lognormal distribution GeoSD = 1.35 | Source: Irwin and Hanna (2005) | lognormal with μ = 0 and s = ln(GeoSD) = 0.30 |
| 2 | *dv*: diurnal variation of emissions | None | Source: Expert judgement (internal discussions) | Amplitude scaling, depending on particular diurnal emission variation profile and adjusting the slope of the temperature correction; see Section 3.1.5. |
| 3 | $\sigma_z$: vertical dispersion length | lognormal distribution with GeoSD = 1.35 | Source: Irwin and Hanna (2005). Value for 'random bias', determined from measurements in the | lognormal with μ = 0 and s = 0.30 |

| | Parameter | Initial uncertainty information | Remarks on method and/or source | Resulting probability distribution |
|---|---|---|---|---|
| | | | vicinity of (inert tracer) sources. | |
| 4 | $z_i$: mixing layer height | normal distribution with standard deviation 25% | Sources:<br>• Analysis of ERA5 ensemble (cds.climate.copernicus.eu): 95% of the hours the ensemble standard deviation is 25% or less.<br>• Review by Reen et al. (2014): uncertainties between 13% and 40%, typical value 20%. | lognormal with μ = 0 and s = 0.24 |
| 5 | $k_{chem}$: chemical conversion Rate | lognormal distribution with standard deviation corresponding to 40% at a standard normal distribution. | From comparison of $NH_4^+$ concentrations from OPS to measurements (3 sites, 6 years (2015-2021)), assuming that differences are due to errors in chemical conversion rate | lognormal with μ = 0 and s = 0.36 |
| 6 | $v_d$: deposition velocity | normal distribution with standard deviation 70% of the mean. | Source: review by Schrader and Brümmer (2014) for $NH_3$. Selection of observations covering 4 seasons, land use "agriculture" and "other nature" | lognormal with μ = 0 and s = 0.55 |
| 7 | $\Lambda_w$, $\Lambda_r$: scavenging rate for washout and rainout respectively | normal distribution with standard deviation at 273K is ~40% of the mean | Source: compilation of Henry coefficient for $NH_3$ by Sander (2023). | lognormal with μ = 0 and s = 0.36 |
| 8 | Meteo: meteorological region | discrete, drawn from 7 sets: 1 based on the national average of all KNMI stations used in OPS; 6 based on data from one representative KNMI station per region | Year: 2015. Considered a normal year regarding precipitation, air temperature, wind speed and radiation (see https:/www.knmi.nl/climate dashboard) | discrete, uniform, n = 7 |

For parameters of which the uncertainty can be described using a continuous probability distribution we decided to apply a lognormal distribution (Figure 3.1). The main advantage over a normal distribution is that unrealistic negative numbers are avoided. Uncertainty information initially described by a normal distribution was translated into a lognormal one (see Section 3.2.1). For disturbance of diurnal variation of emissions (*dv*) a special procedure was followed, which is further described in Sections 3.1.5 and 3.2.2. Furthermore, the choice of the meteorological conditions ('Meteorological region' or 'Meteo') was based on a random selection from a homogeneous discrete distribution, as explained in Section 3.1.11. The following Sections 3.1.4-3.1.11 provide more detail on the probability density functions of the specific parameter values. We apply the same distributions for reduced as well as oxidised nitrogen.

### *3.1.4 Plume rise or emission height, $\Delta h$*

Gaussian models have been shown to be sensitive to plume rise (Miller and Hiverly, 1987; Clegg, 2006; Price et al. 2016). This is a highly parameterised process in most models (e.g. Olesen et al., 2007; Price et al., 2016; Sauter et al., 2023), requiring heat content and/or emission velocity, temperature, exit diameter and the effluents' density along with specification of atmospheric conditions at the exit height (Snoun et al., 2023). Estimates of plume rise come with considerable uncertainty. To estimate this uncertainty, we follow Irwin and Hanna (2005), who reviewed earlier uncertainty estimates of plume rise. Their final estimate of the uncertainty distribution of plume rise is applied (see Table 3.1), irrespective of whether plume rise is due to buoyancy or momentum of the effluent. That is, only the final plume rise estimate by OPS is perturbed. The perturbed plume rise may subsequently affect the inversion penetration and detrained fraction of the pollutant (Sauter et al., 2023). Note that the fraction of mass initially emitted above the boundary layer height, may enter the boundary layer at a greater distance from the source due to entrainment: the process where air above the boundary layer is mixed into the mixing layer due to a growing boundary layer height.
Perturbation of plume rise is applied to both the high and low point source. To the line source, mimicking a road, this method cannot be applied. No plume rise is computed in this case, due to lack of buoyancy or momentum as a source characteristic. Instead, the source height is considered an uncertain parameter in this case. Since source height and plume rise are somewhat akin (plume rise + physical source height = effective source height), we decided to perturb the source height of road emissions using the uncertainty distributions applied to plume rise.

### *3.1.5 Diurnal variation, dv*

OPS uses a yearly averaged emission strength as input. In reality, however, most emissions are not constant in time. For instance, the traffic intensity is higher at the start and the end of the workday than during the night and around noon; $NO_x$ emissions increase and decrease accordingly. In OPS, the yearly averaged emission strength is multiplied by so-called emission correction factors to account for such effects.
OPS uses a statistical description of meteorological conditions, in which weather conditions are divided into a number of classes in advance. It cannot simulate temporal variations per se. This precludes application of

diurnal variations in the literal sense. However, when deriving the meteorological statistics for OPS, the hours included in each meteorological class are kept track of, determined by wind direction and stability (Sauter et al., 2023). This allows for emission correction factors to be linked to specific meteorological conditions and to become part of the meteorological statistics used in OPS. As an example for traffic: classes associated with higher numbers of nighttime hours will have a lower emission correction factor, that is, nighttime emissions are implicitly reduced.
In OPS, fixed, specific daily sets of emission correction factors can be used for some emission categories, for example, to specify the diurnal variation of emissions due to traffic emissions. In such cases, diurnal variation of the emissions correction factors is provided in twelve two-hour blocks. In another group of emissions, the correction factors are linked to the weather conditions. An important example in the context of the present study are ammonia emissions from livestock farm systems, which are linked to air temperature (Sauter et al., 2023).
To our knowledge, no information is available in scientific literature on uncertainty in the diurnal variation of emissions for application in uncertainty assessments. After ample discussion and intermediate applicability tests, we decided to proceed as follows.
Typically, the diurnal variation of emissions, and hence of emission factors, approximately takes the form of a sinusoid, with more emissions during the day and fewer during the night. By scaling this sinusoid, we can examine the effect of the distribution's amplitude. We note that in the case of motorway emissions, maxima occur around specific times of the day, but in spite of this, the same scaling method can be applied to this source category. In all cases, special care must be taken to avoid implicit scaling of emission strength instead of just its diurnal variation. Furthermore, emissions may not become negative. We also do not allow the sinusoid to be inverted, causing the sinusoid to flip. This is further described in Section 3.2.2. For the emissions from the livestock farm, the emission correction factor is additionally linked to a temperature effect. Perturbation of this temperature effect is also described in Section 3.2.2.

### *3.1.6 Vertical dispersion length, $\sigma_z$*

The vertical dispersion length $\sigma_z$ (m) is the standard deviation of the concentration distribution of the Gaussian plume in the vertical direction at a given distance from the source. As such, it is a measure for the depth of the plume starting from the plume's axis. Its value depends on the atmospheric conditions, as influenced by the weather conditions, and the plume height. This parameter is expected to play an important role close to the source in particular, where it determines the modelled dilution of the compound in the atmosphere, the location where the plume reaches the ground and the top of the mixing layer (atmospheric boundary layer). Therefore, it may also affect the distribution of mass among atmospheric layers over distance, and hence the results of the simulations at greater distances from the source.
Irwin and Hanna (2005) reviewed results of various dispersion experiments using inert tracers. They also consulted experts to judge the uncertainty in this parameter. It was concluded that the uncertainty in $\sigma_z$ may be characterised by means of a lognormal distribution, with a

GeoSD of 1.35. This means that roughly 95% of samples fall within a factor of 1.82 around the median value.

### 3.1.7 *Mixing layer height, $z_i$*

It has long been recognised that consideration of atmospheric boundary layer properties is crucial for modelling and interpretating dispersion and deposition of air pollution. Mixing layer height $z_i$, is an important parameter in dispersion models (e.g. Gryning et al., 1987). Higher $z_i$ leads to lower concentrations and vice versa, particularly at greater distances from the source. This affects deposition as well. Unfortunately, assessment of $z_i$ introduces quite some uncertainty, due to measurement issues and the many different diagnosis tools and model-based approaches (Seibert et al., 2000). Complex land surface – atmosphere interactions render linking $z_i$ to local, station-based observations, as is done in the meteorological preprocessor of OPS, an extremely difficult task (Beamesderfer et al., 2024).
Reen et al. (2014) reviewed uncertainties reported (on the basis of modelling or comparison to observations) or assumed (expert judgement) in scientific literature. They found uncertainties to range between 13% and 40% of the mean, with a typical value of 20%. Some studies report a tendency towards (much) larger uncertainties during nighttime (stable) conditions (e.g. Han et al. 2008). Duyzer and Erbrink (2022) assumed an uncertainty of 20% during daytime (unstable or neutral) conditions, but 50% during nighttime conditions. Here, we complemented these earlier assessments of $z_i$ uncertainty, using boundary layer heights from the ERA5 reanalysis (Hersbach et al., 2020), with a focus on the Netherlands. Our analysis is based on an 8-year timeseries of ensemble $z_i$ values, at 3 and 12 UTC. The results suggest that about 95% of the values of the coefficient of variation (CV; standard deviation divided by the mean) from the ensemble was within 0.25, but without a clear distinction between nighttime and daytime conditions (see Appendix 1 for more information).
On the basis of the review by Reen et al. (2014) and considering the results of the ERA5 data analyses, we decided to assume a standard deviation of $z_i$ of 25% of the mean, which translates into a lognormal error distribution with m=0 and s=0.24. At the present stage of development, we ignore possible differences between stable and unstable or neutral conditions for simplicity.

### 3.1.8 *Chemical conversion rate, $k_{chem}$*

Chemical conversion rate $k_{chem}$ will affect conversion of primary material into secondary material, resulting in a loss of primary species and a production of secondary species. Concurrent effects on deposition of primary and secondary components will depend on their respective deposition velocities.
At present, chemical conversion rates used by OPS are derived from calculations with the EMEP model (Simpson et al., 2012). For primary components, the total amount of mass in the mixed layer converted during a year according to EMEP, is compared to the total input due to the emissions. From this mass budget, a spatially explicit field of annual conversion rates is derived (Sauter et al., 2023).
The conversion rates evaluated from the EMEP calculations depend upon a combination of meteorological conditions and source strengths, and on distributions of various components that drive the chemical conversion

processes. To the best of our knowledge, information on the uncertainty in the rates derived in the aforementioned way is not available. Hence, instead of imposing a generic uncertainty range, we proceed as follows. Observations of $NH_4^+$ concentrations during six years (2015-2021) at three locations in the Netherlands are compared to the concentrations computed with OPS. We assume that the differences between the computed and observed concentrations represent the uncertainty in the chemical conversion rate. This is expected to be an overestimation, since the differences will also be affected by other processes. However, we consider this estimate a reasonable first guess for the *a priori* uncertainty range we need in the present study. We also assume that a similar uncertainty applies to conversion rates of $NO_x$.
The analysis of deviations between modelled and observed $NH_4^+$ concentrations suggests a standard deviation of the residuals of ~40% of the mean observed value. Hence, we use a lognormal error distribution with μ=0 and s=0.36. See Appendix 2 for further details.

### 3.1.9 *Deposition velocity, $v_d$*

A significant amount of pollutant mass may be removed from the atmosphere by dry deposition. Hence, dry deposition can have a strong impact on concentration. In most air quality models, dry deposition is computed as the product of deposition velocity, $v_d$, and concentration, $C$. Both should be evaluated at the same height in the atmosphere. This approach is also applied in OPS. However, we note that OPS uses a so-called effective $v_d$ in the case of $NH_3$. The effective $v_d$ takes into account the effect of non-zero concentrations at the surface (compensation concentration, also called compensation point; Wichink Kruit et al., 2010; Van Zanten et al., 2010). As such, a compensation point reduces deposition and, in some conditions, leads to re-emission instead of to deposition (Massad et al., 2010). This distinction is not an issue in the present study.
The uncertainty in $v_d$ is known to be considerable. Schrader and Brümmer (2014) reviewed $v_d$ data for ammonia and for various land use types. We analysed their collection of $v_d$ values for land use categories "agriculture" and "other nature", only including datasets in which estimates for four seasons per year were available. We also included observations from the so-called COTAG sites, run by RIVM, at which dry deposition is measured and from which $v_d$ can be obtained (Rutledge-Jonker et al., 2023). The coefficient of variation (CV; standard deviation divided by the mean) from this (extended) dataset was found to be 70%, which translates into a lognormal uncertainty distribution with μ=0 and s=0.55 (see also Section 3.2.1). The reader is referred to Hoogerbrugge et al. (2023) for further information.
We note that the aforementioned uncertainty also includes uncertainties due to the compensation point of $NH_3$: the measurement data listed by Schrader and Brümmer (2014) as well as the data from the COTAG sites are based on net exchange of ammonia. Therefore, the measurements implicitly include possible effects of the compensation point. The uncertainty estimate also contains uncertainty in measurement setup, for example, due to unspecified height. However, a possible overestimation of the $v_d$ uncertainty is not a problem for the *a priori* uncertainty estimate intended here, since this should simply provide a wide enough, though realistic, range of parameter values to examine maximum uncertainty ranges. Upon examining possible physically

unrealistic outcomes for some parameter combinations, uncertainty ranges may be reduced to result in *a posteriori* estimates. We apply the perturbation of $v_d$ to both $NH_3$ and $NO_x$, as well as to $v_d$ of secondary products such as $NH_4^+$ and $HNO_3$ / $NO_3^-$ aerosols.
In the present approach, removal by dry deposition over a trajectory is implemented in terms of a depletion factor, which depends on the average $v_d$ over the trajectory (Sauter et al., 2023). A distinction is made between the well mixed phase of the plume and the phase where the plume is not yet well mixed. The disturbance is applied directly to the deposition velocity calculated separately for each phase. OPS takes into account the effects of dry deposition on the atmospheric concentration profile (Sauter et al., 2023). Such effects are related to interactions between the dry deposition rate of the compound and the shape of the concentration profile. This is because faster uptake leads to steeper profiles and vice versa. However, for the time being, we ignore possible effects of the *perturbed* depletion on this profile adjustment. Thus, we implicitly assume that the relative perturbation of $v_d$ is the same at all heights in the atmospheric surface layer and in all phases of plume development. This is considered a reasonable approximation because we expect the largest part of the uncertainty in $v_d$ to be related to uncertainty in the height-independent surface resistance.
So far, we only considered effects of $v_d$-perturbation on the depletion across the trajectory path. However, dry deposition has to be assessed locally as well, that is, at the receptor points defined in this study. For practical reasons, we decided to obtain an estimate of disturbed deposition at the receptor points that is consistent with the perturbation of $v_d$ (separately for the primary and secondary material) over the trajectories, in a post-processing step (i.e. after the simulations have been finished). This method assumes that local changes in deposition do not affect local atmospheric concentrations and that the concentration at the receptor point includes depletion in the trajectories. Ignoring effects on the local concentration profile, an estimate of the local, perturbed deposition can then be obtained by multiplication of the annual effective dry deposition calculated using OPS (which includes the perturbed source depletion) with the $v_d$ perturbation factor applied in the trajectories (see the online Appendix document, 2025-0081-appendix). This method assures consistency of the $v_d$ uncertainty assessment for specified land use types and between great distances and local estimates. Another option would be to choose differing perturbation factors at the receptor and over the trajectory, as was the case in Duyzer and Erbrink (2022). The problem whether or not to choose a different disturbance between the local and trajectory $v_d$ is somewhat akin to the one of $v_d$ disturbances that may differ among patches in heterogeneous landscapes. Implications of such differences for our uncertainty estimates will be assessed later (see discussion in Chapter 5 and Appendix 3).

### 3.1.10 *Scavenging rates, $\Lambda_w$ and $\Lambda_r$*

In accordance with the description in Section 3.1.2, OPS distinguishes two wet scavenging processes, washout and rainout. Washout describes removal by falling precipitation below the cloud's baseline. This can be relatively important near pollutant sources, where there has been no interaction of the pollutants with clouds yet. There are some indications based on measurements that washout may have been underestimated

until now (Yao et al., 2024). Rainout describes the uptake of pollutant by precipitation being formed within clouds. This process is thought to contribute most to the total wet deposition and has an effect on depletion and deposition at greater distances in particular (Hales, 1978). Wet scavenging is the result of a set of complex micro-physical interactions. However, in most commonly used air-quality models, simple parameterisations are applied to reduce the computational burden (e.g. Gong et al., 2011; Vivanco et al., 2017). OPS relies on a form of the so-called scavenging rates $\Lambda_w$ and $\Lambda_r$ for washout and rainout, respectively. Computational details of these coefficients may depend on the species (Sauter et al., 2023). We consider $\Lambda_{w,pri}$ and $\Lambda_{r,pri}$ for primary components and $\Lambda_{w,sec}$ and $\Lambda_{r,sec}$ for secondary components, respectively. For readability we maintain $\Lambda_w$ and $\Lambda_r$ where the distinction is irrelevant, and the *treatment* of these parameters is the same.
In order to derive an uncertainty distribution for $\Lambda_w$ and $\Lambda_r$, we acknowledge that the distribution of a substance over water and air plays a pivotal role in both $\Lambda_w$ and $\Lambda_r$. In this context, the Henry coefficient $K_h$ governs air-water exchange and the distribution of mass of the two media to a large extent. Hence, we decided to base the uncertainty distribution for $\Lambda_w$ and $\Lambda_r$ on the uncertainty in $K_h$ for ammonia. The uncertainty distribution of $K_h$ was derived from a compilation of $K_h$ values published in scientific literature (Sander, 2023). The value of the coefficient appears to be quite uncertain, due to uncertainty in both solubility and vapor pressure. There is also uncertainty in the temperature dependence of $K_h$. Computing the average and standard deviation from the compilation, using reports that include temperature dependence, leads to a coefficient of variation of almost 40% at 273 K. Furthermore, we ignore possible temperature effects on the derived *uncertainty* and assume a lognormal uncertainty distribution. This distribution can then be described as μ =0 and s=0.39. This distribution is also considered appropriate to $NO_x$. For example, from the compilation by Sander (2023), one can derive a CV (standard deviation divided by the mean) for $NO_2$ of 45% at 273 K. Note that $K_h$ values for $NO_x$ are much smaller than for $NH_3$. Likewise, the same uncertainty is assumed for the secondary species.

### *3.1.11 Meteorological conditions, Meteo*

It may be obvious from Section 3.1.2 that specification of the meteorological conditions (Meteo) to be used in OPS is crucial. Meteo affects many parameter values and is used to establish the properties of the simulated trajectories, including their direction and length. In the present context, it is thus essential to assess effects of uncertainty in Meteo. We note that variation of Meteo will also lead to variation in values of that were selected for perturbation in the present study. However, we consider meteorological uncertainty an independent source of uncertainty. As will be explained next, assessment of sensitivity of OPS to Meteo is not a trivial task.
The meteorological input used by OPS actually represents statistical properties of meteorological conditions, derived in a meteorological preprocessor. These statistics are offered for so-called meteorological regions or districts (Sauter et al., 2023). In OPS, meteorological information must be available in some spatial detail. To this end, six meteorological regions (1-6) are distinguished, mainly on the basis of the average wind speed regime over the Netherlands. In each district,

the meteorological conditions used in OPS are derived from measurements performed at automatic weather stations run by the Royal Netherlands Meteorological Institute (KNMI). A pre-processor is used to derive from these measurements the average meteorological conditions per district (Regions 1-6) and for the Netherlands as a whole (called 'Region 0'). Regional output includes hourly solar radiation, air temperature and relative humidity, duration of precipitation, wind speed and direction averaged over the districts, as well as daily values of the intensity and length of rainfall events. In a second pre-processor, these results are used to derive important secondary variables such as mixing layer height and friction velocity. Per region, statistical properties regarding both primary and secondary weather conditions are derived for each of the meteorological classes distinguished in OPS. National averages ('Region 0') are used to construct the trajectories from wind speed and direction, including the trajectory characteristics in terms of primary and secondary meteorological variables. This is carried out using the METPRO preprocessor. During an OPS run, local meteorological conditions for sources and receptors are determined on the basis of their location and an interpolation of meteorological data from the three nearest regions or on the basis of a single regional set. Furthermore, the origins of the trajectories and the corresponding properties are determined. Recall that OPS currently applies the same meteorological dataset for construction of trajectories throughout the country, so that slight differences in meteorological statistics are obtained due to the differing origins of the paths. For more detailed information on the use of meteorological data the reader is referred to Sauter et al. (2023).

When testing uncertainty due to Meteo, variation of one single specific meteorological variable should be avoided since this may lead to inconsistencies in Meteo within or between the regions. Therefore, we chose to vary meteorological datasets as a whole. Furthermore, we consider the main uncertainty to be related to the spatial distribution of the weather conditions, for instance, country average versus regional, or coastal regions versus inland regions. In the present operational setup of OPS, the same national averages of temperature, humidity and global radiation are applied to each region because regional deviations are assumed to have a small impact on the model outcome only (Sauter et al., 2023). Also, national averages of wind speed and direction are used to construct the trajectory paths. This strongly reduces the differences between Meteo in different regions, and therefore, spatial differences between regions are expected to be underestimated. Hence, we decided to proceed as follows.

For each region, one representative KNMI weather station was selected. Note that at present, some regions are covered by one station only. Then, measurements from the selected station were assumed to represent the weather conditions of the entire Netherlands. For example, the weather conditions observed in Maastricht also apply to Groningen, Vlissingen, etcetera. See Table 3.2 for the list of weather stations used to define meteorological conditions for the sensitivity runs.

*Table 3.2 Stations used to describe meteorological conditions in sensitivity runs.*

| Standard OPS region | Selected KNMI station | WMO number |
|---|---|---|
| I | Leeuwarden | 06270 |
| II | Rotterdam | 06344 |
| III | Twenthe | 06290 |
| IV | Vlissingen | 06310 |
| V | De Bilt | 06260 |
| VI | Maastricht | 06380 |

Measurements from the selected weather stations (year 2015) were processed by the meteorological pre-processors as if they would be used operationally. This resulted in six new meteorological data sets, each containing Meteo for 7 districts (0-6), as before. Within each new set, largely the same Meteo information applies to all individual regions. Despite using data from one station only, small differences remain due to correction of wind speed for regional roughness length and the related spatial interpolation, averaging of trajectory properties, and subsequent classification of weather conditions. However, the differences between the new datasets will be comparatively large. For the sake of completeness, we mention that background maps of concentration and chemical conversion rates are left unchanged. These are generated at a European scale, using simulations with a mesoscale weather model. As such, they are nearly independent of specific weather observations in the Netherlands.
In addition to these single station-related new Meteo sets, the standard OPS set was retained and used to define our reference situation. Thus, we have seven Meteo sets in total. During the sensitivity runs, one of the seven Meteo sets was randomly selected. Of the selected set, always the meteorological conditions for district 0, i.e. the national averages, are prescribed in the present sensitivity analysis. The use of these single station-related new Meteo sets is expected to lead to an estimate of the maximum uncertainty due to spatial patterns of Meteo within the Netherlands, unaccounted for in OPS until now. Note that this does still not fully appreciate uncertainty due to the fact that the construction of the trajectories is at present independent of the location within the Netherlands (for example, the wind speed and direction used to set up the trajectories is exactly the same in Groningen and Maastricht). The present model set-up precludes assessment of uncertainty due to this choice.

## 3.2 Sampling procedure

Model parameters are sampled from probability distributions on the basis of the uncertainties given in Table 3.1. Analyses such as the Sobol' index analysis, described in Section 3.5, require the parameters to be drawn from a uniform distribution across the range [-1, 1]. However, this interval does not reflect our prior knowledge about the uncertainty in the parameters. To properly express this knowledge, the uniformly sampled values are transformed to their respective distributions using the inverse transform sampling method. This method uses the inverse of the corresponding cumulative probability distribution function to transform a sample from the uniform distribution to a distribution of our choice, as is illustrated in Figure 3.4. Using this technique, all relevant

parameters are transformed to their respective probability distribution. Some of these distributions require additional parameters to determine their shape and, consequently, the uncertainty they represent. These distributions and their parameters are described below.
For completeness we mention that the *Meteo* parameter is not scaled, but randomly drawn from one of the seven prescribed meteorological data sets (described in Section 3.1.11).

*Figure 3.4 An example of inverse transform sampling. (a) A sample from the uniform distribution is transformed using the inverse of the cumulative density function of the desired distribution. (b) Transforming a regular sequence of points shows how the density of the sampled points changes. (c) A density estimate of the transformed samples reveals the probability density function of the desired distribution.*

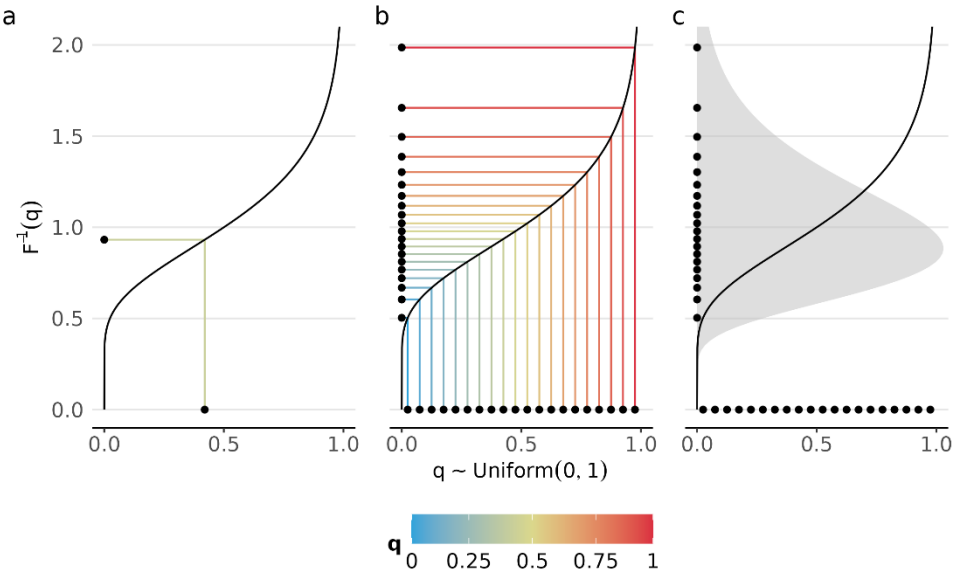


### 3.2.1 *Lognormal scaling factors*

Since the variables/processes (parameters) outlined in Table 3.1 are not allowed to become negative, most parameters for this sensitivity analysis are perturbed using non-negative scaling factors. This makes using the lognormal distribution a natural choice as it only supports positive values. The lognormal distribution, with probability density function

$$p(X = x) = \frac{1}{x\sigma\sqrt{2\pi}} \exp\left(-\frac{(\ln x - \mu)^2}{2\sigma^2}\right),$$

is described by two parameters, $\mu$ and $\sigma$, that control the location and spread, respectively.
Since we make no assumptions about whether the current parameter values in OPS ought to be moved in any particular direction, we fix the median of the distribution at a value of $m = 1$. This choice is applied to each parameter distribution wherever applicable. Only Meteo, being a categorical variable, has no definition of the median. For the lognormal distribution, the median is defined as $\mu = \ln(\mathrm{m}) = 0$.

The spread parameter, $\sigma$, represents the uncertainty in our parameter and is therefore derived from either the standard deviation $s$ or the *geometric* standard deviation $s^* = exp(\sigma)$ (the *geometric* standard deviation, *GeoSD*, is a measure of the extent to which data points are spread out from the geometric mean). As the latter is defined in terms of $\sigma$ already, it is more easily interpretable as a spread parameter. When the standard deviation $s$ is given, we can use the definition of the variance of a lognormally distributed random variable $X$ to find the value of $\sigma$:

$$s^2 = \mathrm{Var}(X) = [exp(\sigma^2) - 1]\, exp(2\mu + \sigma^2)$$

As we have already defined $\mu = 0$, the expression can be simplified to a second-degree polynomial in $exp(\sigma^2)$ and be solved accordingly:

$$0 = exp(\sigma^2)^2 - exp(\sigma^2) - s^2$$

$$exp(\sigma^2) = \frac{1}{2} + \frac{1}{2}\sqrt{1 + 4s^2}$$

$$\sigma = \sqrt{ln\left(\frac{1}{2} + \frac{1}{2}\sqrt{1 + 4s^2}\right)}$$

This approach ensures that samples generated by the lognormal distribution have a (geometric) standard deviation that reflects the uncertainties as described in Table 3.1.

### *3.2.2 Diurnal variation scaling*

The diurnal variation is a distribution of emissions over a single day for a particular source type. Twelve emission weights, each representing a two-hour block, are provided for each source type. Typically, this distribution roughly resembles a sinusoid, with more emissions during the day – or specific times of day in the case of motorway emissions – and fewer during the night. By scaling this sinusoid, we can examine the effect of the distribution. However, some care must be taken during this scaling. For example, summing up the twelve two-hour emission weights of a given diurnal variation distribution yields a constant value representing 100% emission over the course of a day. Scaling these contributions uniformly or individually would lead to this sum deviating from 100%, thereby effectively scaling the emission strength of the source.

To retain the normalisation property, we subtract the average weight $\overline{w} = \frac{1}{N}\sum_{n=1}^{N} w_n$ — with $N$ the number of two-hour blocks in a day — from each individual weight $w_n$ before scaling and finally adding the average back by the same amount afterwards. Formally, a diurnal weight $w_n \in \{w_1, w_2, \cdots, w_N\}$, is perturbed by a scaling factor $\phi$ resulting in the perturbed individual weight $\widehat{w}_n$:

$$\widehat{w}_n \equiv \phi(w_n - \overline{w}) + \overline{w}.$$

However, an unbounded scaling factor applied this way runs the risk of producing negative weights. Since we do not intend to model negative emissions, the scaling factor $\phi$ must be constrained to the interval:

$\left[\frac{\bar{w}}{\bar{w}-w_+}, \frac{\bar{w}}{\bar{w}-w_-}\right]$, where $w_+$ and $w_-$ are the largest and smallest weights available among all two-hour blocks of a given diurnal distribution, respectively. Under most circumstances, as the scaling factor moves towards its lower bound, the amplitude of the diurnal variation would be inverted, causing the sinusoid to flip. To prevent this, the lower bound of the scaling factor is further constrained to 0, resulting in the asymmetric interval: $\phi \in \left[0, \frac{\bar{w}}{\bar{w}-w_-}\right] = [0, \phi_{\max}]$.

To perform sensitivity analyses, it is again necessary to express the parameter uncertainty over the bounded scaling factor $\phi$. Since this parameter has both lower and upper bounds (to prevent a sinusoid flip and negative emissions, respectively), we require a distribution that reflects this property as well as characteristics featuring in other parameters, such as being able to keep the median fixed at a factor of 1. To this end, we constructed a linear piecewise probability density function. The function is composed of two right-angled triangles, one representing the probability over values in the interval 0 up to 1, the other representing values from 1 up to $\phi_{\max}$. Both triangles have the same area, ensuring that the probabilities of drawing a scaling factor below or above 1 are equal – in other words, setting the median at 1. Figure 3.5 shows the resulting piecewise probability density function. Due to its simple formulation, the inverse of the cumulative density function – which is required for transforming the samples to the desired distribution – is simply a piecewise second-degree polynomial.

*Figure 3.5 Piecewise linear probability density function used to model the uncertainty in the diurnal variation scaling factor. Note that the slope of the rightmost segment depends on the difference between 1 and $\phi_{\max}$ to preserve the total area.*

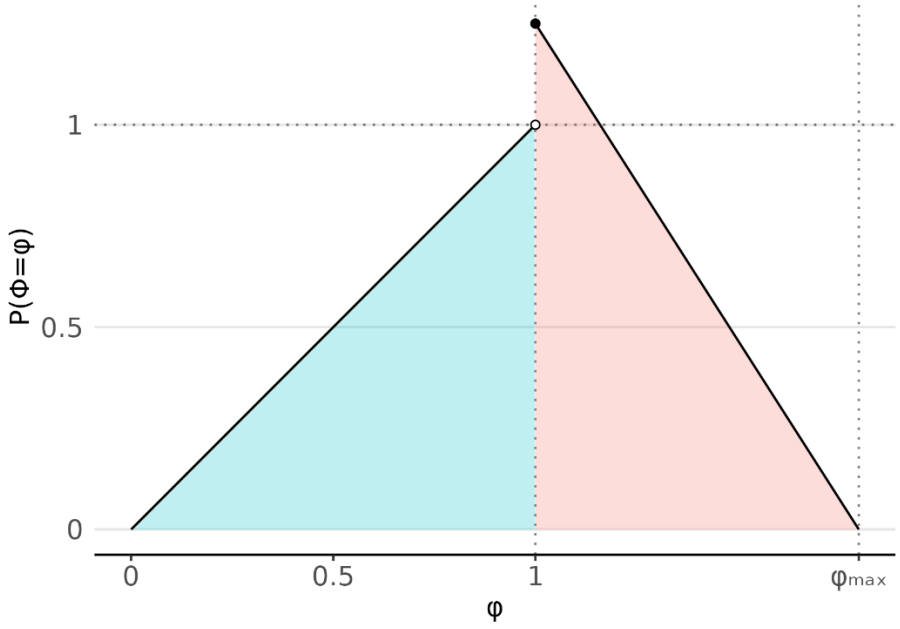


Similarly to the other parameters, the scaling factor is obtained by sampling a scale index from a uniform distribution over the range [0, 1] and transformed to the desired distribution over $\phi$ using inverse

transform sampling. This scale index is a value between 0 and 1, where 0 pulls the distribution closer to a uniform distribution (less variation during the day) and 1 pulls the distribution's extremes (peaks and valleys) apart (more extreme variation during the day). A scale index of 0.5 results in no change in the distribution. This scale index is what is provided as input in the OPS model to perform the sensitivity analysis. Since the default sinusoid can differ between source types, the imposed bounds on these distributions may also differ between source types. Therefore the prescribed perturbation will differ depending on the source type. As an example, Figure 3.6 shows the effect of scaling the diurnal variation for 'average industrial activity' as a function of the transformed scaling factor $\phi$.

*Figure 3.6 The effect of scaling the diurnal variation weights for 'average industrial activity'. The maximum scale is bounded by the four o' clock weight as scaling any further would make it negative. A scaling factor of 0 results in a flat distribution. The black line represents the original variation without any scaling.*

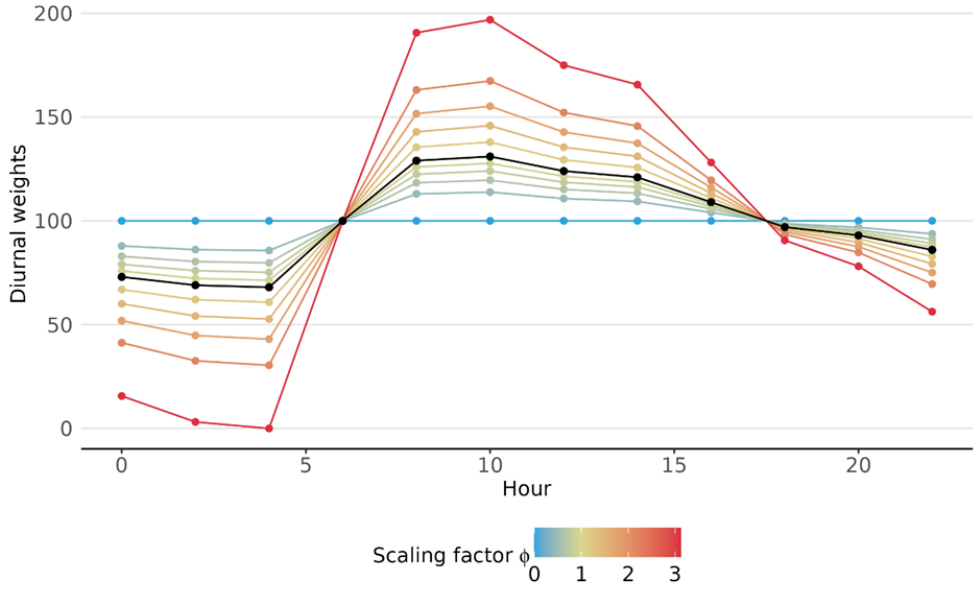


As stated at the start of this section, OPS takes into account diurnal variation using twelve two-hourly blocks. For the industrial stack, this distribution is according to the (average) industrial activity during a working day. For the motorway source, this is according to the (average) traffic intensity. For the livestock farm, the diurnal variation consists of two parts, each representing half of the total variation. These parts are perturbed in a different way as follows.
The first part of the variation equals half the variation imposed on industrial emission as an estimate for the day-night rhythm. This part is perturbed according to the aforementioned scaling method for industrial stacks.
The second part is implemented in OPS as a temperature correction (emission correction *EC*), which for livestock farms is:

$$EC_{livestock\ farm} = \max\left(1 + 0.0294\left(T - T_{avg}\right), 0.2\right).$$

Here, $T$ is the outdoor temperature of the current stability, wind direction and distance class and $T_{avg}$ the long-term average outdoor temperature, which is set at 10 °C. The temperature correction is not allowed to be lower than 0.2. This minimum correction factor needs to be set at temperatures below -17.2 °C. It is unlikely that this occurs in the meteorological classes in OPS for which multiple hours have been averaged in the meteorological pre-processor. Therefore, the resulting mean temperatures of the classes will not show extremely large deviations from the mean. Note that for yearly runs, this function implies that the emission total for a year, with an average temperature other than 10 °C, changes. In general, this function gives a higher emission correction factor for temperatures exceeding 10 °C and a lower emission correction when temperatures are below 10 °C.
This emission correction function based on temperature also needs a perturbation, as otherwise only half the diurnal variation, the industrial part, is perturbed. Similar to the twelve two-hourly blocks, a scale index of 0.5 gives no change in the temperature correction. A scale index of 1 increases the slope of the temperature correction by 20%, and a scale index of 0 decreases the slope by the same amount. As such, this either strengthens or reduces the temperature impact on the emission.

## 3.3 Model version

For the sensitivity analysis performed in this study, the OPS-LT model version v5.3.1.0 was used (released at https://github.com/rivm-syso/OPS/releases/tag/v5.3.1.0). This is the model version applied for the production of the GCN2025 maps (Large scale Concentration and Deposition Netherlands produced in 2025 for year 2024) and is expected to be used in AERIUS later this year. The version also includes the OPS adjustments that were incorporated to enable the sensitivity analyses. Technical details on these adjustments are provided in the online Appendix (2025-0081-appendix).
Meteorological conditions were prescribed using observations from the year 2015. In the present-day climate, this year represents an average year regarding precipitation, air temperature, wind speed and solar radiation (see https:/www.knmi.nl/climate dashboard). A further description of the processing of the meteorological data used in this analysis is given in Section 3.1.11 as well as in Section 2.7 of the online Appendix (2025-0081-appendix).
Other data required to run OPS include background concentrations and chemical conversion rates. To this end, the set of digital maps applied for the year 2015 in GCN2025 was used. These maps provide the best representation, using the most recent insights, of the background concentrations (calibrated to the observations) and the chemical conversion rates in this year, consistent with the meteorological conditions. For the roughness lengths and land use spatial data, maps based on LGN2020 (Landelijk Grondgebruik Nederland; lgn.nl) at 250 x 250 $m^2$ resolution were applied.

## 3.4 Source types and characteristics and source-receptor configuration

The aim of this research is to study the uncertainty in the annual nitrogen deposition on a nature area caused by a single source, up to great distances from the source (here, 400 kilometres was decided

upon). Three different source types are studied: a livestock farm, an industrial stack and a motorway. It was decided to use the same source types as in the benchmark study at local scale (Kooi et al., 2025a). The latter study is conducted within the SAGEN project. It focuses on the local scale (up to 5 km) and addresses the estimation of the uncertainty in a different way. While in the present project the uncertainty is estimated by performing a sensitivity analysis following from uncertainty in various parameterisations, the benchmark study focuses on uncertainty obtained by using various models (see also Section 2.1). Note that the benchmark study consists of two parts: a model intercomparison study and a model validation. For the present study, we align with the model intercomparison study (Kooi et al., 2025a). The specific source characteristics are provided in the sections below.
For the location of the sources we choose the central point of the Dutch national coordinate system, the RD coordinates (in Dutch: Rijksdriehoekscoördinaten (RD) with unit m). This central point is located near the centre of the Netherlands, in the centre of the city of Amersfoort. Its coordinates are [155000; 463000] RD (latitude = 52.15517$^{o}$N, longitude = 5.387204$^{o}$E).
Regarding the receptor configuration, it was decided to study the sensitivity of the OPS in twelve different directions. These correspond to the centre of the wind direction classes used in OPS. The centre point of the receptor configuration is set equal to the centre point of the sources. The distances were selected in such a way that the highest point density is near the source starting from 1 km, with greater distances between the receptors at further distances:

- From 1 km until 2 km: a receptor point every 100 m
- From 2 km until 25 km: a receptor point every 500 m
- From 25 km until 50 km: a receptor point every 1 km
- From 50 km until 100 km: a receptor point every 5 km
- From 100 km until 400 km: a receptor point every 10 km

This results in 122 receptors in each of the 12 directions, which yields a total of 1464 receptor points. The array of 122 receptors in one specific direction will also be referred to as ‘spokes’. The default receptor height of 4 m is applied.
An overview of the receptor points and source locations is provided in Figure 3.7.

*Figure 3.7 Overview of the receptor locations and the source locations of the livestock farm, industrial stack and motorway. The centre point of the source locations is identical to the centre point of the spokes with receptor points.*

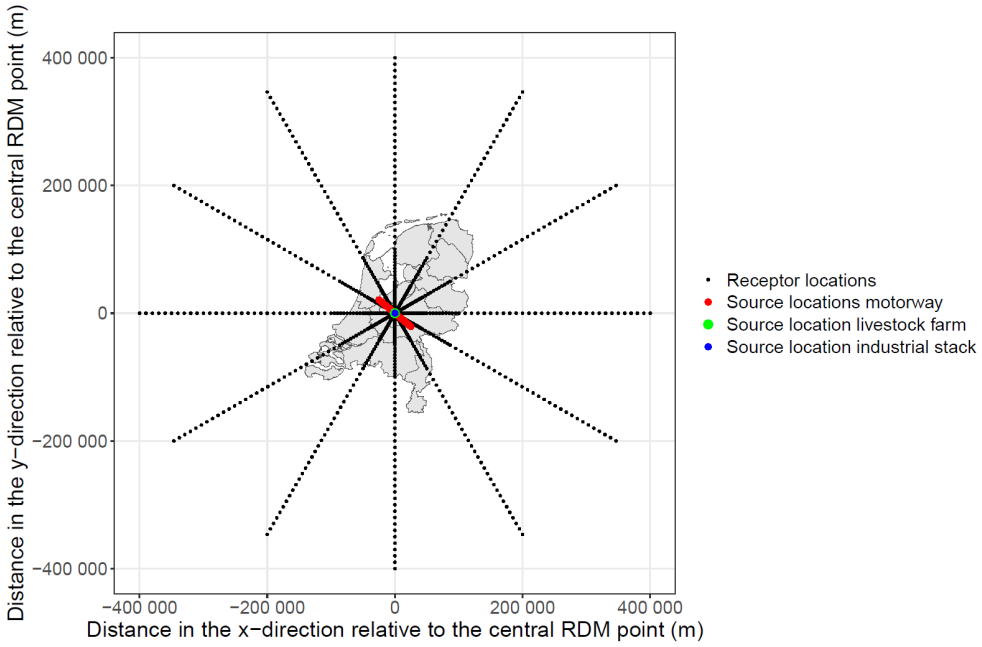


### 3.4.1 *Livestock farm*

In the model intercomparison of the benchmark study by Kooi et al. (2025a), two different setups for the livestock farm were investigated: one with and one without building effects. In the present study, the characteristics of the livestock farm without building effects are selected. This is because the focus is on the greater distances where building effects are expected to be insignificant.
In contrast to the benchmark study, diurnal variation was imposed on yearly average emission rates and only one emission point was considered (not: four). Both choices are consistent with default settings when using OPS for permit application and in the production of the GCN/GDN maps (largescale concentration/deposition maps Netherlands). In the model intercomparison of the benchmark study, no diurnal variation was imposed as it was desired to have consistent input across the models. The total emission strength was kept identical to the one used by Kooi et al. (2025a) (see below).
Note that all animals are assumed to remain inside the animal house, so that all emissions originate from there.

*Table 3.3 Input values for the livestock farm.*

| **Livestock farm** | |
|---|---|
| Substance | $NH_3$ |
| x-coordinate | 155000 m (RDM) |
| y-coordinate | 463000 m (RDM) |
| Emission rate | 0.04 g/s |
| Emission height | 4.4 m |
| Initial vertical dispersion length | 0.0 m |
| Source heat content | 0 MW |

| **Livestock farm** | |
|---|---|
| Exit temperature | Not applicable (missing value:-999.0 °C) |
| Exit diameter | 1 m |
| Exit velocity | 0.5 m/s |
| Diurnal variation code | 4 (livestock farm) |

A summary of the input values is provided in Table 3.3. The source characteristics presented in the table were defined using an internal database with descriptions of 5782 animal houses. First, the dataset was used to determine the 40$^{th}$ and 60$^{th}$ percentile values of emission height, exit velocity, exit diameter, emission strength, building height, building width and building length to width ratio, respectively. In the case of three sources, all parameter values were within the 40$^{th}$-60$^{th}$ percentile range. The mean emission height, exit velocity and exit diameter of these three sources were then used to define the livestock farm case. The average source strength in the unfiltered database is 0.013 g/s. In order to increase numerical accuracy of model output, a conservative estimate of 0.04 g/s has been chosen by Kooi et al. (2025a) and divided over four emission points. Here, we use the same value, but assume it is emitted from one emission point only.

### *3.4.2 Industrial stack*

In the model intercomparison of the benchmark study, a tall source containing buoyancy and momentum was selected. In the present study, all input values except diurnal variation are identical to the input values used in the model intercomparison study by Kooi et al. (2025a). In the present study, diurnal variation was set to the code for average industrial activity to allow investigating the influence of uncertainty in this parameter on total uncertainty.

*Table 3.4 Input values for the industrial stack.*

| **Industrial stack** | |
|---|---|
| Substance | $NO_2$ |
| x-coordinate | 155000 m (RDM) |
| y-coordinate | 463000 m (RDM) |
| Emission rate | 0.74 g/s |
| Emission height | 50 m |
| Initial vertical dispersion length | 0.0 m |
| Source heat content | Determined in OPS via exit temperature, diameter and velocity (here missing value: -999.0 MW) |
| Exit temperature | 60 °C |
| Exit diameter | 2.5 m |
| Exit velocity | 1 m/s |
| Diurnal variation code | 1 (average industrial activity) |

The source characteristics are provided in Table 3.4. The "industry" category involves a wide range of economic activities, from small enterprises to large refineries and power plants. Emission characteristics (source strength, stack height, stack diameter, emission temperature and exit velocity) of industrial stacks vary considerably. Available data

sets did not include data for all of these parameters. The case included in Table 3.4 is merely an example. The stack height of 50 m is much greater than the average height of industrial stacks (between 15 and 20 m). This was a deliberate choice, since this height results in more contrast with the cases with low sources. The emission strength of 0.74 g $NO_x$/s in $NO_2$ equivalent mass is also relatively large compared to the emission strengths in the consulted data sets.

### *3.4.3 Motorway*

In the benchmark study by Kooi et al. (2025a), two different setups for the motorway were investigated: one with and one without a noise barrier. In the present study, only the motorway without a noise barrier was selected since this is custom for permit application and production of the GCN/GDN maps. Except for diurnal variation, source characteristics were identical to the values used in the benchmark study (see Table 3.5). The orientation of the motorway is on the line from 130° to 310°, relative to the North. In order to define the line source, 2611 separate point sources with 25 m spacing in between are simulated. However, in the context of the present study, these point sources should rather be considered segments of one single line source. The centre point of the motorway is located at the centre point of the receptor configuration and equals the location for the livestock farm and industrial stack. For an overview, see Figure 3.7.

*Table 3.5 Input values for the motorway.*

| **Motorway** | |
|---|---|
| Substance | $NO_2$ |
| Location centre point of all sources | x = 155000 m, y = 463000 m (RDM) |
| Location most western source | x = 130000 m, y = 483977 m (RDM) |
| Location most eastern source | x = 179984 m, y = 442036 m (RDM) |
| Emission rate | 0.184 g/km/s (= 0.00461 g/s per source segment) |
| Emission height | 2.5 m |
| Initial vertical dispersion length | 1.25 m |
| Source heat content | 0 MW |
| Exit temperature | Not provided |
| Exit diameter | Not provided |
| Exit velocity | Not provided |
| Diurnal variation code | 3 (average traffic intensity) |

Emission strength for motorway traffic depends on traffic intensity and differs between regions due to variation in population density. An average emission strength was determined by dividing the total $NO_x$ emission from motorways combined with the length of motorways in the Netherlands. The emission strength used in the model intercomparison study and in the present study is 0.184 g/km/s in $NO_2$ equivalent mass. This strength is somewhat greater than the annual average value for all Dutch motorways.

## 3.5 Uncertainty analyses

### *3.5.1 Monte Carlo Analysis*

The effects of some of the parameters on the model can interact with one another. These interactions can result in a reinforced effect – for example, reducing the plume rise while simultaneously increasing the deposition velocity – could result in a change that is greater than the sum of its parts. Conversely, interactions can conceivably cancel out the effects of individual parameters. It is difficult to enumerate, understand and account for all of these effects. To this end, we also perform a straightforward Monte Carlo sensitivity analysis, from which we estimate the uncertainty.

For this analysis, values for all parameters are sampled from their respective probability distributions simultaneously. We use a sample size of five thousand runs. To ensure this sample is representative of the variability of the uncertainty distributions, a random Latin hypercube design is used for sampling. By looking at smaller subsets the number of five thousand runs appeared quite sufficient. The model's total sensitivity is expressed as a coefficient of variation relative to the reference result: $CV = \frac{\sqrt{Var(X)}}{|X_{ref}|}$, where Var$(X)$ is the variance of the model results over all Monte Carlo runs. This is also our measure of uncertainty. Note that this deviates from the standard definition of CV, where the standard deviation divided by the mean (as used to define parameter uncertainties in Section 3.1). In this report we generally use the CV from the equation above and will mention explicitly where we deviate from this function.

### *3.5.2 Sobol' Sensitivity Indices*

While the Monte Carlo analysis is useful for estimating the total uncertainty, implicitly capturing the subsequent parameter interactions, it does not provide any additional insight in the contribution made by particular interactions. Sobol' Sensitivity Indices provide a decomposition of the model variance into fractions of first- and higher-order parameter effects. Sobol' indices are computed by fitting a metamodel using Polynomial Chaos Expansion into the results of the five thousand Monte Carlo runs. The coefficients from this metamodel can then be used to analytically compute the Sobol' Sensitivity Indices (Gauchi et al., 2017).

To account for most interactions, we computed indices up to the third order. Since computing these indices for each receptor would be too time consuming, approximately 10% of receptors are selected at random. Sensitivity indices for these receptors are computed and then displayed as a function over distance. These results are then smoothed out to more clearly visualise the general trends.

By definition, all Sobol' indices combined add up to 100% of the model variance. Since there are too many possible parameter combinations to meaningfully present, only the top eleven most significant effects, based on the combined importance across the three cases, are shown. Therefore, the same parameters and combinations are shown in each case. The sum of the other parameters and their combinations are shown as "other".

### 3.5.3 *One-at-a-time sensitivity analysis*

In support of the interpretation of the results of the Monte Carlo analysis and the Sobol' Sensitivity Indices, we also performed a set of one-at-a-time sensitivity analyses, targeted at the most influential parameters according to the Sobol' Sensitivity Indices. In contrast with the Monte Carlo analysis, each parameter is now being varied individually, while keeping the values of the other parameters fixed at their 'default' values (see Section 3.2). The value of each parameter tested is now also varied within the domain of their prior uncertainty distributions, but parameter values are taken to be the percentiles of the distribution. The 50$^{th}$ percentile (the median) represents the parameter's default value (see Figure 3.8). To prevent too extreme parameter values, the lowest (0%) and highest (100%) percentiles are excluded, leaving 99 parameter values for which the model is evaluated. In this way, nearly the entire bandwidth of the distribution is covered, with a slight focus on higher-density parts.

A notable exception to this approach is the Meteo parameter. As this is a discrete parameter with seven possible outcomes, only as many model evaluations are performed per source configuration.

*Figure 3.8 Example of a lognormally distributed scaling parameter. The coloured vertical lines represent the positions of the percentiles, the values for which the model is evaluated. The dotted line represents the median or the 50$^{th}$ percentile.*

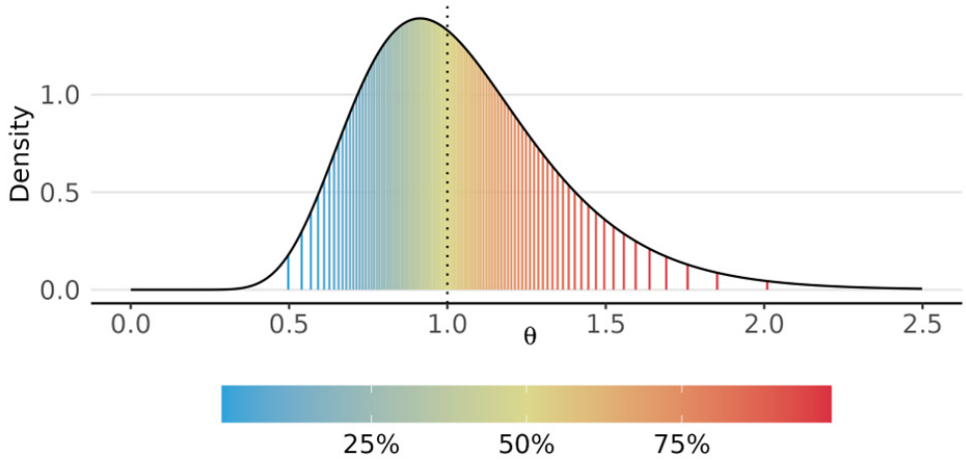


Every model evaluation yields estimates of concentration and deposition at receptors along each of the twelve spokes described in Section 3.4. Therefore, varying a parameter results in a response surface that describes the outcome of the model for a given parameter setting over distance from the source for each spoke. In order to obtain a visual understanding of the sensitivity of changing a parameter, each model result $X_i$ (based on parameter set $i$) is taken relative to the corresponding result from a reference model run in which all parameters are kept at their default values $X_{i,\text{rel}} = \frac{X_i - X_{\text{ref}}}{|X_{\text{ref}}|}$, for non-zero reference value $X_{\text{ref}}$. Finally, the mean of the relative differences is taken across the twelve spokes.

## 3.6 Uncertainty Analysis Tool

The prior uncertainty distributions of the various perturbation parameters are considered to be independent. However, a comparison between measurements and representative model results corresponding to these sampled parameters is likely to reveal that certain combinations of parameters generated by the priors lead to unrealistic model results. This measure of 'realism' was heuristically determined by modelling the concentrations at receptor locations corresponding to measuring stations from the MAN (Measuring Ammonia in Nature) network for a large set of real-world emission sources. Model results for all parameter value combinations were evaluated by computing the Root Mean Squared Error (RMSE) between the model results and the measurements at the MAN stations. The parameters with the highest RSME values are considered as unlikely. The sensitivity of the uncertainty, for the removal of these unlikely results, has been tested. This test, used for illustrative purposes only, was applied to an older version of OPS. Due to the small differences in results regarding the CV between both OPS versions, the time-consuming calculations of these illustrations were not updated.

# 4 Results

In this chapter, we will present and analyse the sensitivity obtained from the Monte Carlo analysis and Sobol' Sensitivity Indices obtained from this. From the results of the five thousand runs, at each receptor point the Coefficient of Variation (CV: standard deviation divided by the reference value) was computed for total deposition (dry + wet of both primary and secondary material) as well as for concentration of the primary material. These CV values are used to quantify the model sensitivity. Because realistic uncertainty distributions for each parameter are used and propagated in the model, we expect that the sensitivities from the Monte Carlo analysis represent reasonable estimates for the model uncertainty.

We use relative differences to express sensitivity. This choice is motivated by looking at the absolute $NH_3$ concentrations. Figure 4.1 shows the results of one of the one-at-a-time analyses. In this particular case the deposition velocity of the primary material ($v_{d,pri,}$) was varied (see also Sections 3.5.3 and 4.4.1). Red and blue lines represent increased and decreased $v_{d,pri}$, respectively. This figure shows a typical example of the behaviour of concentration as a function of distance from a source, in this case the livestock farm. Distance is plotted logarithmically. Concentration is plotted in two ways: linearly (left) and logarithmically (right). As expected, the concentration strongly reduces with distance from the source, by about two orders of magnitude in the first 20 to 25 kilometres. Differences between various runs can be seen quite clearly over this distance in the linear plot (right). Beyond 25 km, absolute differences seem to disappear in the linear plot but become clearly distinguishable in the logarithmic plot (left). This shows that there is a strong signal of sensitivity or uncertainty over greater distances. Since an important aim of the present study is to determine uncertainty at such greater distances, we decided to study relative sensitivity, even though differences in absolute contributions may be small. Note that in practice at greater distances, many small contributions, each with an uncertainty, may contribute to the total concentration and deposition, which still makes the relative sensitivity at greater distances for an individual source relevant.

*Figure 4.1 $NH_3$ concentration as a function of distance from the livestock farm, for varying $v_{d,pri}$ and keeping other parameters fixed at their default value. Colours represent perturbation factors for $v_{d,pri}$. Left: with linear scale to plot concentration; right: with logarithmic scale to plot concentration. The distance from the source is plotted logarithmically in both cases.*

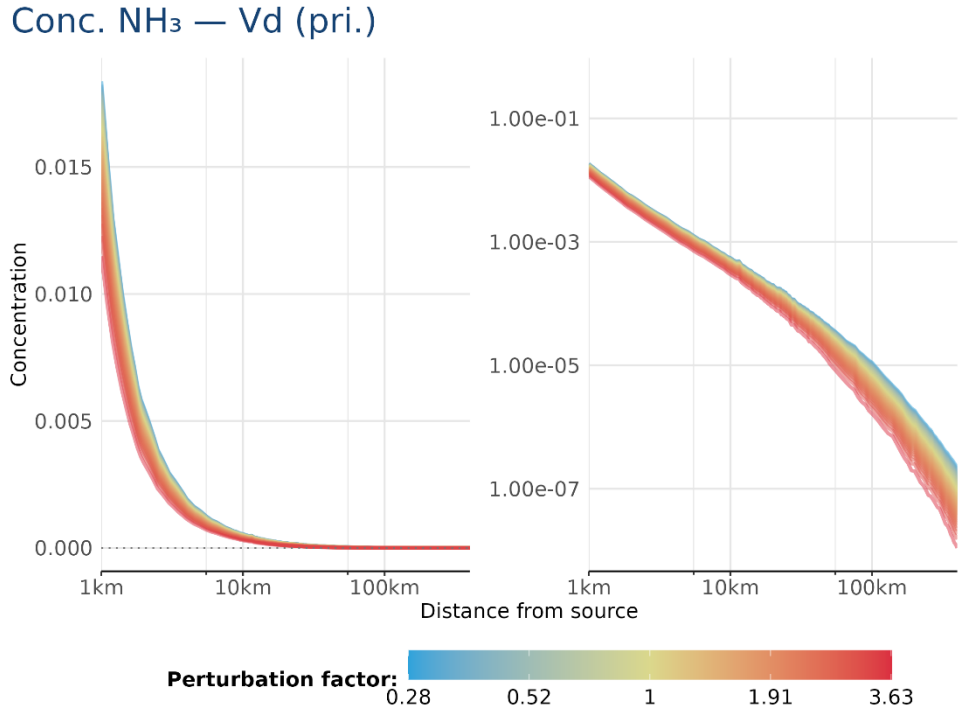


The sensitivity results were analysed further, as described below. The analyses are introduced by first showing results for the livestock farm in some detail. These more detailed results are used to explain the figures, and the underlying choices that were made to create them, and for the other source types as well. Subsequently the results are interpreted further, using the one-at-a-time sensitivity analysis for the most influential parameters common to the three source types.

## 4.1 Sensitivity results for the livestock farm ($NH_3$ concentration and total $NH_x$ deposition)

Figure 4.2 shows the total sensitivity (defined as the CV from the five thousand runs) to the twelve parameters for the ammonia concentration and the total deposition of the sum of ammonia and ammonium ($NH_x$). The plot shows the median of the spoke CV values at a given distance (thick lines). We choose to analyse median CV values since the results show some extreme CV values on individual spokes that would affect an average value disproportionally. Extreme values can occur for locations with a high compensation point. Then, dry deposition due to this source can be very low with extreme effects of parameter scaling. To avoid domination by these extreme values, the application of the median rather than the average is considered more appropriate. Because the extreme values also dominate the calculated standard deviation, we choose the scaled Median of Absolute Differences ($MAD = median(|X_i - median(X)|)$ MAD [Median absolute deviation - Wikipedia]) as the

indicator for the spread of results. The MAD is scaled using a factor of 1.48, making it an estimator of the standard deviation. From here on, further mentions of the MAD refer to this rescaled estimate. The shaded areas in Figure 4.2 indicate the corresponding range of 1 MAD and 2 MAD to indicate the spread.
The sensitivity for total deposition is relatively high near the source, with a median CV of just over 60%. It gradually decreases to just below 25% at distances ranging between 50 and 100 km. For even greater distances, the sensitivity slightly increases again. The median CV for concentration in general indicates a relatively small sensitivity of 40% close to the source, which increases to around 60% for greater distances up to 10 km. Sensitivities then decrease until 50 km again, to 40%, and increase again after 100 km. For the whole domain, the sensitivities seen for $NH_3$ concentration, as quantified with the median CV, range between 40 and almost 70%.
The CV of the $NH_3$ concentrations is lower than the CV of total $NH_x$ deposition for small distances, up to 3 km. By contrast, the CV of total $NH_x$ deposition is lower than the CV for concentrations for greater distances. This difference is caused by compensating effects for the amount of deposition. For instance, if the dry deposition is underestimated, more of the ammonia will stay airborne and will be available for deposition. Such compensating effects are not present in the uncertainty in the concentration.

*Figure 4.2 Coefficient of Variation of $NH_3$ concentrations (red) and total $NH_x$ depositions (dry and wet, blue) of a livestock farm in which all model parameters are varied. The median is used as central indicator (thick line) and 1 respectively 2 MAD values are used to indicate the spread in the spokes (darker and lighter shade respectively).*

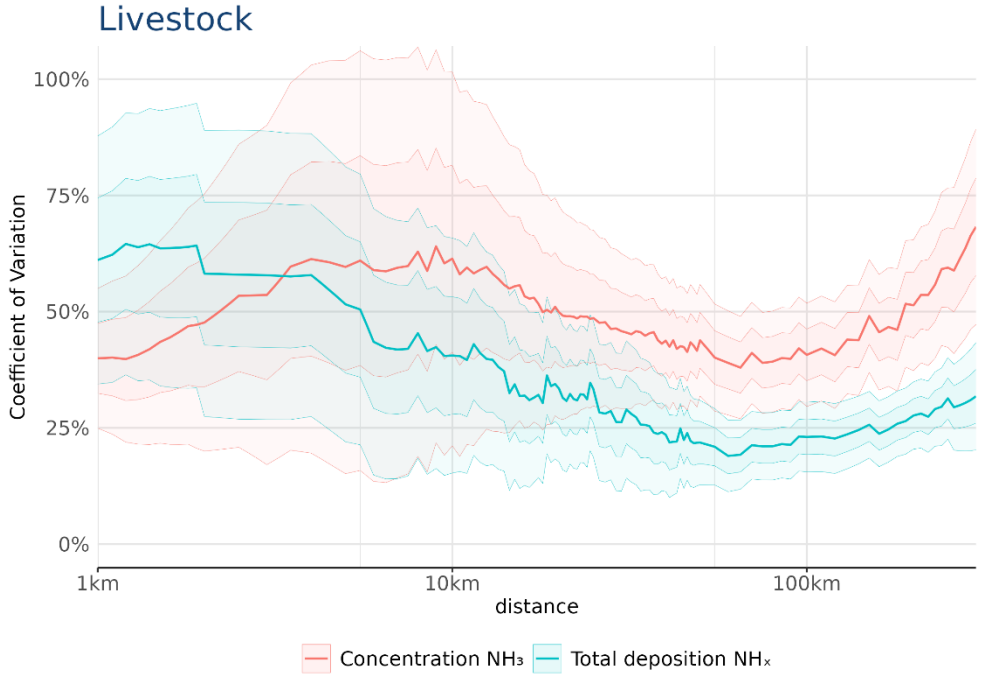


The contribution made to the CV by the various parameters is analysed using the Sobol' Indices (Figure 4.3; see also Section 3.5.2). The set of

the eleven most influential parameters and parameter combinations are shown individually. All other parameters and combinations, of which the individual contribution is very small, are shown in the "other" category. The Sobol' Indices plots for the other two sources use the same set of selected parameters as the selection was based on the most influential parameters common for the three source types. The results show that the relatively high sensitivity in the concentration close to the source is caused to a large extent by the variation in the parameters that dominate the dispersion process, such as the vertical dispersion length $\sigma_z$ and the mixing height $z_i$. In the case of the livestock farm, such parameters determine the initial dilution of emitted material. After a few kilometres from the source, the influence of especially $\sigma_z$ on the concentration diminishes as ammonia becomes better mixed over the boundary layer. After several tens of kilometres also the influence of $z_i$ decreases. After about 10 kilometres, the removal by dry deposition of the primary material increasingly influences the development of the concentration. Hence, the uncertainty in the dry deposition velocity of the primary material ($v_{d,pri}$) becomes more important in the CV.

*Figure 4.3 Relative contribution by the various parameters to the variation (Sobol'-indices) for concentration ($NH_3$) and total $NH_x$ deposition (dry and wet) for a livestock farm.*

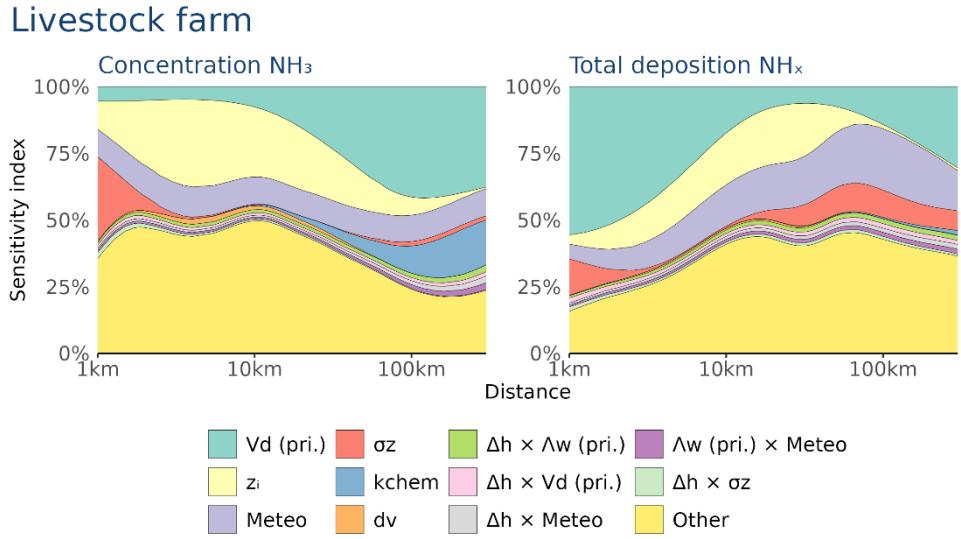


By contrast, the CV of the total $NH_x$ deposition is initially large due to the uncertainty in the dry deposition velocity of the primary material. Beyond a distance of about 10 km from the source, the feedback of the concentration on the dry deposition process is starting to play an important role. This leads to a smaller dependence of the dry deposition sensitivity on $v_{d,pri}$. Therefore, the contribution by the variation in the deposition velocity diminishes at greater distances up to about 50-100 km. For even greater distances, the crossover point is passed, and sensitivity starts increasing.
In both figures the sensitivity meteorological conditions is also substantial. The modelled $NH_3$ concentrations at great distances are sensitive to the chemical reaction velocity. The sum of sensitivities of all other individual parameters and second- and third-order combinations

are shown as "other". For example, the largest individual parameter, included in "other", contributes up to 1% to the total sensitivity.

## 4.2 Sensitivity results for the industrial source ($NO_x$ concentration and total $NO_y$ deposition)

Figure 4.4 shows the CV for the $NO_x$ concentrations and total $NO_y$ deposition for the industrial source. For the concentration of $NO_x$ the CV close to the source (1 km) is small: less than 20%. For distances up to 25 km the CV gradually increases up to about 50%. For distances larger than 25 km the CV-values decrease to around 30-35%. The Sobol' Indices in Figure 4.5 show that near the source variations are mostly due to the uncertainty in the vertical dispersion length which determines the initial mixing of the plume. After a few km, the mixing height gains relatively more importance. In the case of the industrial source, these parameters also determine where the plume touches the surface. This has a great impact on the CV values. Meteorological conditions are of importance at all studied distances. In general, after 5 km meteorological conditions and mixing height together contribute to -roughly- 25-50% of the CV. After about 50 km the relative influence of chemical conversion on concentration increases.

*Figure 4.4 Coefficient of Variation of $NO_x$ concentrations (red) and total $NO_y$ depositions (dry and wet, blue) of an industrial source in which all model parameters are varied. The median is used as central indicator (thick line) and 1 2 MAD values are used to indicate the spread in the spokes (darker and lighter shade, respectively).*

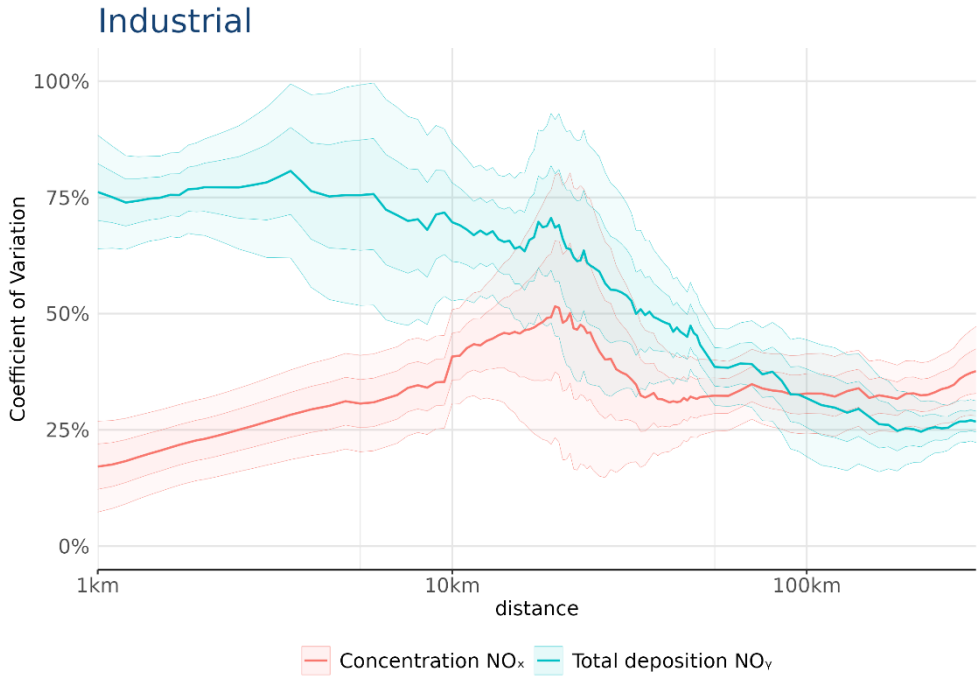

*Figure 4.5 Relative contribution by the various parameters to the variation (Sobol'-indices) for concentration ($NO_x$) and total $NO_y$ deposition (dry and wet) for an industrial source.*

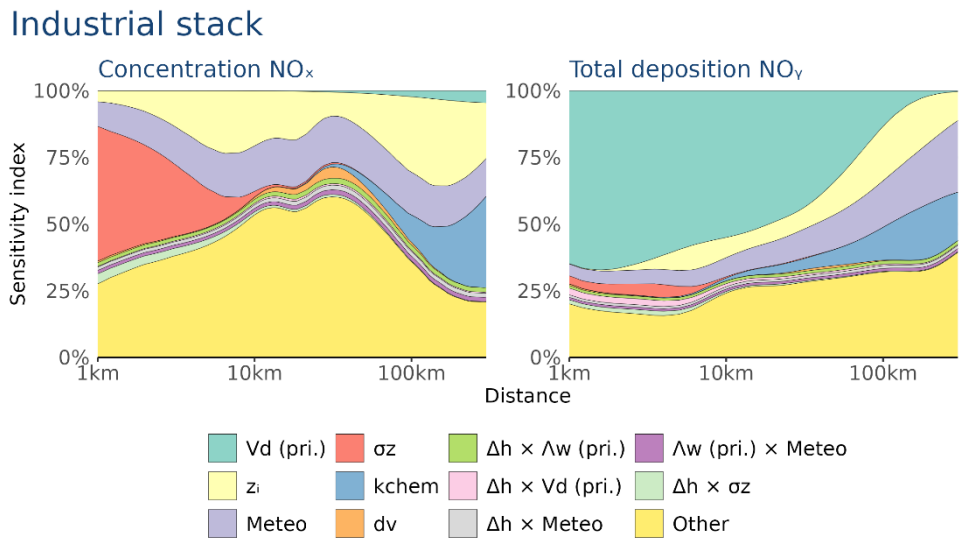


The CV for total $NO_y$ deposition, Figure 4.4, is quite large, about 70-75%, up to 20 km. For greater distances from the source the CV decreases to 25-30% beyond 100 km. The Sobol' indices (Figure 4.5) reveal that the CV of deposition is dominated by the sensitivity to the deposition velocity of the primary material up to 50-100 km from the source. For greater distances, the impact of $v_{d,pri}$ is reduced because the feedback process plays a role here as well (similar to ammonia, see previous section). At greater distances, over 10 km, the uncertainty in the chemical conversion, the mixing height and the meteorological conditions start to play a more important role in the overall CV for total $NO_y$ deposition.

## 4.3 Sensitivity results for the motorway ($NO_x$ concentration and total $NO_y$ deposition)

The CV of the $NO_x$ concentration close to the source is about 50%, up to approximately 20 km (Figure 4.6). For greater distances, the CV decreases to 30% at about 200 km. The Sobol' indices for $NO_x$ concentration, shown in Figure 4.7 (left), show that the main parameters causing these variations are the vertical dispersion length and mixing layer height, along with weather conditions. Closer to the source, up to a few kilometres from the motorway these parameters dominate the CV of the concentration. The diurnal scaling also shows an effect, presumably since the emission of a motorway is influenced by rush hours, resulting in pronounced diurnal variations of the emissions. At greater distances, the influence of the (local) dispersion parameters diminishes, and the CV drops towards a minimum. From then on, the CV slowly increases. At these greater distances, the CV is determined to a large extent by uncertainty in the combination of meteorological conditions, mixing layer height, dry deposition of the primary material and chemical conversion.

As for the other sources, the CV of the deposition, is large near the source, just over 80% (Figure 4.6). For distances greater than 5 km, the CV decreases to around 25% for distances around 100 km and beyond. The Sobol' indices for deposition (Figure 4.7, right) show that uncertainty in the dry deposition velocity of the primary material contributes to the CV by about 50% up to a distance of around 50 km. Up to about 20 km, the vertical dispersion length also has a significant effect. From 50 km onwards, uncertainties in meteorological conditions, mixing layer height and chemical conversion are the main contributors to the CV.

*Figure 4.6 Coefficient of Variation of $NO_x$ concentrations (red) and total $NO_y$ depositions (dry and wet, blue) for a motorway source in which all model parameters are varied. The median is used as central indicator (thick line) and 1 respectively 2 MAD values are used to indicate the spread in the spokes (darker and lighter shade respectively).*

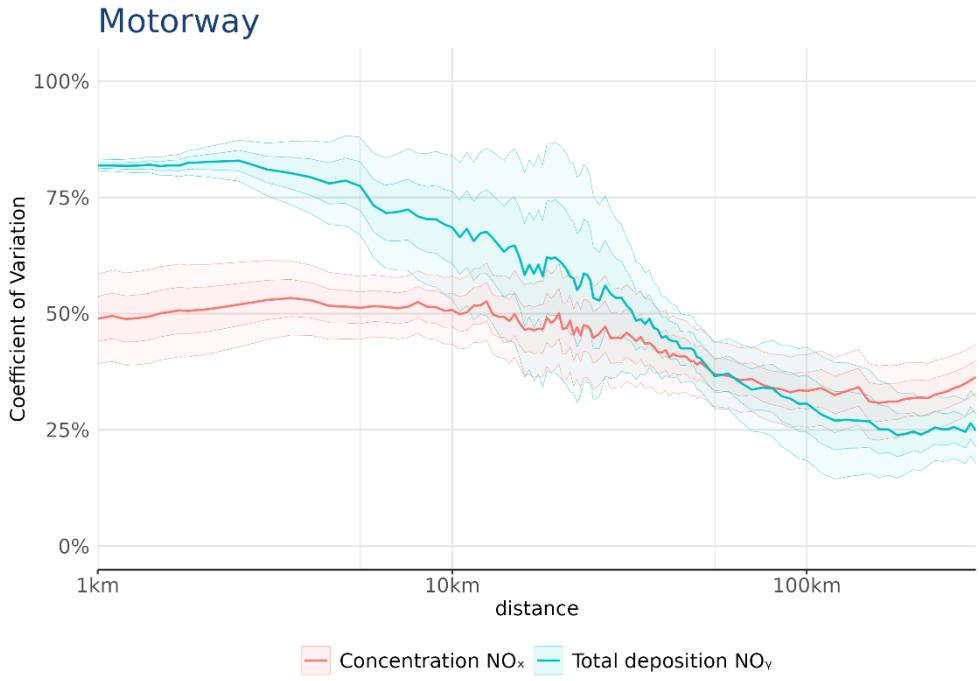

*Figure 4.7 Relative contribution by the various parameters to the variation (Sobol'-indices) for concentration ($NO_x$) and total $NO_y$ deposition (dry and wet) for a motorway.*

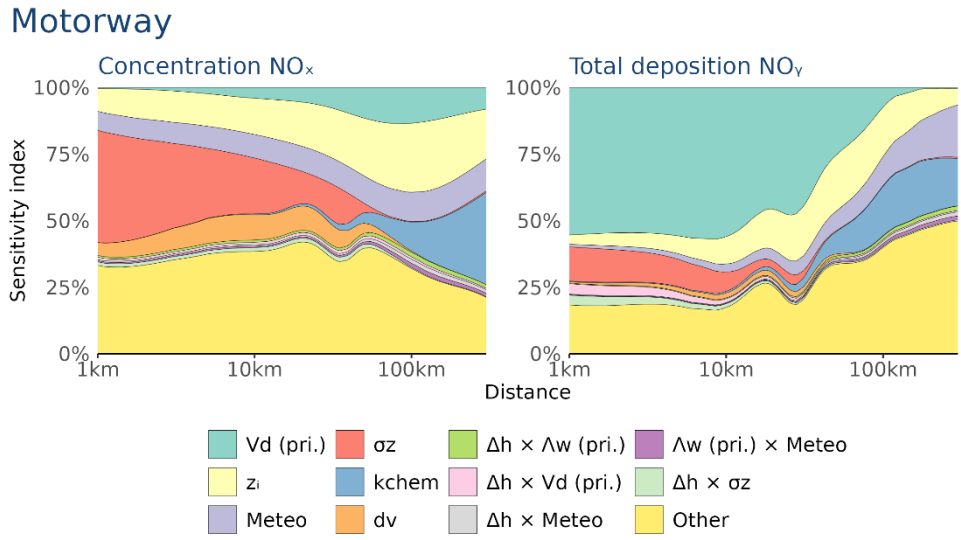


## 4.4 Sensitivity to individual parameters

The results presented in the previous sections were further interpreted using the sensitivity study for individual parameters (Section 3.5.3). Considering the scope of the present report, we focus on the most influential parameters that are common to all sources. The Sobol' Sensitivity Indices indicate major impacts of the uncertainty in:

- the deposition velocity of the primary compound, $v_{d,pri}$;
- mixing layer height, $z_i$;
- vertical dispersion length $\sigma_z$;
- chemical conversion rate $k_{chem}$;
- meteorological conditions, *Meteo.*

This major influence applies to concentration of the primary material, to total deposition, or both. Uncertainties in this parameter set determine 50-75% of the total uncertainty for all sources, depending on source type and distance. A more detailed analysis of the sensitivity to all parameters is available in an online Appendix (2025-0081-appendix). In the next sections, we will present the model response as a function of distance, obtained by averaging the responses over the twelve receptor spokes at a given distance (see Figure 3.7). Regarding concentration, we primarily focus on the relative differences for the primary components, $NH_3$ and $NO_x$. With respect to the sensitivity to $k_{chem}$ the concentrations of the secondary material are studied as well, i.e. $NH_4^+$ and $NO_3^-$+$HNO_3$, respectively. Regarding dry deposition, wet deposition and total deposition, the results are shown for the total amount of material, i.e. the sum of the primary and secondary components ($NH_x$ and $NO_y$).

### 4.4.1 *Sensitivity to $v_{d,pri}$*

The dry deposition velocity of the primary material ($v_{d,pri}$) was adjusted simultaneously for both the trajectory (source depletion) and at the receptor (local effect). This has the following impacts:

- Increasing $v_{d,pri}$ results in a decrease of concentration, since more material will be removed from the atmosphere due to source depletion over the trajectory. The reverse will be true for a decrease in $v_{d,pri}$. The effect increases with distance since there has been more time for source depletion to take place. The relative sensitivity of concentration is much stronger for $NH_3$ than for $NO_x$ (Figure 4.8; Figure 4.3, Figure 4.5 and Figure 4.7). This is because $NH_3$ deposits more readily than $NO_x$ (i.e. $v_{d,pri}$ is higher for $NH_3$).
- Initially, close to the source, a given relative change in $v_{d,pri}$ leads to an equally large relative effect on dry deposition at the receptor. Hence, we see a strong contribution by this parameter to the uncertainty in dry deposition close to the source. However, due to depletion, dry deposition affects concentration over greater distances. Because the effect on concentration increases with increasing distance, the initial effect of $v_{d,pri}$ on the dry deposition gradually decreases with distance. It can be shown that – theoretically – this feedback loop may ultimately lead to a crossover point, where the effect of $v_{d,pri}$ on the dry deposition is reversed. This occurs at a distance from the source that depends on the magnitude of $v_{d,pri}$. The crossover point is found closer to the source for $NH_x$ than for $NO_y$, again due to the more effective dry deposition for the former as compared to the latter. Around this crossover point, the sensitivity and hence the contribution made by this parameter to the uncertainty is minimal (Figure 4.9; Figure 4.3, Figure 4.5 and Figure 4.7). Many complicating factors may obscure the effect, rendering the location of the crossover point rather unpredictable in practice.
- Since wet deposition is a strong function of the mass in the atmospheric column, the sensitivity of wet deposition roughly follows the one of concentration (Figure 4.10).
- The sensitivity pattern of total deposition to $V_{d,pri}$ largely resembles the one of dry deposition. However, the contribution by wet deposition causes the crossover point to shift somewhat towards the source (Figure 4.11).
- Concentration of the secondary material is impacted as well (not shown), because less (increased $v_{d,pri}$) or more (decreased $v_{d,pri}$) primary material can be converted to secondary material. Since the deposition velocity of the secondary components is not adjusted in this part of the study, impacts on the dry and wet deposition of the secondary material will mirror the impact of $v_{d,pri}$ on the concentration of secondary compounds. However, such impacts of the secondary components are hardly distinguishable in the sensitivity of total deposition to $v_{d,pri}$.

*Figure 4.8 Relative difference in concentration compared to the reference run (average over the various directions) when varying dry deposition velocity of the primary material $v_{d,pri}$ for both the trajectory and at the receptor (%). Top left: livestock farm $NH_3$; top right: industrial stack $NO_x$; bottom: motorway $NO_x$.*

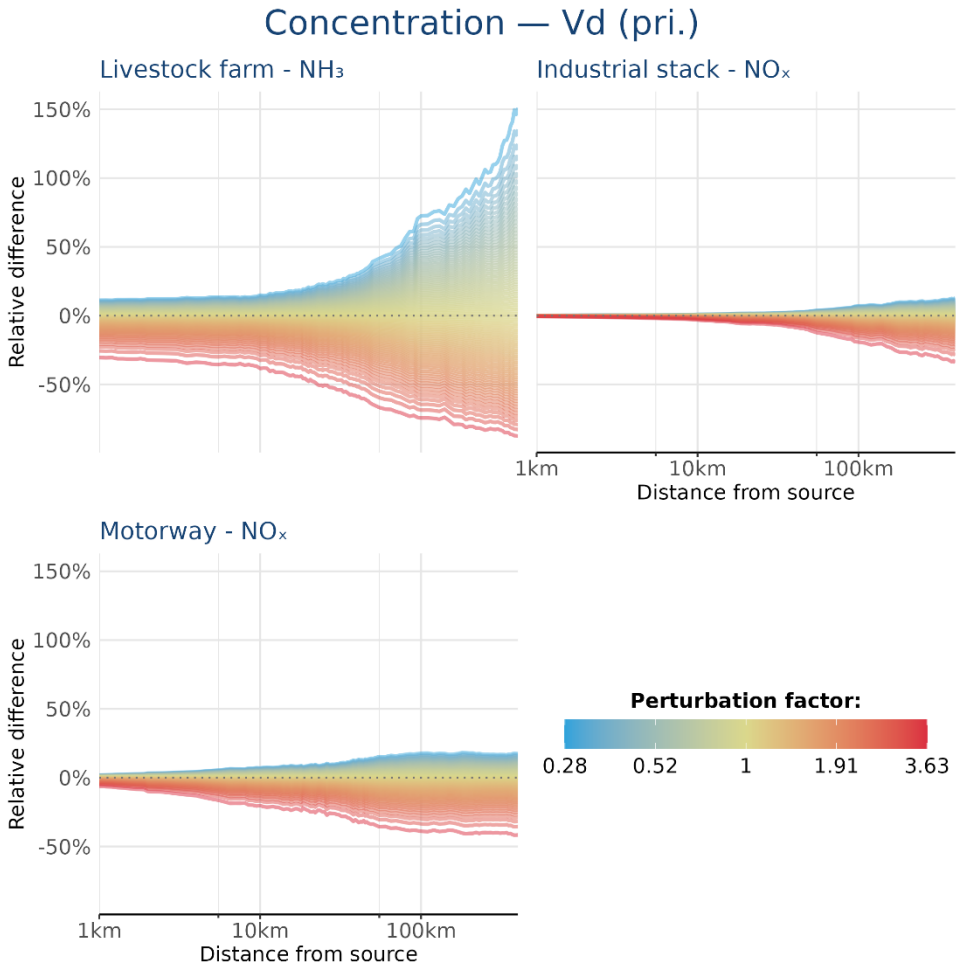

*Figure 4.9 Relative difference in dry deposition compared to the reference run (average over the various directions) when varying dry deposition velocity of the primary material $v_{d,pri}$ for both the trajectory and at the receptor (%). Top left: livestock farm $NH_x$, top right: industrial stack $NO_y$, bottom: motorway $NO_y$.*

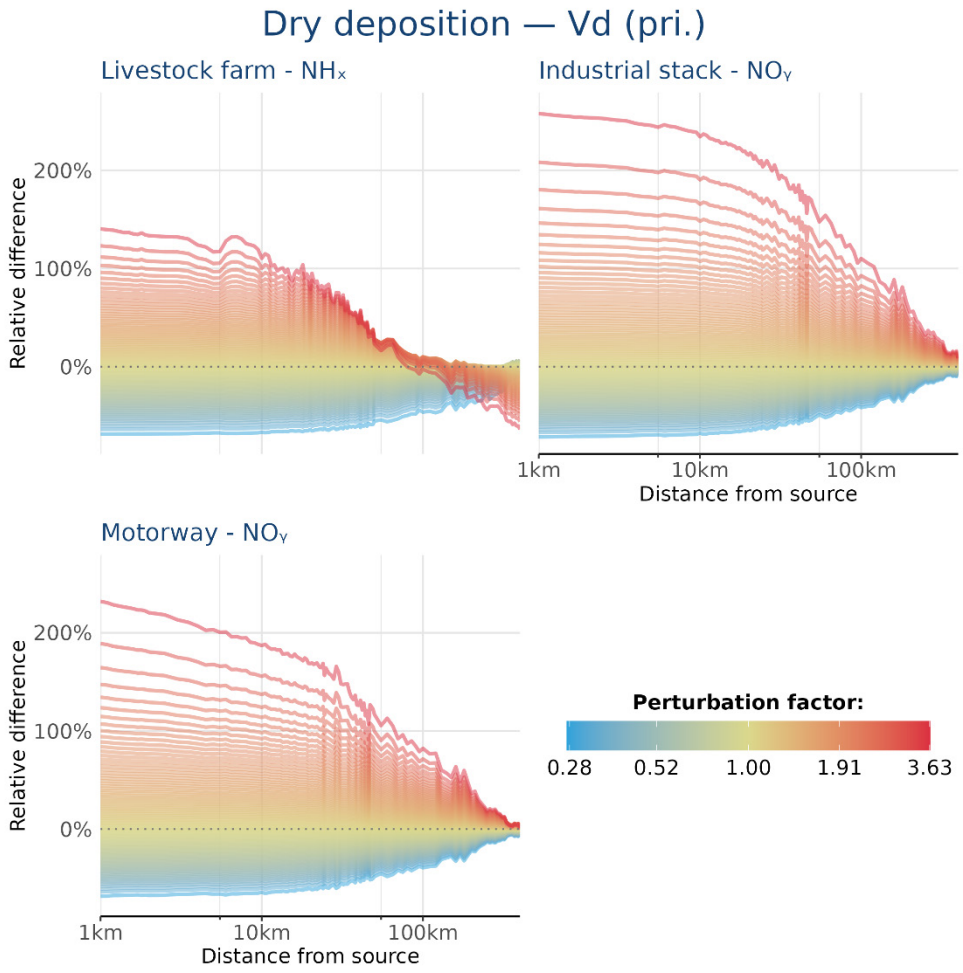

*Figure 4.10 Relative difference in wet deposition compared to the reference run (average over the various directions) when varying dry deposition velocity of the primary material $v_{d,pri}$ for both the trajectory and at the receptor (%). Top left: livestock farm $NH_x$, top right: industrial stack $NO_y$, bottom: motorway $NO_y$.*

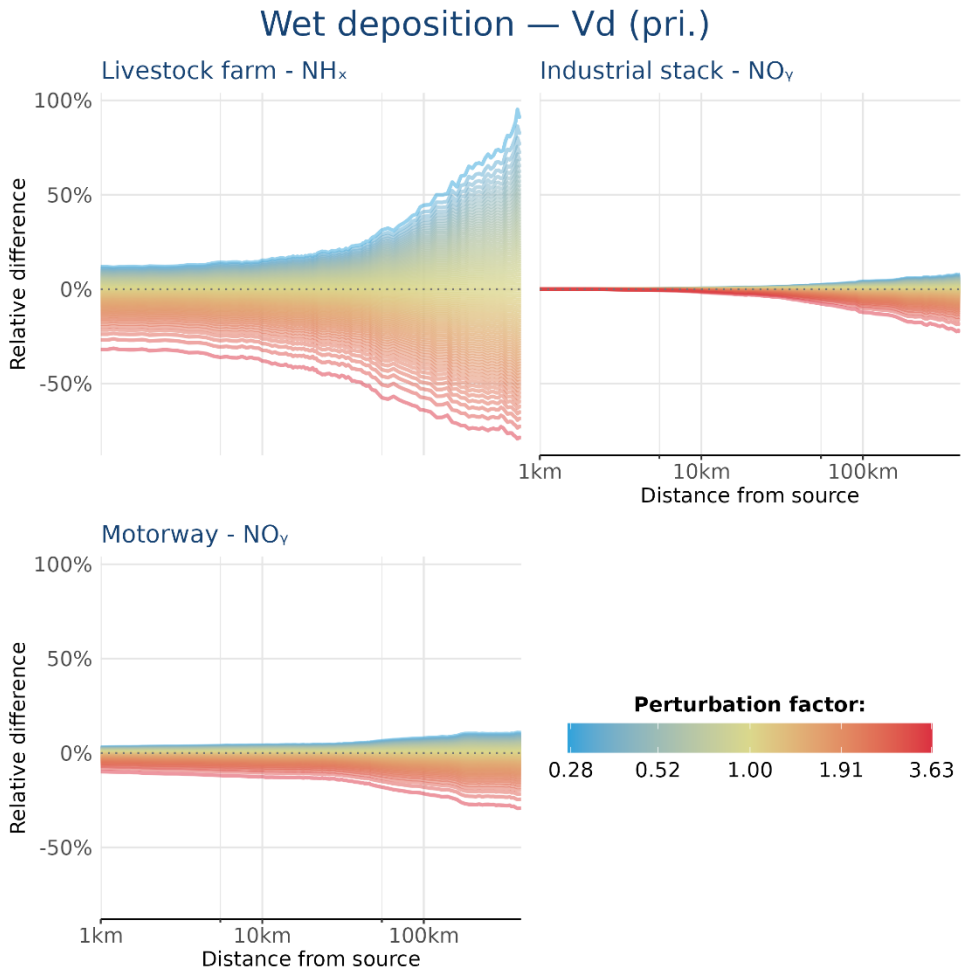

*Figure 4.11 Relative difference in total deposition compared to the reference run (average over the various directions) when varying dry deposition velocity of the primary material $v_{d,pri}$ for both the trajectory and at the receptor (%). Top left: livestock farm $NH_x$, top right: industrial stack $NO_y$, bottom: motorway $NO_y$.*

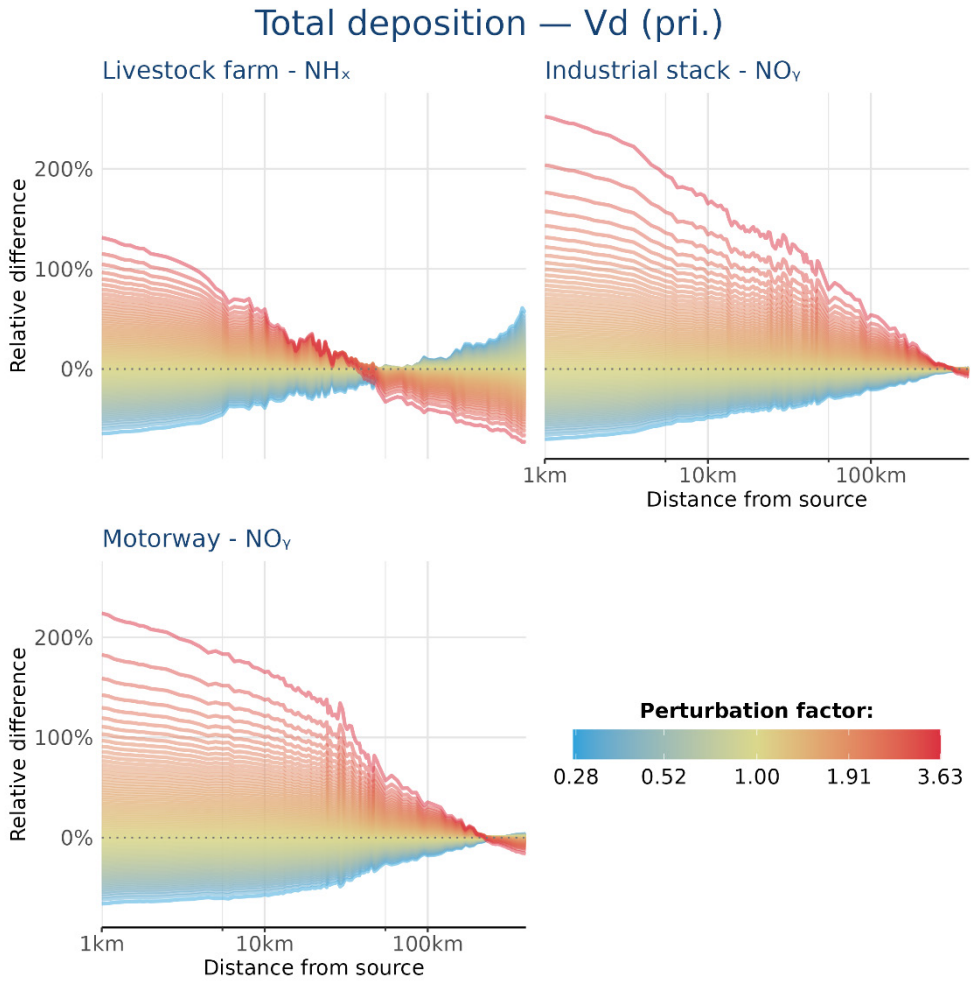


### 4.4.2 *Sensitivity to* $\sigma_z$

A change in vertical dispersion length ($\sigma_z$) has several effects:

- Increasing $\sigma_z$ yields deeper plumes. The plume depth affects dilution of the plume and thus impacts the concentration directly. Depending on the receptor location, this can result in higher or lower concentrations:
  - An increased $\sigma_z$, and hence a deeper plume, can lead to higher concentrations if the receptor was outside the plume for the reference run while it was inside the plume for the increased $\sigma_z$ run. However, if the receptor was already near or at the plume axis, a deeper plume, which is more diluted, will reduce the concentration.
  - A reduced $\sigma_z$, and hence a shallower plume, can lead to lower concentrations if the receptor height is no longer reached in the reduced $\sigma_z$ run, or is more towards the edge of the plume. Higher concentrations will be found if the receptor was already near or at the centre of the plume.

- Such effects cause a high sensitivity, especially of concentration, typically within ~10 km from the source (Figure 4.12; Figure 4.3, Figure 4.5 and Figure 4.7). For the low sources, the dilution effect is most important. For the high source, very near the source, the location of the receptor height with respect to the plume height is more important, followed by the dilution effect at slightly greater distances. At greater distances, a crossover point may be reached (see below).
- In the first order, the effect on dry deposition follows the effect on concentration (Figure 4.13). However, there is some modulation by plume characteristics as influenced by $\sigma_z$. Deeper plumes are reflected at the surface and top of the boundary layer at shorter distances, compared to the reference run, and vice versa. This affects source depletion and dry deposition at the receptor, which in turn is affected by the distance at which deposition starts. Vertical dispersion length, combined with mixing height, also impacts the so-called phase of the plume: not yet well-mixed (phase 2) versus well-mixed (phase 3), respectively. The distance at which phase-2 transitions to phase 3 decreases with increasing $\sigma_z$. At a given concentration, the source depletion is expected to be less when $\sigma_z$ increases, and vice versa, because the deposition velocity is larger in phase 2 than in phase 3. The impact of source depletion on concentration causes a crossover point at greater distances, which is also seen in the dry deposition at the receptor.
- The distribution between washout (below cloud) and rainout (in cloud) directly depends on $\sigma_z$. The relative contribution from rainout increases faster with distance when $\sigma_z$ is increased, and vice versa. This impacts the wet deposition, since wet deposition by rainout is larger than by washout. Increased $\sigma_z$ will, therefore, result in a higher wet deposition loss, because of the increased contribution from rainout, and vice versa (Figure 4.14). However, the total loss due to wet deposition also depends on the travel time, which is inversely proportional to the wind speed at the height of the plume axis averaged over the trajectory. Since wind speed in the atmospheric boundary layer usually increases with height, the travel speed also increases with increasing $\sigma_z$, as this parameter affects the plume height after reflection. Hence, the impact on the source depletion factor due to wet deposition is small.
- Sensitivity to total deposition carries the signature of both wet and dry deposition (Figure 4.15). The impact on depletion due to dry deposition tends to cause crossover points. The impact of wet deposition moves the crossover point somewhat closer to the source, which can be seen most clearly for the low sources of the livestock farm and motorway. The distance of the crossover point increases with decreasing $\sigma_z$.

*Figure 4.12 Relative difference in concentration compared to the reference run (average over the various directions) when varying vertical dispersion length $\sigma_z$ (%). Top row: livestock farm $NH_3$; middle row: industrial stack $NO_x$; bottom row: motorway $NO_x$.*

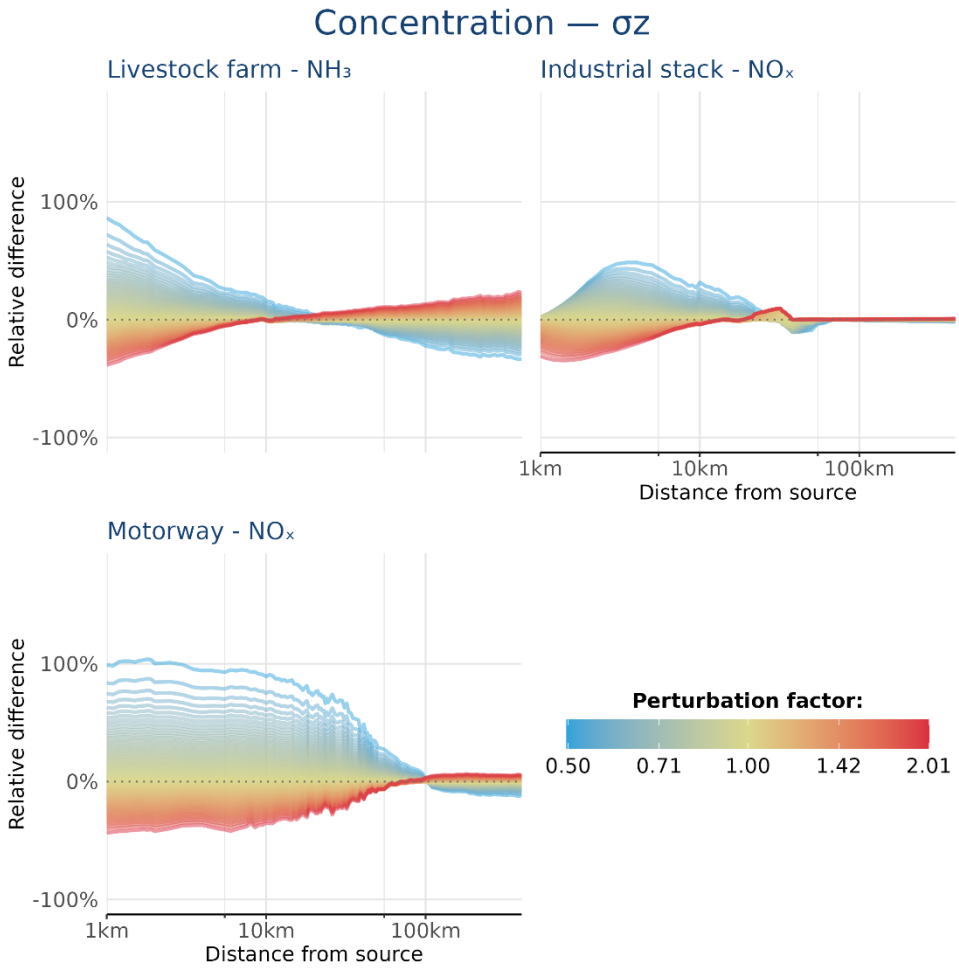

*Figure 4.13 Relative difference in dry deposition compared to the reference run (average over the various directions) when varying vertical dispersion length $\sigma_z$ (%). Top left: livestock farm $NH_x$; top right: industrial stack $NO_y$; bottom: motorway $NO_y$.*

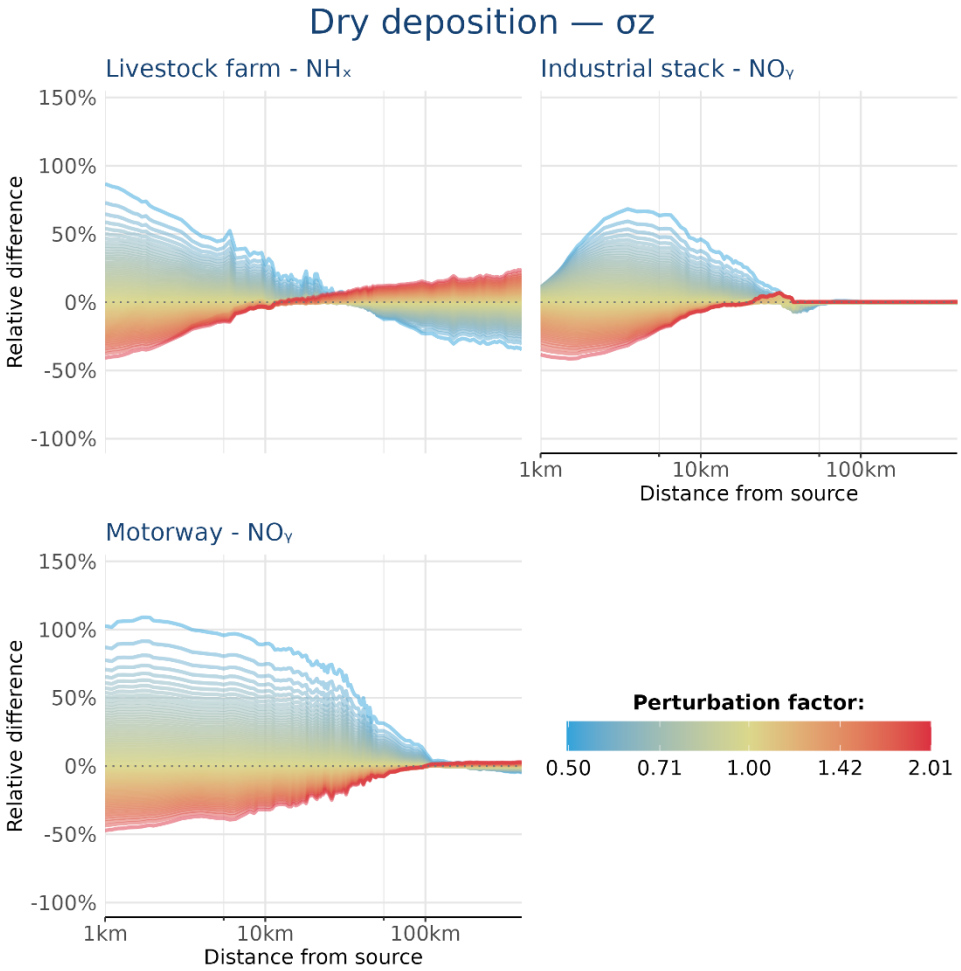

*Figure 4.14 Relative difference in wet deposition compared to the reference run (average over the various directions) when varying vertical dispersion length $\sigma_z$ (%). Top left: livestock farm $NH_x$; top right: industrial stack $NO_y$; bottom: motorway $NO_y$.*

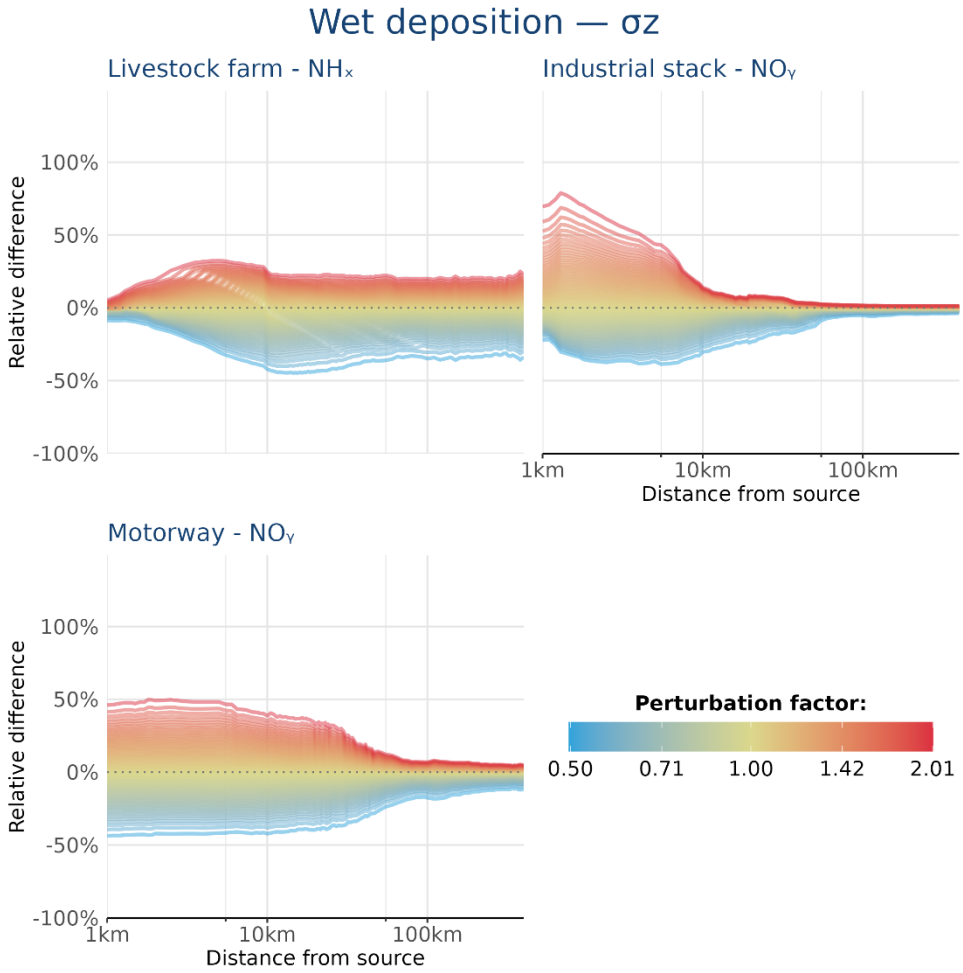

*Figure 4.15 Relative difference in total deposition compared to the reference run (average over the various directions) when varying vertical dispersion length $\sigma_z$ (%). Top left: livestock farm $NH_x$; top right: industrial stack $NO_y$; bottom: motorway $NO_y$.*

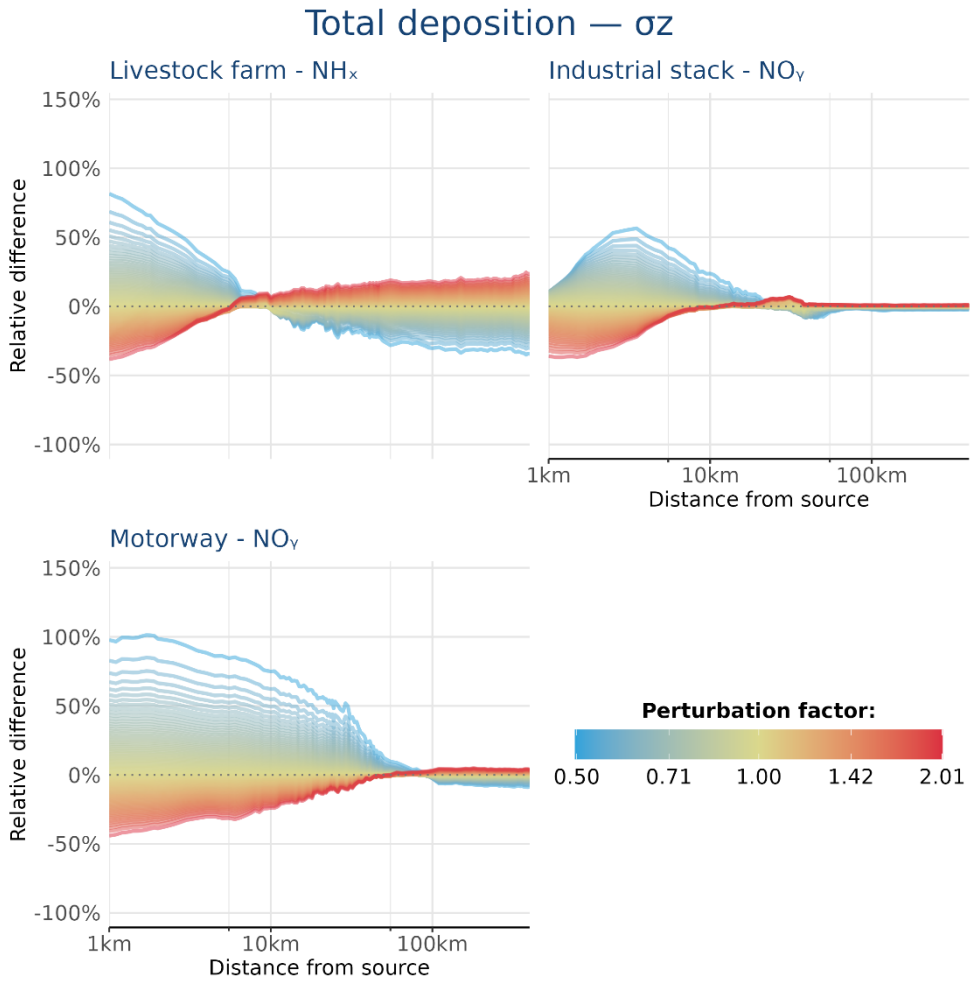


### 4.4.3 *Sensitivity to $z_i$*

A change in mixing layer height ($z_i$) has several, sometimes highly non-linear, effects.

- The volume in which pollutants are mixed is affected. With increased $z_i$, pollutants will generally be more diluted than with decreased $z_i$. This is basically what is visible in Figure 4.16, near the two lower sources (livestock farm, motorway), which may be assumed to emit within the atmospheric boundary layer. The impact is maximum at some distance from the source when the plume depth reaches $z_i$. At greater distances, a crossover point may be reached (see below).
- The pattern for the industrial stack is much more complex. Upon emission, the plume height (including plume rise) may exceed $z_i$. Obviously, the fraction of pollutant emitted above the boundary layer is influenced by $z_i$. As such, lower $z_i$ may cause lower concentrations near the source, and vice versa. At distances further from the source, mixing layer growth may cause entrainment of pollutant from above the mixing layer. In the case

of the industrial stack, this interplay between emission within or above $z_i$ and subsequent entrainment of emitted material, combined with the aforementioned dilution effect, leads to the complex sensitivity pattern displayed in the first 80 km (see Figure 4.16).

- For plumes emitted below $z_i$, the distance at which reflection at the top of the boundary layer height occurs is greater (increased $z_i$) or smaller (decreased $z_i$). Therefore, it may also take longer or shorter, respectively, before the plume becomes well mixed. The plume height and hence plume speed are influenced as well. In general, increased $z_i$ results in higher plume heights and speeds.
- In OPS, the ratio of emission height including plume rise to $z_i$ determines how vertical dispersion length and wind speed at plume height are computed. This results, sometimes strongly, in non-linear effects of $z_i$ on $\sigma_z$. For example, an in-depth analysis regarding the livestock farm revealed that for strongly stable conditions, $\sigma_z$ decreases if $z_i$ increases, whereas for less stable to unstable conditions, $\sigma_z$ increases with increasing $z_i$ (not shown here). For the industrial stack, non-linear effects were found even within the same stability class, or a reversal of effects across distance. It is beyond the scope of the present report to analyse such effects in detail. However, it is clear that they strongly contribute to the complexity of the sensitivity patterns (Figure 4.16 - Figure 4.19) and render interpretation of the sensitivity to $z_i$ an extremely difficult task.
- Source depletion due to dry deposition in the not yet well-mixed phase of the plume shows non-linear impacts similar to the aforementioned ones. For the livestock farm, for instance, source depletion due to dry deposition when the plume is not yet well mixed increases with increasing $z_i$ for strongly stable conditions but decreases for less stable and unstable conditions. Less source depletion due to dry deposition in well-mixed plumes is found for increased $z_i$. Yet, the relative impact of $z_i$ on dry deposition at the receptor is – roughly – similar to the relative impact on concentration for the lower sources (livestock farm, motorway). For the industrial stack, results are more variable again, due to the many non-linear interactions (Figure 4.17).
- The relative contribution from washout (below cloud) and rainout (within cloud) depends on $z_i$ as well as on $\sigma_z$. The contribution from rainout increases faster with *decreasing* $z_i$ and the other way around. This in turn leads to higher loss rates for decreased $z_i$ and lower ones for increased $z_i$ (Figure 4.18). Although the average wind speed and hence travel time is also affected by $z_i$, this does not fully compensate the initial impact on loss rate in this case (cf. effect of $\sigma_z$). At greater distances, a crossover point may be reached for wet deposition at the receptor due to the impact of source depletion on the atmospheric concentration.
- Total deposition roughly carries the signature from dry deposition, with somewhat stronger modulation by wet deposition at greater distances (Figure 4.19).
- The many non-linear interactions may be expected to add to the relatively large contribution of the uncertainty in $z_i$ to the total uncertainty (Figure 4.3, Figure 4.5, Figure 4.7).

*Figure 4.16 Relative difference in concentration compared to the reference run (average over the various directions) when varying the boundary layer height $z_i$ (%). Top row: livestock farm $NH_3$; middle row: industrial stack $NO_x$; bottom row: motorway $NO_x$.*

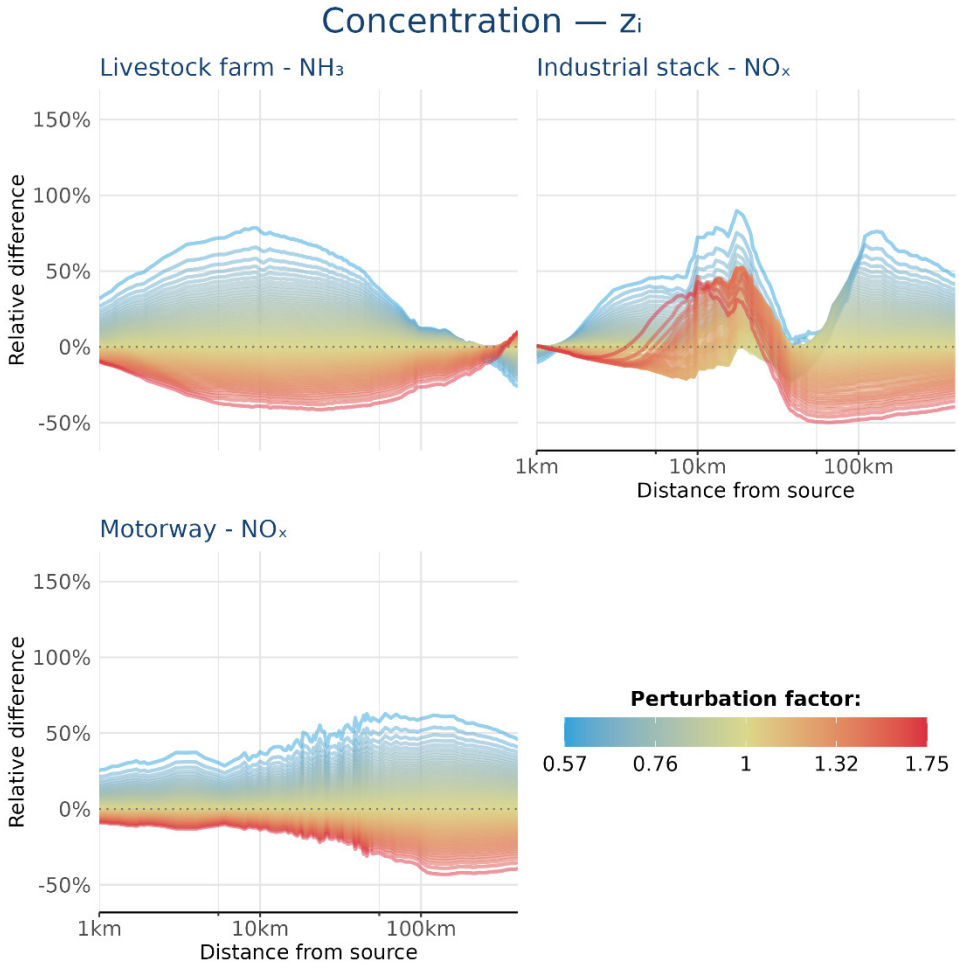

*Figure 4.17 Relative difference in dry deposition compared to the reference run (average over the various directions) when varying the boundary layer height $z_i$ (%). Top left: livestock farm $NH_x$; top right: industrial stack $NO_y$; bottom: motorway $NO_y$.*

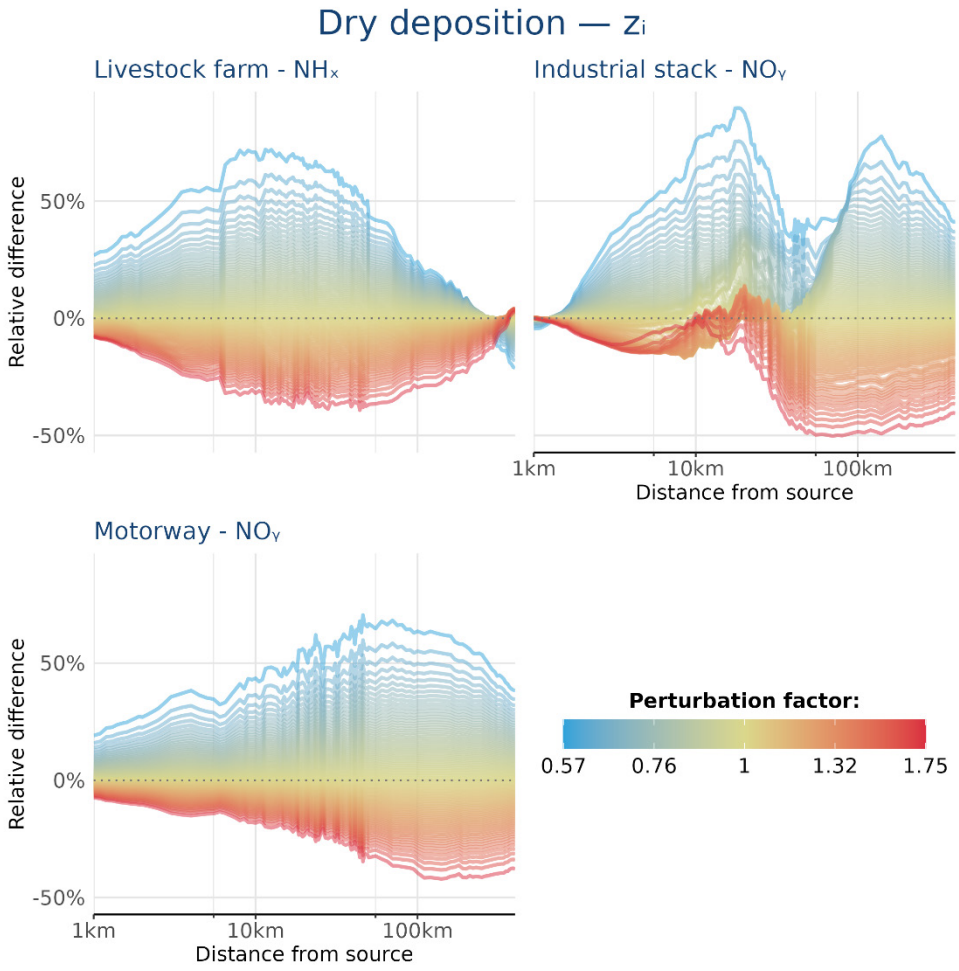

*Figure 4.18 Relative difference in wet deposition compared to the reference run (average over the various directions) when varying the boundary layer height $z_i$ (%). Top left: livestock farm $NH_x$; top right: industrial stack $NO_y$; bottom: motorway $NO_y$.*

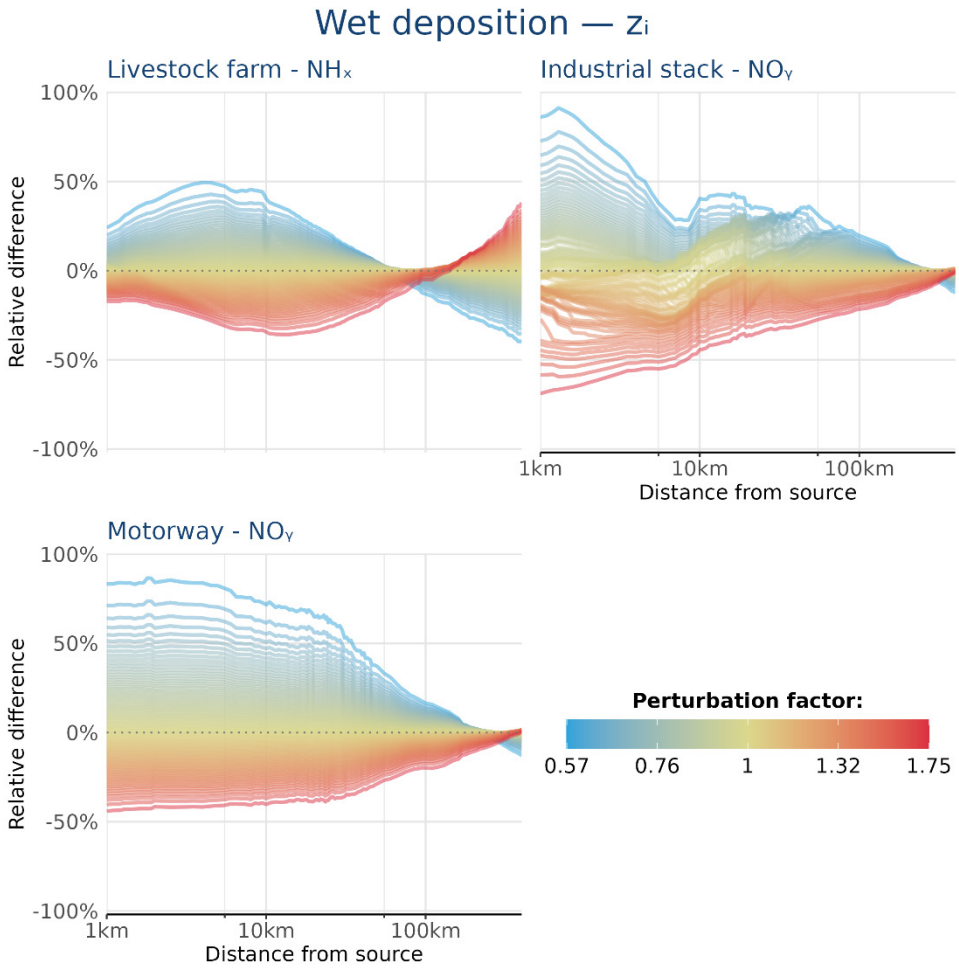

*Figure 4.19 Relative difference in total deposition compared to the reference run (average over the various directions) when varying the boundary layer height $z_i$ (%). Top left: livestock farm $NH_x$; top right: industrial stack $NO_y$; bottom: motorway $NO_y$.*

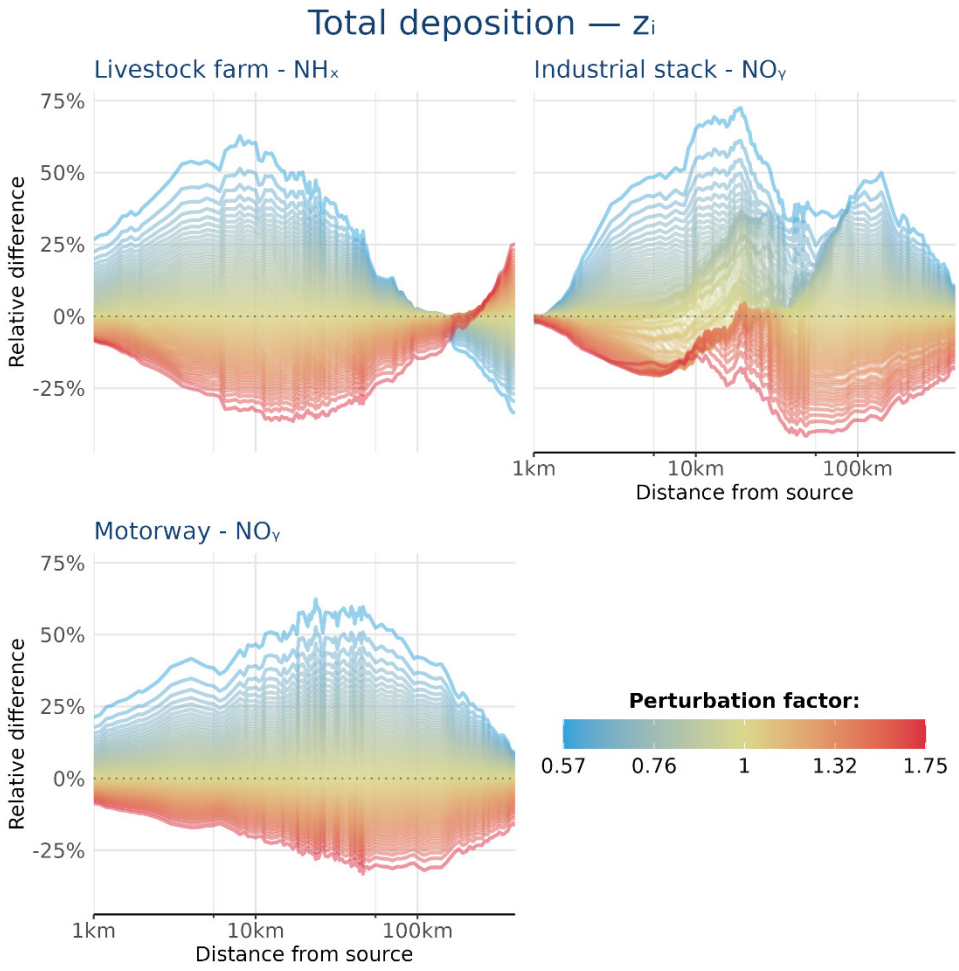


### 4.4.4 *Sensitivity to $k_{chem}$*

The effect of a change in chemical conversion rate, $k_{chem}$, is more straightforward than the parameters described so far. Since $k_{chem}$ controls conversion of primary to secondary compounds, we explicitly retain some information on secondary components in this case. Altering $k_{chem}$ has the following effects:

- Increasing $k_{chem}$ reduces the atmospheric concentration and hence deposition of the primary emitted material and vice versa. In the present – Lagrangian – framework, the effect of $k_{chem}$ on the concentration of primary material can, to first order, be described by an exponential decay. Hence, relative differences between runs can also be described by an exponential function, with the difference in chemical conversion rate being the time constant. This principle is clearly recognised in the left-hand panels of Figure 4.20, showing that differences are smaller near the source and increase with increasing distance. This also explains that the contribution of uncertainty in $k_{chem}$ to the total uncertainty is apparent at greater distances only (Figure 4.3,

Figure 4.5 and Figure 4.7). Second-order effects occur due to other removal processes (dry and wet deposition) and variations in $k_{chem}$ and wind speed among the receptor spokes.

- With higher $k_{chem}$, more secondary material is formed and vice versa (Figure 4.20, right-hand panels). This is complementary to the decay of primary material. Therefore, first-order effects of $k_{chem}$ on formation and concentration of secondary compounds also follow an exponential function, complementary to the one of primary compounds. Hence, the largest relative differences are obtained near the source and decrease with increasing distance. Again, second-order effects are due to other removal processes (dry and wet deposition) and variations in $k_{chem}$ and wind speed among the receptor spokes.
- For primary as well as secondary material, dry deposition is strongly linked to atmospheric concentration. The sensitivity of dry deposition roughly follows the sensitivity of their respective concentrations (Figure 4.21). The dry deposition of their combination ($NH_x$ or $NO_y$) is obviously a combination of the individual effects:
  - For the livestock farm, the sensitivity of the sum of dry deposition of primary and secondary components roughly follows the one of concentration of the primary component. However, compared to concentrations, the sensitivities are somewhat reduced, due to the opposing signal of the secondary component. This is likely to be caused by the more efficient dry deposition of $NH_3$ compared to $NH_4^+$.
  - For the industrial stack and motorway, the sensitivity of the $NO_y$ dry deposition increases with distance. However, differences have the sign of the concentration differences of the secondary material: increasing $NO_y$ dry deposition with increased $k_{chem}$, and vice versa. Hence, the sensitivity of $NO_y$ dry deposition to $k_{chem}$ is mainly driven by dry deposition of secondary material.
  - Strong fluctuations in sensitivity are obtained, due to the contribution from secondary components. The fluctuations are most pronounced for the $NO_y$ runs.
- Wet deposition is also strongly linked to the concentrations, or masses, of the compounds in the atmospheric column. Different impacts are obtained for $NH_x$ and $NO_y$, respectively, with differing contributions from primary and secondary material.
  - Wet deposition is quite effective for both $NH_3$ and $NH_4^+$ but is more effective for the latter component. This causes a rather strong effect on the sensitivity of wet deposition of $NH_x$ to $k_{chem}$ (Figure 4.22, upper left panel). On the one hand, the individual contributions by $NH_3$ and $NH_4^+$ tend to compensate each other, leading to smaller-range relative differences than for concentration at greater distances (cf. Figure 4.20). On the other hand, the sign of the sensitivity follows the one of the $NH_4^+$ concentration, which is opposite to the one of $NH_3$ concentration. The impact of $NH_4^+$ also becomes apparent as the local maximum in the sensitivity at about 10 km.
  - Sensitivity of $NO_y$ wet deposition is mainly driven by $HNO_3$+$NO_3^-$ (Figure 4.22, upper right and lower left panels).

This is explained by the low solubility of $NO_x$, which renders $NO_x$ removal by wet deposition an inefficient process.

- In the total deposition of $NH_x$ further compensation can be recognised between dry and wet deposition. Its sensitivity is limited to within a few (~5) percent (Figure 4.23, upper left panel; see also Figure 4.3, right-hand panel). In the case of $NO_y$ total deposition, the dominant role of dry deposition can be recognised. However, at greater distances, a clear contribution from wet deposition can be distinguished, by means of the gradually increasing sensitivities, to values higher than the ones for dry deposition alone (Figure 4.23, upper right and lower left panels).

*Figure 4.20 Relative difference in concentration compared to the reference run (average over the various directions) when varying the chemical conversion rate $k_{chem}$ (%). Top row: livestock farm $NH_3$ and $NH_4$; middle row: industrial stack $NO_x$ and $NO_3^-$+$HNO_3$; bottom row: motorway $NO_x$ and $NO_3^-$+$HNO_3$.*

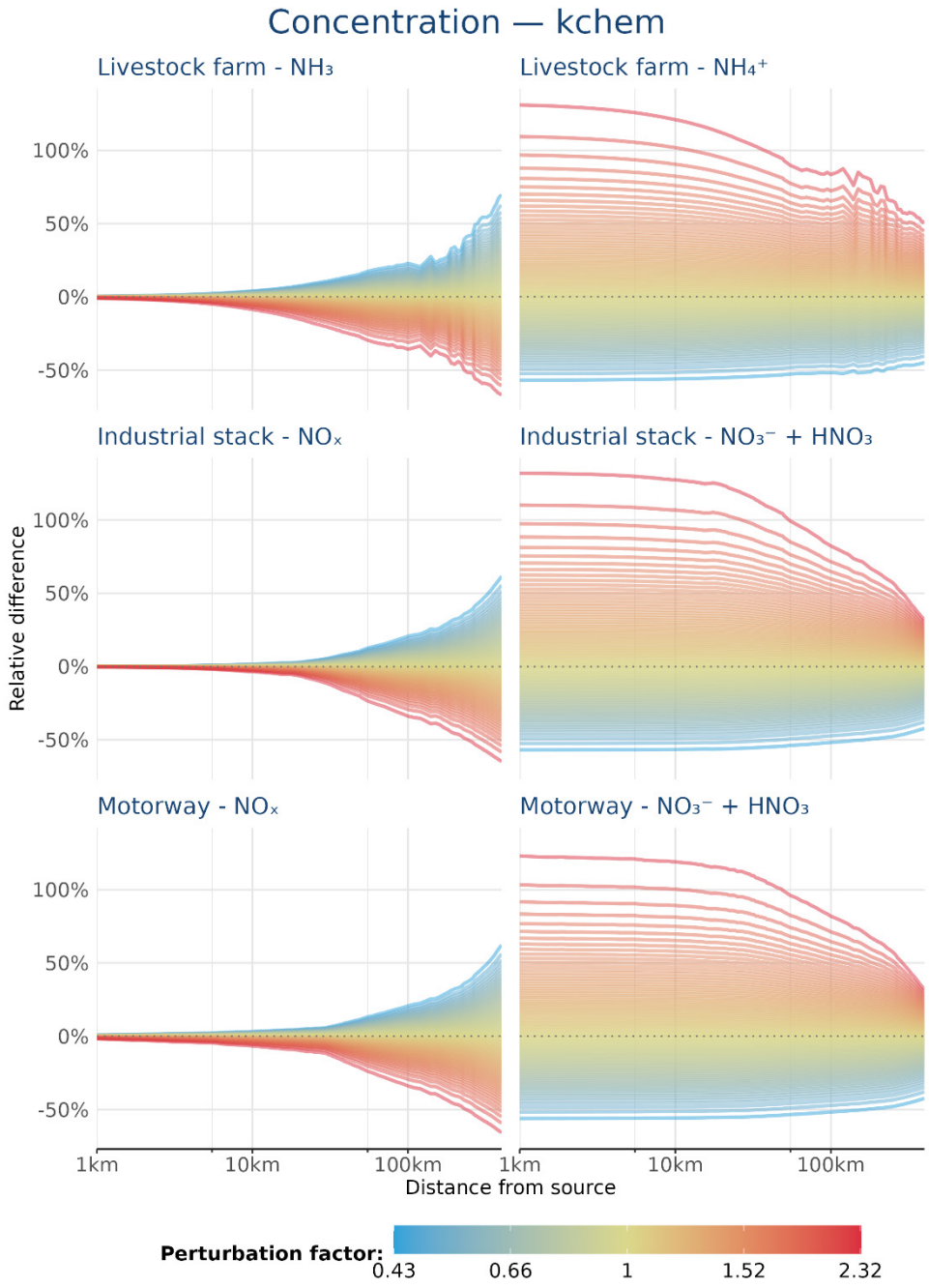

*Figure 4.21 Relative difference in dry deposition compared to the reference run (average over the various directions) when varying the chemical conversion rate $k_{chem}$ (%). Top left: livestock farm $NH_x$; top right: industrial stack $NO_y$; bottom: motorway $NO_y$.*

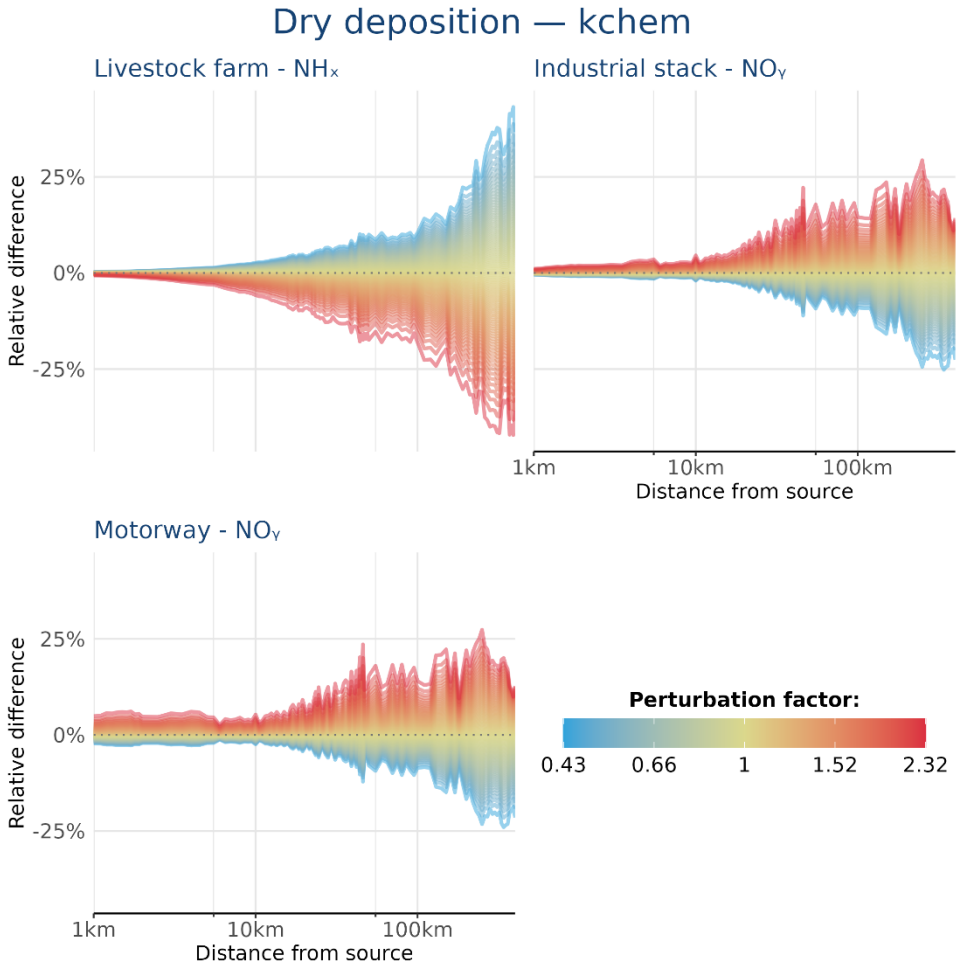

*Figure 4.22 Relative difference in wet deposition compared to the reference run (average over the various directions) when varying the chemical conversion rate $k_{chem}$ (%). Top left: livestock farm $NH_x$; top right: industrial stack $NO_y$; bottom: motorway $NO_y$.*

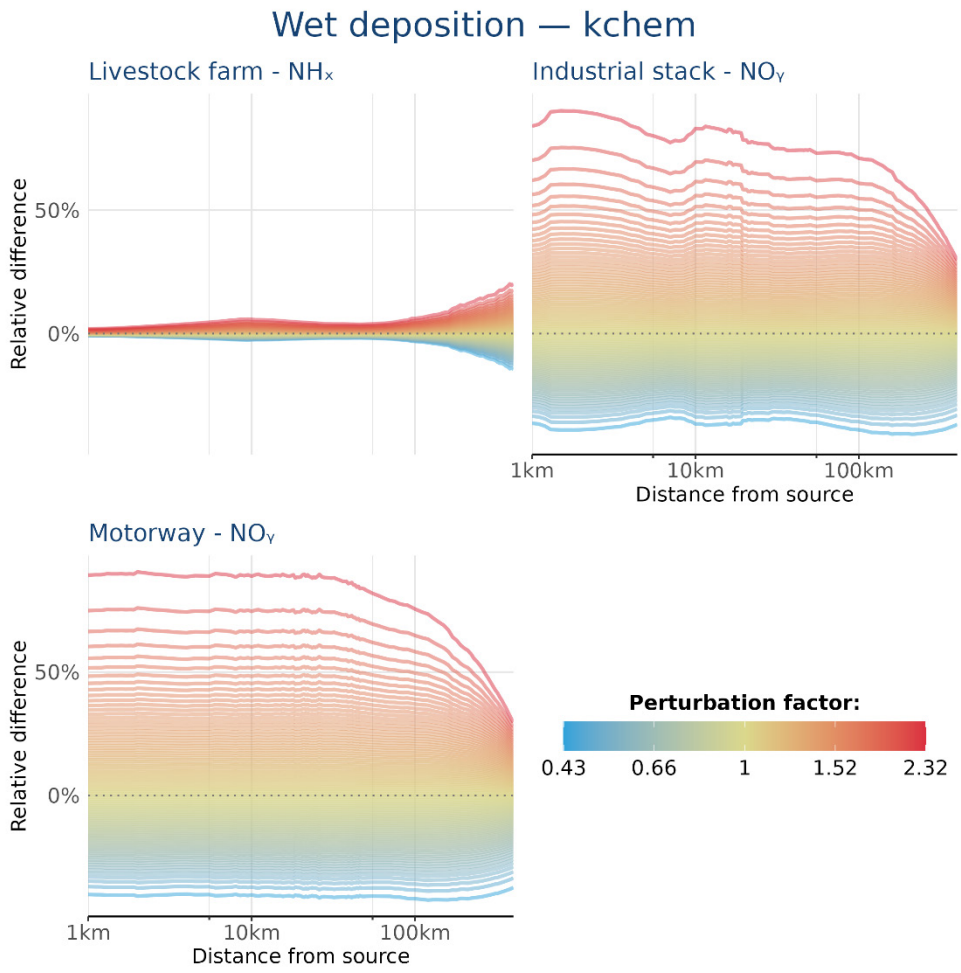

*Figure 4.23 Relative difference in total deposition compared to the reference run (average over the various directions) when varying the chemical conversion rate $k_{chem}$ (%). Top left: livestock farm $NH_x$; top right: industrial stack $NO_y$; bottom: motorway $NO_y$.*

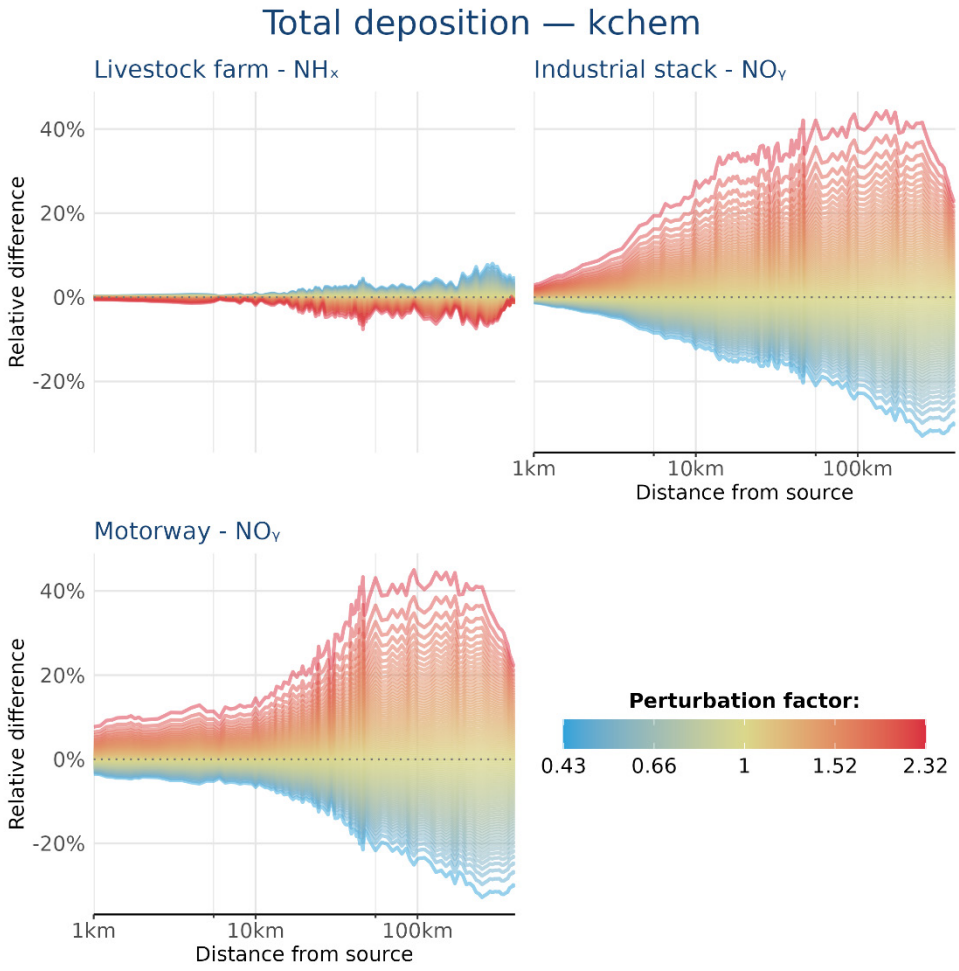


### 4.4.5 *Sensitivity to* Meteo

- Treatment of Meteo is very important, since meteorological conditions are used to construct the trajectories, including their properties. They may affect a suite of processes at once, locally at the receptors and along the trajectories. Important examples are (see Table 4.1 as well): a change in wind speed has a strong effect on friction velocity, $u_*$, which is used as a scaling parameter in the description of surface-atmosphere interactions. As such, wind speed indirectly influences many other, $u_*$-related parameters, such as mixing layer height ($z_i$), vertical dispersion length ($\sigma_z$) and deposition velocity ($v_{d,pri}$ and $v_{d,sec}$). In general, the magnitude of these parameters reduces with decreasing wind speed. This results in higher concentrations, but the magnitude of the effect depends on concurrent changes in other weather conditions as well (Figure 4.24).
- There is a tendency for higher deposition in the case of lower wind speed. This is because of the higher concentrations discussed before. However, since lower wind speeds also reduce

deposition velocity, the effect of higher concentrations is compensated. The latter is more important for $NH_x$, because $v_{d,pri}$ of $NH_3$ is much more sensitive to atmospheric conditions than of $NO_x$ in the case of $NO_y$ deposition (Figure 4.25).

- Wet deposition is strongly related to total mass in the atmospheric column. This explains why, in the case of the low sources, we see some similarities with the sensitivity of concentration: low wind speeds lead to higher concentration and hence, to more wet deposition (Figure 4.26). For the industrial stack, there is hardly any similarity to the patterns in concentration, because of the complex interactions between plume rise and source height, mixing layer development, and vertical dispersion (see previous sections). Because of these interactions, the relation between concentration and mass in the atmospheric column is complex. Effects for all source types are clearly modulated by precipitation effects, namely rainfall probability, intensity and event length. In the case of ammonia, this is most evident for AWS344, which is located in a relatively wet region of the Netherlands. While the concentration only showed moderate deviations from the reference case, up to a maximum of about 30% near the source (Figure 4.24, upper left), the maximum relative effect on wet deposition amounts to about 75% (Figure 4.26, upper left).
- Sensitivity patterns for total deposition look much like the ones for dry deposition (Figure 4.25 vs. Figure 4.27). This is in spite of the fact that relative differences in wet deposition are much larger (Figure 4.26). It confirms that, in absolute terms, dry deposition is the more important removal process in the cases studied here.
- Meteo influences many interactions between parameters. For example, the interaction between plume rise, vertical dispersion and mixing layer development may induce non-linear interactions that strongly affect the sensitivity to weather conditions. In addition, indirect effects may occur as well. For example, in the case of the livestock farm, temperature affects the source strength, with higher temperatures leading to somewhat larger emissions (see also Section 3.2.2). Finally, the statistical classification with respect to wind direction and stability will be affected. This has an important impact on many model parameterisations. Hence, it is no surprise that meteorological conditions are an important driver of uncertainty (Figure 4.3, Figure 4.5 and Figure 4.7).

*Table 4.1 Average wind speed, frequency of dominant wind sector (195-225 degrees in all cases), mixing layer height ($z_i$), friction velocity, air temperature, and precipitation intensity, event length and probability from the seven meteorological datasets, for distance Class 1 (local, 0-50 km). The averages have been determined based on the OPS pre-processor METPRO (Sauter et al., 2023), using measurements from KNMI stations in 2015.*

| Quantity | Reference | AWS260 De Bilt | AWS270 Leeuwarden | AWS290 Twenthe | AWS310 Vlissingen | AWS344 Rotterdam | AWS380 Maastricht |
|---|---|---|---|---|---|---|---|
| Wind speed (m/s) | 3.03 | 2.12 | 2.92 | 2.08 | 4.16 | 2.56 | 2.42 |
| Frequency wind sector 195-225° | 20.3% | 18.2% | 17.5% | 22.4% | 18.1% | 16.1% | 23.7% |
| $z_i$ (m) | 176 | 126 | 180 | 133 | 299 | 155 | 157 |
| Friction velocity (m/s) | 0.205 | 0.147 | 0.212 | 0.156 | 0.339 | 0.182 | 0.180 |
| Temperature (°C) | 10.7 | 10.9 | 10.3 | 10.5 | 11.5 | 11.1 | 11.1 |
| Precipitation | | | | | | | |
| - Intensity (mm/h) | 1.25 | 1.20 | 1.27 | 1.19 | 1.51 | 1.31 | 1.19 |
| - Event length (h) | 1.98 | 2.95 | 2.89 | 3.28 | 2.57 | 2.80 | 3.64 |
| - Probability (%) | 8.16 | 8.54 | 8.05 | 8.67 | 6.59 | 8.11 | 7.29 |

*Figure 4.24 Difference of concentration of primary components compared to the reference run when varying meteorological conditions. Upper left: livestock farm ($NH_3$); upper right: industrial stack ($NO_x$); lower left: motorway ($NO_x$).*

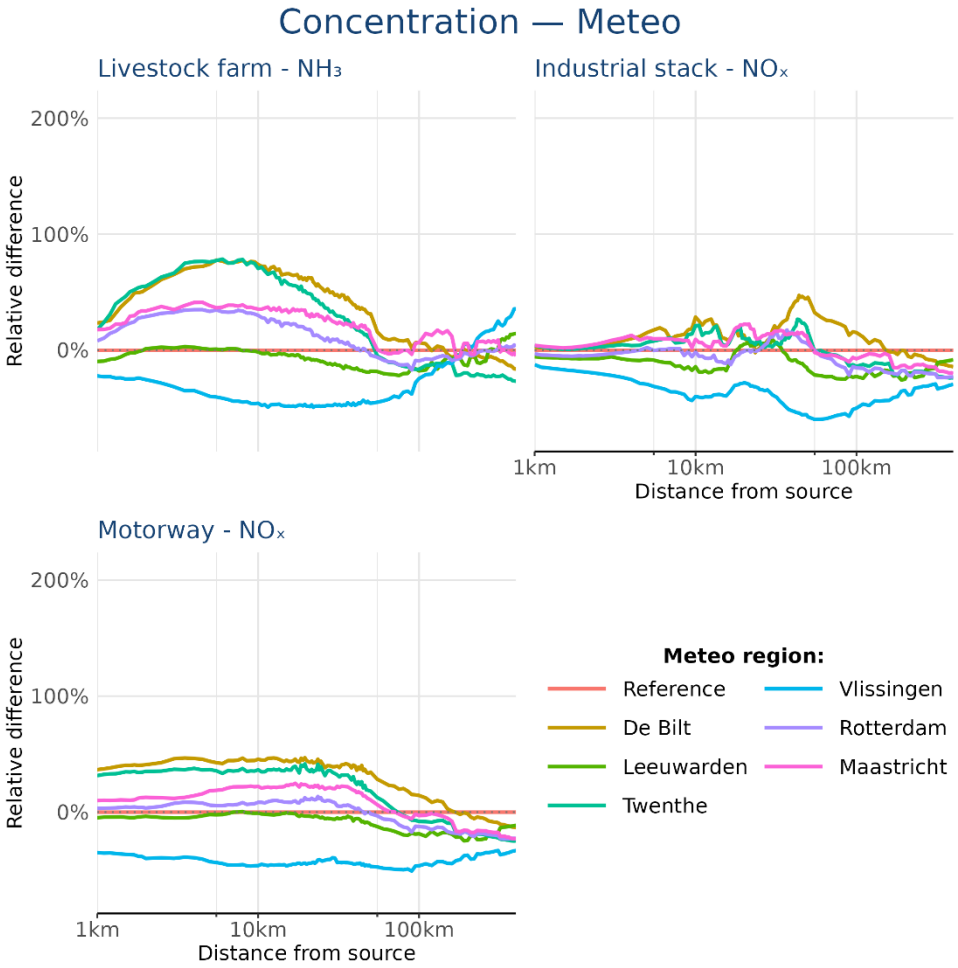

*Figure 4.25 Relative difference of dry deposition compared to the reference run, when varying meteorological conditions. Upper left: livestock farm $NH_x$; upper right: industrial stack $NO_y$; lower left: motorway $NO_y$.*

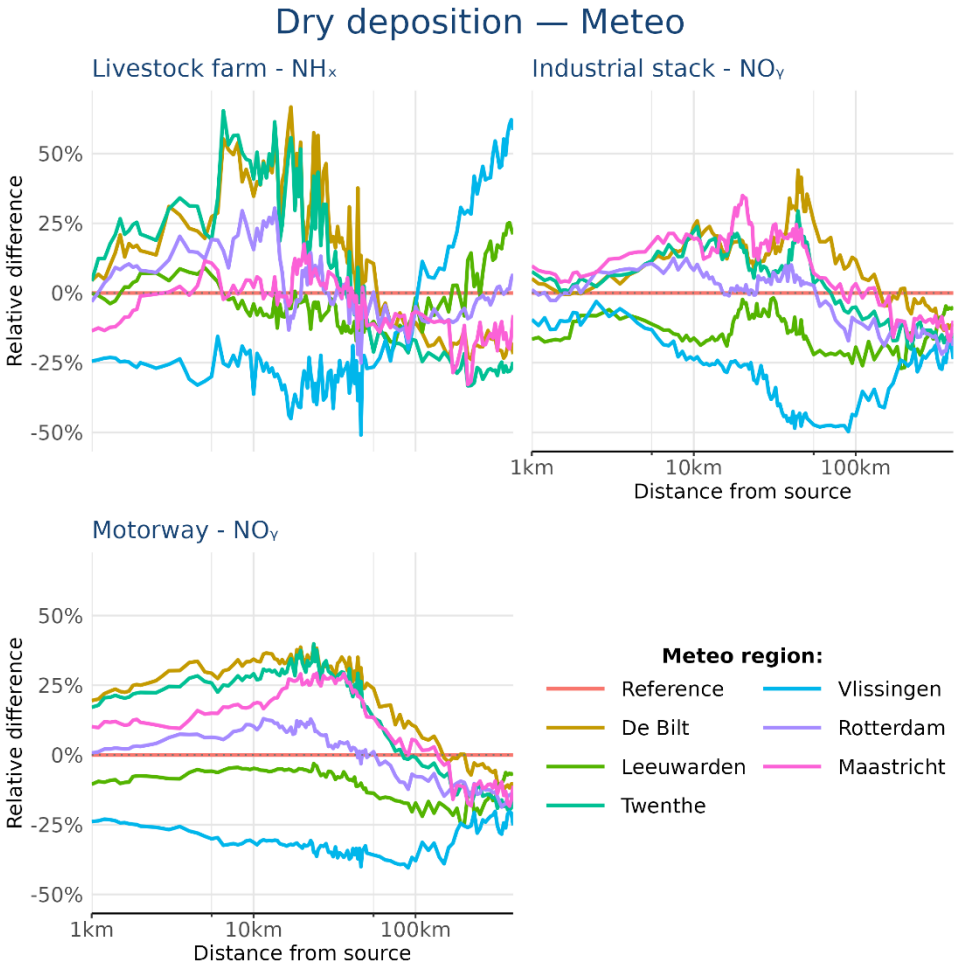

*Figure 4.26 Relative difference of wet deposition compared to the reference run, when varying meteorological conditions. Upper left: livestock farm ($NH_x$); upper right: industrial stack ($NO_y$); lower left: motorway ($NO_y$).*

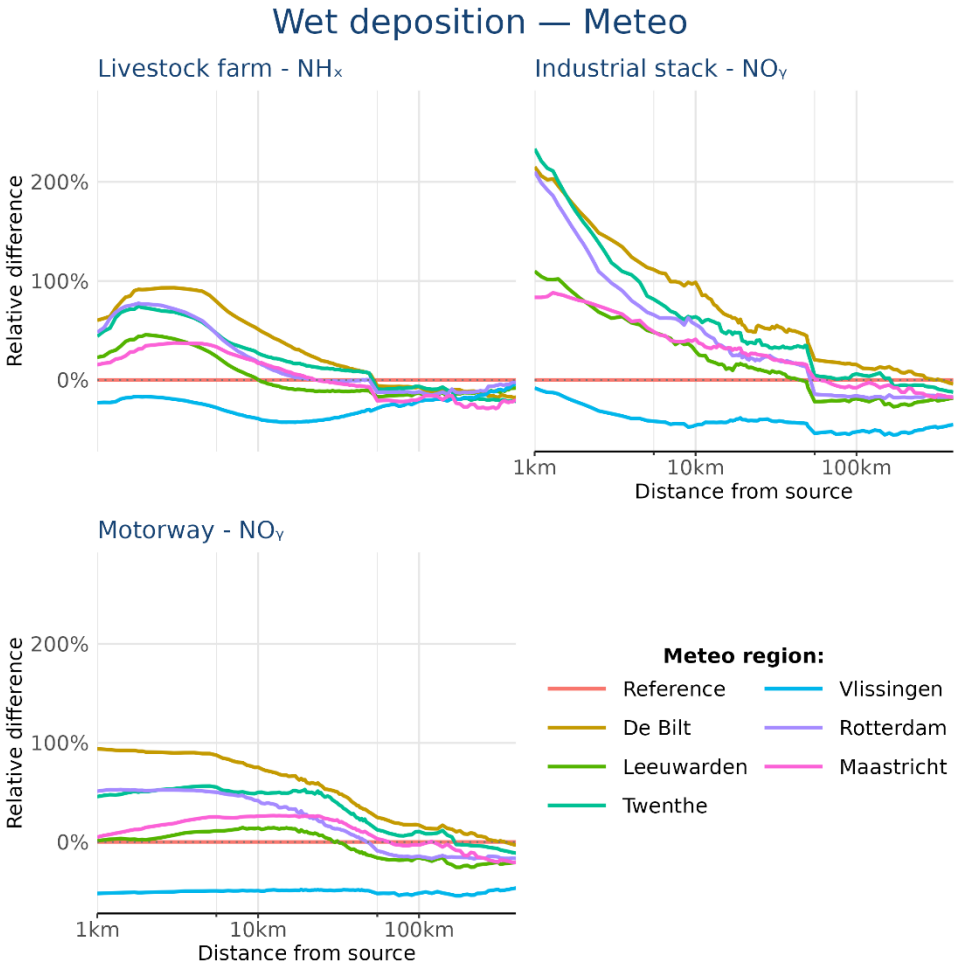

*Figure 4.27 Relative difference of total deposition compared to the reference run, when varying meteorological conditions. Upper left: livestock farm ($NH_x$); upper right: industrial stack ($NO_y$); lower left: motorway ($NO_y$).*

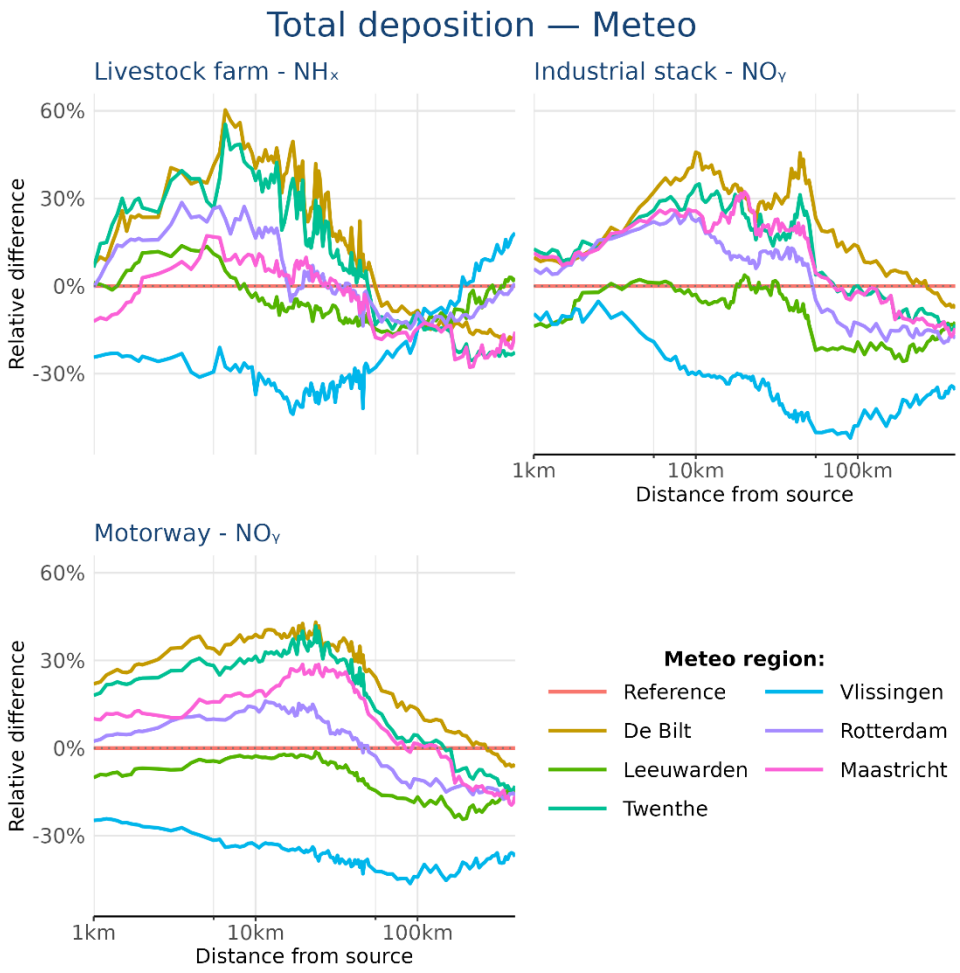


## 4.5 Results based on UAT

For all five thousand Monte Carlo drawings to estimate the sensitivity the modelled concentrations on the MAN locations are also calculated, using the UAT (see Section 3.6). This yields an RMSE between the modelled and measured concentrations. The purpose is to find out if any of the five thousand parameter combinations yields unrealistic results in the 'real world' and to examine their possible effect on the sensitivity results.

To illustrate this, Figure 4.28 shows the five thousand parameter combinations for plume rise and dry deposition velocity of $NH_3$ for the livestock farm case study. The colours used to plot the combinations indicate the magnitude of the RMSE, with more yellowish colours showing larger RMSE values. About 10% of the combinations lead to an RMSE larger than approximately 4 $\mu g/m^3$. The figure shows that these values are mainly localised in the upper right corner of the plot. Note that elsewhere in the picture high RMSE values also occur, presumably due to some of the other parameters. After removal of these high RMSE values, the bandwidth of the joint parameter distribution slightly decreases.

*Figure 4.28 Scatterplots showing a two-dimensional projection of the point cloud representing all of the five thousand sampled parameter combinations for plume rise ($\Delta h$) and dry deposition velocity of the primary material ($v_{d,pri}$) in the Monte Carlo analysis (left). By excluding parameter combinations leading to RMSE values above a given threshold (middle) the point cloud becomes narrower (right), corresponding to a reduced uncertainty bandwidth of the prior distributions.*

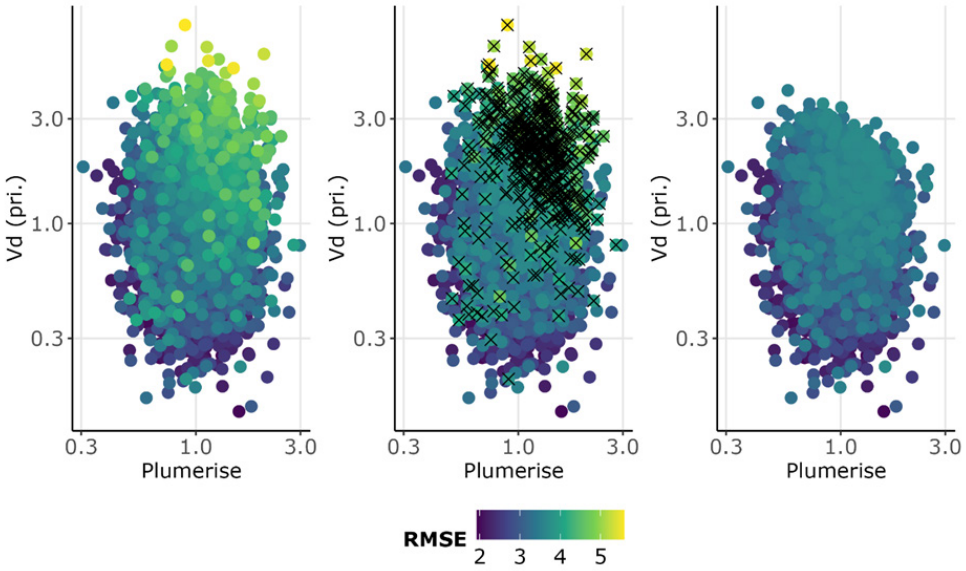

*Figure 4.29 Effect of removal of the 10 percent parameter settings with the highest RMSE's on the calculated CVs. The straight lines show the result with the original prior distribution of parameter uncertainties. The dashed lines show the result after elimination.*

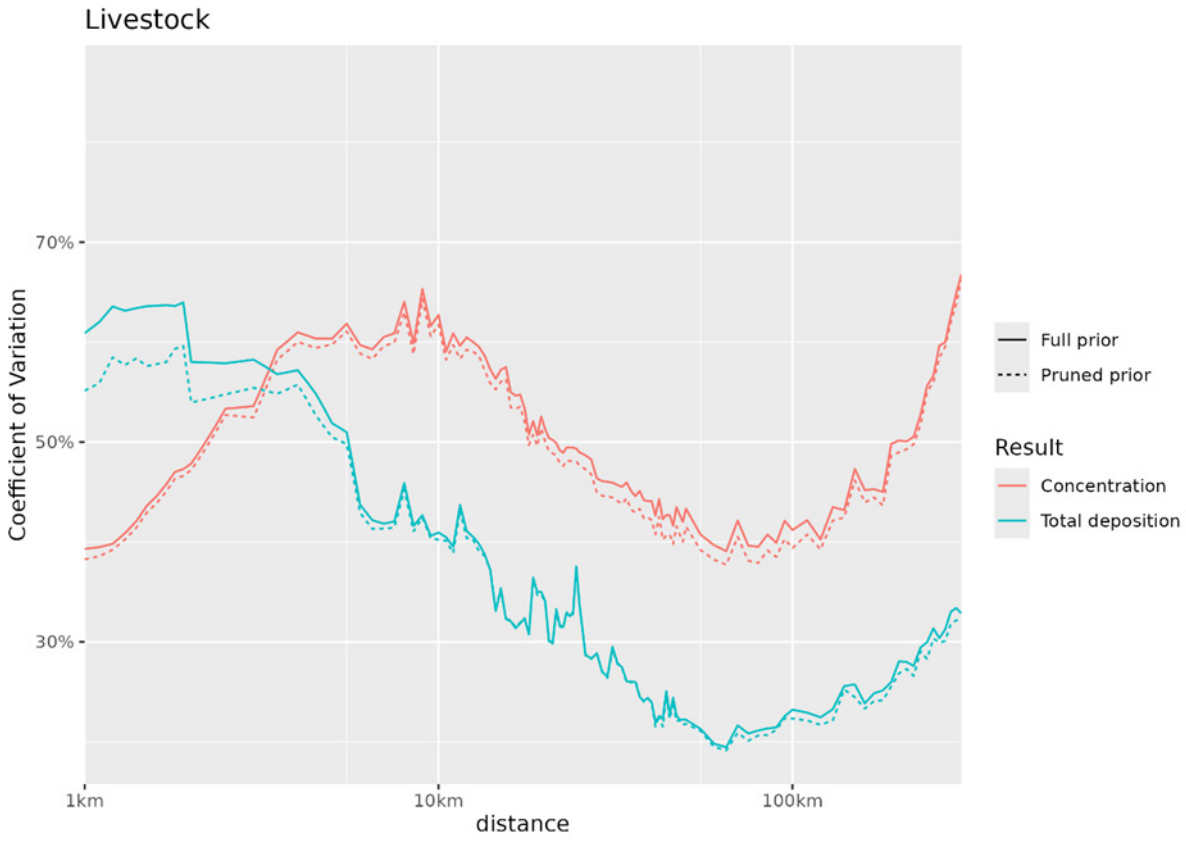


Figure 4.29 shows the effect of the removal of the 10% parameter settings with the highest RMSE. The effect on the uncertainty in the contribution from a single source is very small for greater distances and only slightly larger near the source. On the basis of this result, it is concluded that the results of this study are not extremely sensitive to a small portion of unlikely combinations. Such an evaluation by selective elimination, therefore, does not seem very fruitful in the context of the present study. However, a more comprehensive analysis of the likelihood of the various parameter settings is expected to yield useful information on the model parameters, emissions and uncertainties for simulations of real-world situations. Such an analysis is beyond the scope of the present work and is part of a study to be conducted in the near future.

# 5 Discussion

## 5.1 Discussion of this study

### *5.1.1 Study design*

In this report, we present an uncertainty assessment of contributions from an individual source of $NH_3$ or $NO_x$ to deposition and concentrations of nitrogen compounds at a great distance from the source, up to 400 km. The assessment has been conducted via a Monte Carlo-type sensitivity analysis of the OPS outcomes. On the basis of surveys in scientific literature and expert judgement, a selection was made of the set of the most important parameters to be investigated.

It is important to note that the selection was made in the context of the operational use of OPS. While the selection of the parameter set is to some extent similar to the set chosen in Abbott et al. (2003) and in Duyzer and Erbrink (2022), both studies being partially akin to the present one, there are also some differences because of the differing context. For example, uncertainty in deposition velocity, mixing layer height and scavenging rate are considered in all of the three studies. By contrast, chemical conversion rates, treated in a simplified way in the present study, were considered in quite some detail in Abbott et al. (2003), but were not varied in Duyzer and Erbrink (2022). Differences also reflect the various model characteristics. Although all three modelling approaches are Lagrangian in nature, the models applied by Abbott et al. (2003) apply a box model and a layered model, respectively, rather than a Gaussian plume formula. This allows them to study chemical processes in more detail, amongst other things. The model used by Duyzer and Erbrink (2022) applies a Gaussian approach, but without an extension with trajectories.

Uncertainty distributions of the selected input parameters have been identified on the basis of literature surveys, expert judgement, and sometimes additional data analyses. Parameter uncertainty is propagated in the model by randomly drawing combinations of parameter input values. The set of model outcomes is then statistically analysed. While the method is accepted as a reasonable approach to estimate uncertainty (e.g. Uusitalo et al., 2015) it should – again – be recognised that it is applied within the modelling context. The impact of unknown processes and alternative parameterisations cannot be assessed in this way, which is likely to lead to some underestimation of the uncertainty (Abbot et al., 2003). This is one of the reasons why we will assess our results in a wider context in Section 5.2, using results from other studies, which are partly based on other methods.

The list of parameters selected here is not exhaustive. Expanding it would probably lead to slightly higher estimates of the uncertainties than we obtained in the present study. On the other hand, the uncertainty distributions might have been too pessimistic regarding the uncertainty in some of the parameters. For example, in the uncertainty in chemical conversion rate, $k_{chem}$ has been derived assuming that all deviations between model outcomes and, a limited number of, observations are entirely due to $k_{chem}$.

In particular, if the uncertainty in input parameters is overestimated, random drawings of parameter values may lead to unrealistic sets of

input values. We examined the possible consequences of this in a combined study, in which we ran OPS with the five thousand sets of parameter values, using all emissions in the Netherlands and abroad. This allowed for a comparison to the measurements of the MAN (the Measuring Ammonia in Nature network). The results indicated that the uncertainties in the estimates for the single-source contribution are probably overestimated, although we are not yet able to quantify this further. Probabilistic assessment of overall uncertainty with comparison to measurements is considered an important method in uncertainty research (Abbott et al. 2003) and is foreseen in the near future.
The present research results show the uncertainties across the distance domain from 1000 m to 400 km. It should be stressed that the design of the study was aimed at distances from 20 to 400 km, with the lower boundary roughly corresponding to a typical hourly atmospheric travel distance at a wind speed of 5 m/s. This choice means that the results for very short distances in particular may not be entirely representative, especially regarding source configurations. For example, the uncertainty as a result of possible building effects and other obstacles was not explicitly included in this study. It is likely that the analysis based on a comparison to the measurements from the MAN has more added value for the greater distances than for short distances. After all, the MAN is mainly focused on nature reserves, and measurement locations close to a local source are avoided as much as possible.

### *5.1.2 Meteorological conditions*

Since calculations of transport, dispersion and deposition rely on modelling atmospheric processes, meteorological conditions may be an important source of uncertainty, albeit sometimes indirectly. In contrast with approaches that do not depend on trajectory calculations and where only wind speed and direction are varied (Abbott et al., 2003; Duyzer and Erbrink, 2022), we decided to vary complete meteorological datasets here, within the bounds of Dutch meteorological observations. This has the advantage that meteorological conditions are varied in a consistent way for all parameters involved. However, some limitations may be noted.
The way meteorological properties of the trajectories are currently implemented in OPS does strongly reduce variations of these properties among the trajectories. For example, the trajectory path for a plume exiting a source in the East of the Netherlands is the same as the path for a plume exiting a source in the West. Only slight differences in meteorological statistics due to the differing paths are obtained. In reality, different trajectories will be followed due to varying wind speeds and directions as well as to other meteorological conditions. Testing the sensitivity in OPS to this effect implies a major adjustment in the code and would be outside the scope of this study, which is based on the current operational version of OPS. The purpose of selecting meteorological stations that represent a comparatively large variation in meteorological conditions across the Netherlands was to obtain a large enough impact of meteorology for the present sensitivity analysis. The present setup results in relative differences up to several tens of percents, and noticeable contributions to the variance of the parameters. Efforts are underway to improve trajectory estimates, based on gridded output from weather forecasting models, but implementation of such a method also requires major code changes.

Another limitation is related to the current use of a limited number of fixed meteorology classes in OPS. The classes comprise six stability classes, twelve wind direction classes and four distance classes. On the basis of hourly data, the METPRO preprocessor divides the trajectories across these classes and calculates representative averages for a number of meteorological variables. As such, the temporal variation is reduced in the meteorological statistics. The choice in the number and types of classes affects the impact of the meteorological conditions on the model outcomes. For example, when including effects of *dv,* it might be desirable to use additional temperature classes. Also, the number of stability classes and wind direction classes could be increased to refine the statistical input. In this study, the sensitivity of the model outcomes to such choices could not be tested either, since this would imply too large a change in the code of OPS to enable tests in this regard.

### *5.1.3 Impact of deposition velocity*

The uncertainty in deposition velocity is quite large (e.g. Flechard et al., 2011; Schrader and Brümmer, 2014). This conclusion must lead to the use of quite a large uncertainty range in this parameter in studies like the present one. Hence, it is also no surprise that the present study confirms that uncertainty in deposition velocity of the primary components, $v_{d,pri}$, is the most important driver of uncertainty in nitrogen deposition, in particular near the source. In the case of $NO_y$ deposition, it is a dominant source of uncertainty within approximately the first 50 km from the source, for $NH_x$ deposition up to about 10 km from the source. In the case of $NH_x$, uncertainty in $v_{d,pri}$ is also an important cause of uncertainty in concentration far from the source. The importance of this parameter was also reported by Abbott et al. (2003) for $SO_2$, albeit at a greater distance from the source, and for oxidised nitrogen very close to the source, within a few tens of kilometres. These authors found that, in the latter case, uncertainty in details of chemical conversion rates, wind speed and wind direction and wet deposition of aerosols became the most important source of variance at the distance at which the maximum deposition of oxidised nitrogen occurred (200-300 km from the source). At such distances, the impact of $v_{d,pri}$ on $NO_y$ deposition has also virtually disappeared in the present study, and important drivers of uncertainty are $k_{chem}$, and *Meteo*, along with $z_i$. Duyzer and Erbrink (2022) also conclude that uncertainty in deposition velocity is the most important driver of the variance of $NH_3$ deposition, but note that such an impact is almost absent for $NO_x$ deposition. They explain the latter finding by the much lower deposition velocity of $NO_x$. However, we argue that they might have referred to *absolute* variances, since the *relative* sensitivity of $NO_y$ deposition to $v_{d,pri}$ must initially be strongly related to that parameter. This is particularly the case near the source, where not much depletion by any mechanism has occurred yet. Also, note that in Duyzer and Erbrink (2022), depletion across the trajectory due to dry deposition and local deposition velocity were varied independently and used different uncertainty ranges.

In this study, we found that sensitivity of nitrogen deposition to $v_{d,pri}$ reduces at distances further away from the source and may then increase again, beyond the crossover point. This behaviour is consistent with the atmospheric feedback mechanism, by which increased $v_{d,pri}$ leads to reduced concentration and vice versa. This mechanism requires

time to become noticeable. Thus, it is effective at larger spatial scales only, typically 10 km or more. Ultimately, it leads to a crossover point, around which the sensitivity of deposition to $v_{d,pri}$ is strongly reduced.
Although the results regarding the impact of $v_{d,pri}$ are in agreement with results from other studies, some explanatory remarks are in place.
First, although the mechanism of the compensation seems straightforward at first sight, it is complex in reality, due to the possible role of the secondary components and $v_{d,sec}$. Their impact on relative differences due to changes in $v_{d,pri}$ is clearly visible at greater distances. However, not only is estimation of chemical conversion a difficult task in the context of Gaussian plume models (Dore et al., 2015, Van Der Swaluw et al., 2021), $v_{d,sec}$ is quite uncertain as well (Hoogerbrugge et al., 2023).
Second, for practical reasons, in the present study, $v_{d,pri}$ as well as $v_{d,sec}$ has been perturbed with the same factor for all land use types. To explore the implications of this choice, a theoretical analysis was performed with land use-dependent perturbations of $v_{d,pri}$ in heterogeneous landscape, consisting of 20% forest and 80% grassland (Appendix 3). It was found that the choice to use the same perturbation factor of $v_{d,pri}$ for both has a noticeable, but limited effect on the estimated uncertainty, as long as the perturbations have the same sign for the two landscape types (see Appendix 3 and Section 5.2). The latter assumption is not unreasonable for natural vegetation, of which $v_{d,pri}$ is driven by the same large-scale phenomena, such as precipitation, temperature, humidity, and solar radiation. Anomalies in such drivers would lead to similar anomalies of –at least partly overlapping – eco-physiological drivers of $v_{d,pri}$. For example, lack of precipitation in a region would lead to large-scale drought. Ultimately, such a precipitation anomaly would have similar effects on soil moisture, atmospheric humidity and temperature, and hence on leaf wetness and surface resistance of both grassland and forest. Thus, effects of such changes are expected to go in the same direction for all the natural vegetation in the Netherlands, albeit with differing response times and end points (cf. Hoek van Dijke et al., 2023).
Third, depletion will have an impact on the concentration profile in the lower atmosphere, the surface layer. In OPS, this effect depends on the distance from the source and the timescale at which the profile adjusts to the standard atmospheric theories on surface-atmosphere exchange (Sauter et al., 2023). The timescale of adjustments depends on $v_{d,pri}$, but this effect could not be accounted for in the present study. Apart from this spatial effect, there is a quasi-local effect of the interaction between $v_{d,pri}$ and the concentration profile in the surface layer. This effect has been ignored as well. It is a consequence of the so-called flux-profile relationships in surface layer theory. This theory, also implemented in OPS, dictates that larger $v_{d,pri}$ and hence larger dry deposition rates must lead to larger concentration gradients in order to sustain the larger deposition rates. The reverse is true as well. Effects of $v_{d,pri}$ changes on the atmospheric concentrations can be particularly strong in stable conditions. However, in practice, these effects become small when averaging over many atmospheric conditions. Therefore, in the context of the present study, our approach is considered reasonable.

## 5.2 Comparison to other studies and general discussion

Model uncertainties are preferred to be determined by comparing the model results to measurements. Unfortunately, there are no/few measurements available for deposition and there are also few direct comparisons to measurements for concentration calculations at individual sources. This is especially true for greater distances. Therefore, this study mainly looked at the sensitivity of the OPS calculations to uncertainties in preselected model parameters, which were selected in such a way that they cover the main aspects of model uncertainties with the focus on the greater distances. This method can lead to an underestimation of the uncertainty in the model calculation because not all sources of uncertainty have been included. First, there are additional uncertainties because the model system does not exactly correspond to the physical and chemical processes. Usually, the mathematical model is a simplification of reality.
Second, there are uncertainties in the model results due to uncertainties in the emissions. The uncertainty in the emission of an individual source strongly depends on the type of source and the emitted component. Indicatively, an uncertainty of a factor of 2 (2 sigma) for the annual mean emission is estimated for relatively well-known sources. Examples are particulate matter and $NO_2$ from a large factory or highway. For smaller sources and sources with limited information, the uncertainty can be at least a factor of 2 higher. Information on uncertainties in emissions can be found at the Dutch Emissieregistratie [Methoderapporten | Emissieregistratie]. Because the uncertainty in emissions probably hardly correlates with the uncertainty in the model calculation, the uncertainty in the emission can easily be added quadratically to the uncertainty in the model calculation.
The effect of model simplifications is more difficult to estimate. Insight can be gained by comparing model results to other models. A number of other sensitivity and/or uncertainty studies have recently been carried out. Some were part of the NKS ('Nationaal Kennisprogramma Stikstof') programme. The results of the present sensitivity study ('*sensitivity OPS*') have been compared to these other studies. The other studies, in chronological order, are:

1) In 2021, RIVM made an initial assessment of the uncertainties in contributions from individual sources to deposition (Roest et al., 2021).
2) In 2022, TNO published an uncertainty assessment for a single source, based on a Monte Carlo-type sensitivity analysis with the SRM-3 model Stacks ("*sensitivity TNO Stacks"*) for a limited number of parameters and model runs (Duyzer and Erbrink, 2022 / TNO, 2022).
3) In 2023, RIVM conducted an uncertainty analysis of nitrogen deposition at various spatial scales in the Netherlands (Hoogerbrugge et al., 2023). The calculation of nitrogen deposition accounted for contributions from many sources (both from the Netherlands and from abroad). Thus, the deposition at each location is the sum of contributions from a very large number of sources. The uncertainties were calculated on the basis of a comparison to measurements ("*uncertainty OPS based on comparison measurements"*). Because this analysis focused specifically on total nitrogen deposition (mainly in nature areas),

the comparison to the uncertainty in calculating the deposition contribution from an individual source is more challenging.

4) In 2024, Meijer and Van Loon (2024) published the report "Een ondergrens in de berekening van stikstofdepositiebijdragen voor vergunningverlening", which also extensively examined the uncertainties in the deposition contribution from individual sources.
5) In 2025, Kooi et al. (2025a) published a model comparison study ("*benchmark"*) with eight different models including OPS-LT. The variation in the various model outcomes provides more insight into how uncertain the calculated nitrogen deposition is. However, the variation may be limited because of similarities in model choices.
6) Finally, we add a variation of the present sensitivity study that accounts for the possibility that the scaling of dry deposition velocity depends on the land use. In this variant, only the dry deposition velocity of forests is varied ("*sensitivity OPS forest"*).

The variant of the sensitivity study (6) is included since the observed significant compensation effects might differ in effectivity for other than the dominant land uses. Appendix 3 describes a small study to estimate the additional uncertainty for a typical minority land use situation due to dry deposition. As might be expected, this addition in uncertainty in deposition at the receptor is small near the source (compensation by increased source depletion is not yet as effective) and increases for receptors at greater distances (when source depletion becomes more important).

*Figure 5.1 Uncertainties/sensitivities of the calculated total $NH_x$ deposition due to ammonia emission from a livestock farm. The studies shown are described in the text. The uncertainty that follows from the comparison to the measurements cannot be linked to an individual source, and therefore a distance, and is therefore shown separately from the distance scale.*

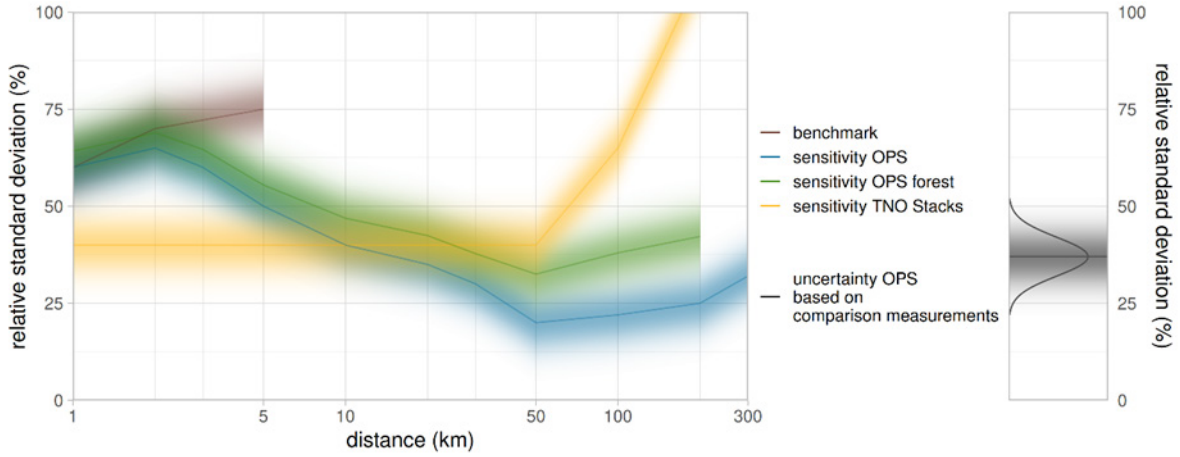


Figure 5.1 shows the results of the present study as well as four out of the six studies (studies 2, 3, 5 and 6 from the list above) for model results of the livestock farm. Below, the results of the present study are put into perspective with regard to the six aforementioned studies:

1) In 2021, RIVM made an initial estimation of the uncertainties in deposition contributions from individual sources (Roest et al., 2021). At local scale, an uncertainty factor of 2 was estimated. Further away from the source (>25 km), the uncertainty was presumed to be significantly higher, with the caveat that this uncertainty could only be determined through model calculations.
Figure 5.1 presents the results of such modelling studies. The estimation of a factor of 2 (corresponding to a CV of 70%) close to the source is confirmed. However, the expectation that uncertainties would increase significantly beyond 25 km turned out to be incorrect. Instead, uncertainties decrease up to a distance of around 100 km. At very great distances >100 km, uncertainties do increase but they do not exceed a factor of 2 up to at least 400 km.
Air quality modelling aims at 50% of the model results falling within a factor of 2 of the measurements. Translated to this uncertainty study, this corresponds to a CV of approximately 100%. The results in Figure 5.1 generally meet this target by a wide margin. This also applies to the results of the sensitivity analyses for the industrial stack and the motorway.

2) The sensitivity analysis with *TNO Stacks* shows a lower sensitivity at short distances compared to the present sensitivity study. This is likely because the TNO study assumes a smaller uncertainty in the dry deposition velocity. In the present study, the sensitivity to dry deposition velocity appeared to be particularly high close to the source. As a result, the sensitivity in TNO Stacks is likely underestimated for short distances when compared to the present study. At greater distances, such as around 100 km from the source, the sensitivity of OPS decreases, whereas the sensitivity in TNO Stacks increases. The latter may be explained by the fact that the TNO Stacks study treats the dry deposition velocity used to describe local deposition and the dry deposition velocity as a loss term along trajectories as two independent parameters. Hence, they are also perturbed independently. As a result, the compensation effect, which plays a significant role in OPS, is disabled in TNO Stacks. In general, Stacks is less focused on deposition at great distances from sources compared to OPS.

3) The sensitivity of deposition calculations for an individual source to uncertainties in the parameters results in roughly the same uncertainty at great distances from a source as the uncertainty derived from the *comparison to measurements*. At first glance, this may seem counterintuitive, as random uncertainties tend to average out when contributions from different individual sources are summed. However, some major sources of uncertainty, such as the dry deposition velocity, are location-dependent, which means they average out far less when aggregated. Additionally, in the comparison to measurements, the uncertainty in the measured deposition and in emission strength also plays a significant role.

4) In Meijer and Van Loon (2024), it is stated that the uncertainties in deposition calculations may be a factor of 2-3 larger than the uncertainties of the concentration calculations. The present sensitivity study does not support this statement, especially at greater distances from the source. Instead, it suggests that the sensitivity in deposition

calculations is of the same order of magnitude as the sensitivity in concentration calculations. The sensitivity does, however, depend on the component and, to a lesser extent, on the type of source.

5) In the present sensitivity study, the same sources were used as in the model comparison of the *benchmark study* (Kooi et al., 2025a). However, the benchmark study focused on the immediate vicinity of the source, up to 5 km, whereas the present study aimed to assess uncertainties at great distances. The benchmark study potentially provides a more complete picture of uncertainties close to the source than the sensitivity studies, as it also includes differences *between* models. Comparison between the present sensitivity study and the benchmark study shows that the relative standard deposition in the calculated dispersion is not heavily underestimated. This suggests that, for distances up to 5 km from the source, no major sources of uncertainty are missing.

6) Finally, Figure 5.1 also shows a variation on the present study that accounts for differences in perturbations of dry deposition velocity between grass and forest. With varying perturbations for different landscape types, the coupling between the dry deposition velocity along the trajectory and the local deposition velocity weakens. As a result, the compensation becomes less effective. In the figure, around 100 km, we observe a less pronounced decrease in sensitivity compared to the optimal compensation scenario, where the deviation is the same for each landscape type.

A similar comparison for $NO_x$ cannot be made since the $NO_x$ source included in the TNO study was neither a stack, nor a motorway, but a livestock farm (Duyzer and Erbrink, 2022). Nevertheless, for the purpose of illustration only, we combined our results for $NO_x$ emissions from an industrial stack with those from the model intercomparison of the local benchmark study (Kooi et al., 2025a) and the results from Duyzer and Erbrink (2022) (Figure 5.2, showing results of the present study, and studies 2 and 5 from the list at the start of Section 5.2). Also included are the results of the uncertainty study by Hoogerbrugge et al. (2023) (right-hand panel of the figure, study 3.).

*Figure 5.2. Uncertainties/sensitivities of the calculated deposition due to $NO_x$ emission from an industrial stack (for TNO: a livestock farm). The studies shown are described in the text. The uncertainty that follows from the comparison to the measurements cannot be linked to an individual source and therefore a distance and is therefore shown separately from the distance scale.*

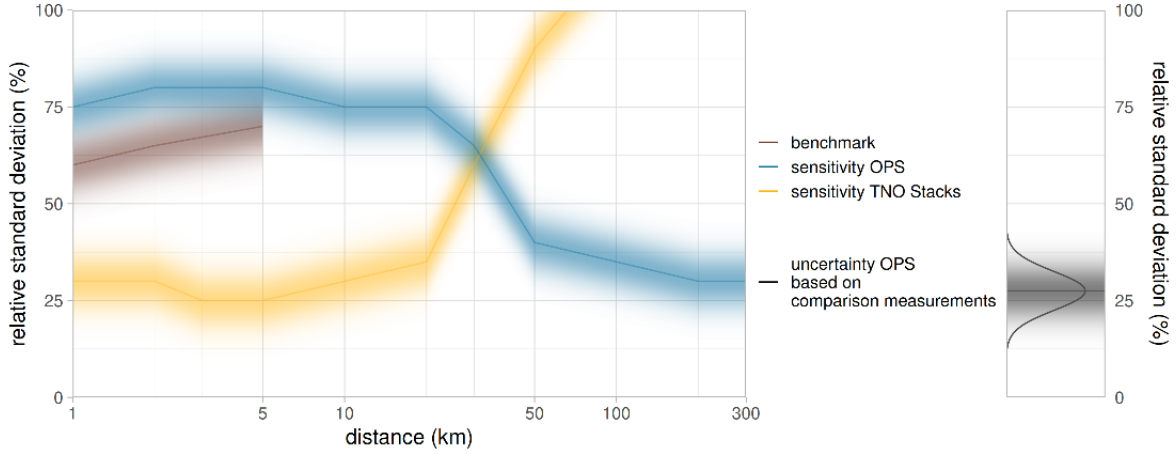


Despite the conceptual differences between the studies, we notice some similarities in the results. For example, for the $NO_x$ source, the uncertainty from our sensitivity analysis and from the benchmark are quite comparable. This indicates that, presumably, no major source of uncertainty is missing. Also, the CV from our sensitivity study decreases with increasing distance, due to compensation. By contrast, the CV from the TNO study increases with increasing distance. Just as in the $NH_3$ case, the compensation in the TNO result is eliminated, since perturbations in the deposition velocity, locally and on the trajectory, are not connected. Finally, as was also the case for $NH_3$ emissions from the livestock farm, the sensitivity for an individual source at a great distance from our study yields about the same spread as the uncertainty derived from the comparison to measurements when using all sources.

# 6 Conclusion on uncertainty

The aim of this study was to determine the uncertainty in the annual nitrogen deposition on a nature area caused by a single source up to several hundreds of kilometres from the source. This was carried out via a model sensitivity analysis where preset variables (twelve in total) were perturbed on the basis of variable-specific estimated uncertainty distributions. To calculate the combined sensitivity, five thousand Monte Carlo calculations were performed, using values from the uncertainty distribution of each of the variables. Runs were performed for three types of sources as a function of distance to the source in twelve different directions. Subsequently, the median Coefficient of Variation (CV) was determined for the separate receptors in each direction, after which the median of absolute differences was chosen to express the sensitivity.

Results of our study indicate that the uncertainty in the annual nitrogen deposition does not necessarily increase with distance, but may show a tendency to decrease, at least in the distance domain studied here. For ammonia deposition from a livestock farm, the sensitivity up to 10 km is more than 60%. For distances around 100 km, the sensitivity is considerably less (around 25%), and then slightly increases again for greater distances. For an industrial source, the sensitivity to the uncertainty in the deposition parameters for small distances from the source up to about 20 km is also highest (about 70-75%). Here too, the sensitivity decreases (to 25-30%) for greater distances (> 100 km). Similar results are seen for the motorway with a sensitivity of just over 80% near the source, which decreases to around 25% for distances around 100 km and beyond. These sensitivities compare relatively favourably to the uncertainties that follow from the reported comparison to measurements [Hoogerbrugge 2023]. The sensitivity to parameters in the deposition calculation also compares favourably to the sensitivity of the concentration to the same parameters for greater distances (>50 km) from the source. Compensation plays a major role in both these aspects. After all, an assumed higher deposition velocity leads to greater deposition close to the source. Further away, the concentration decreases more sharply because more deposition across the trajectory takes place as well, which leads to a reduction in deposition at a greater distance.

The important parameters influencing the concentrations of the primary material close to the source are the ones that determine the dispersion of the initial plume. In particular, the vertical dispersion length and the mixing layer height are most influential. At greater distances from the source, the effect of dry deposition velocity (of the primary material) and chemical reactions on the atmospheric concentration become more important, as well as the diurnal variation for the motorway. For all distances, meteorological conditions are influential for the concentration uncertainty as well.

For total deposition (sum of primary and secondary compounds), the dry deposition velocity of the primary material dominates the CV, both in the near and far ranges from the source. The vertical dispersion length, mixing layer height, and meteorological conditions are influential as well. For the $NO_x$ sources, chemical conversion is important for the total

deposition at very great distances (>100 km). This is not seen for the livestock $NH_3$ source.

**Recommendations for further research**

This study was performed with a particular focus on the greater distances. In the course of the study several important observations were made that can improve the results of a similar study in the future. Upon a more comprehensive understanding of the uncertainty in the deposition contribution from a single source obtained in this particular study, we make the following recommendations:

- Uncertainty in the dry deposition velocity of the primary material dominates the uncertainty in total deposition. Further factorisation of this parameter, covering various stages of the deposition process, is recommended. This could also include differentiation of perturbation factors per land use category.
- The Uncertainty Analysis Tool currently under development, compares model outcomes on the basis of emissions from all known sources to various sets of measurements. The tool can lead to more likely model parameter settings in combination with smaller parameter uncertainties. A simple first attempt is made in this study for illustration purposes. Further research and application of the results of the model improvement tool is recommended.
- The *Meteo* parameter also contributes significantly to the uncertainty in concentration and deposition. Because of the complexity of the meteorological impacts and related effects on various model outcomes, simple scaling was replaced by regional categorisation. Although typical differences in Dutch meteorological conditions are taken into account in a consistent manner, an alternative approach is recommended for future research in general, and for the development of the Uncertainty Analysis Tool in particular.
- The uncertainty in calculated deposition of individual sources can be relevant for policy decisions, especially if the termination of current sources is used to allow for the emission of new sources. In the propagation of uncertainties towards the difference between the old and new situations, the incorporation of the correlation between the uncertainties in both situations is recommended as well.
- This study focuses on greater distances. Therefore, some sources of uncertainty close to the source, such as building effects, are not included in this study. However, we did notice that the relative uncertainties in the total, wet and dry, deposition close to the source are large compared to relative uncertainties at great distances. If a follow-up of this study is required, more focus on uncertainty close to the source is recommended.

# Acknowledgements

We want to acknowledge Wouter Lefebvre, Hans Hooyberghs (both VITO) and Maarten Krol (WUR) for reviewing a draft manuscript of our report and for supplying valuable comments and suggestions. The processing of these comments and suggestions remains the authors responsibility.

# References


Abbott, J., Hayman, G., Vincent, K., Metcalfe, S., Dore, T., Skeffington, R. A., et al., 2003. Uncertainty in acid deposition modelling and critical load assessments. R&D Technical Report P4-083(5)/1 Bristol, UK Environment Agency.

Bennett N.D., B.F.W. Croke, G. Guariso, J.H.A. Guillaume, S.H. Hamilton, A.J. Jakeman, et al., 2013. Characterising performance of environmental models. Environ. Mod. Soft., 40, 1-20.

Briggs, G. A., 1984. Plume rise and buoyancy effects. Atmospheric science and power production, 327, 366.

Cox, W. M. and J. A. Tikvart, 1990. A statistical procedure for determining the best performing air quality simulation model. Atmos. Environ., 24A(9): 2387-2395.

Dore, A. J., Carslaw, D. C., Braban, C., Cain, M., Chemel, C., Conolly, C., et al., ,2015. Evaluation of the performance of different atmospheric chemical transport models and inter-comparison of nitrogen and sulphur deposition estimates for the UK. Atmospheric Environment, 119, 131-143.

Duyzer J. en H. Erbrink. (2021) Afbakening in de modellering van depositiebijdragen van individuele projectbijdragen (Fase 1), Referentie 100340309, TNO Utrecht 6 juli 2021. https://open.overheid.nl/documenten/ronl-1847540a-636e-43db-bc05-ecc160308b6b/pdf

Duyzer, J. en H. Erbrink (2022). Afbakening in de modellering van depositiebijdragen van individuele projectbijdragen (Fase 2) Versie 3. Referentie 100342643. TNO Utrecht 26 april 2022. www.eerstekamer.nl/overig/20220727/afbakening_in_de_modellering_van/document

EEA 2011 The application of models under the European Union's Air Quality Directive, A technical reference guide, EEA Technical report No 10/2011 ISSN 1725-2237.

Flechard, C.R. et al., 2011. Dry deposition of reactive nitrogen to European ecosystems: a comparison of inferential models across the NitroEurope network. Atmospheric Chemistry and Physics, 11(6): 2703-2728, https://doi.org/10.5194/acp-11-2703-2011.

Fox, D.G., 1984. Uncertainty in air quality modeling. Bull. Am. Meterol. Soc., 65(1), 27-47.

Gauchi, J.-P., Bensadoun, A., Colas, F., Colbach, N., 2017. Metamodeling and global sensitivity analysis for computer models with correlated inputs: A practical approach tested with a 3D light interception computer model. Environmental Modelling & Software.

Gong, W., Stroud, C., Zhang, L., 2011, Cloud processing of gases and aerosols in air quality modeling (2011). *Atmosphere*, **2,** 567 - 616.

Gryning, S.-E. and E. Lyck, 1984. Atmospheric Dispersion from Elevated Sources in an Urban Area: Comparison between Tracer Experiments and Model Calculations. J. Appl. Meteorol. Climatol. 23 (4), 651-660. Doi: 10.1175/1520-0450(1984)023<0651:ADFESI>2.0.CO;2.

Hales, J.M., 1978. Wet removal of sulfur compounds from the atmosphere. Atmospheric Environment 12, 389-399.

Hanna, S.R., B.A. Egan, J. Purdum and J. Wagler, 2001: Evaluation of the ADMS, AERMOD, and ISC3 dispersion models with the OPTEX, Duke Forest, Kincaid, Indianapolis and Lovett field datasets. Int. J. Environ. Pollut., 16, 301-314.

Haugen, D.A., and Fuquay, J.J., (Editors), (1963): The Ocean Breeze and Dry Gulch Diffusion Programs, Vol. I. Air Force Cambridge Research laboratories and Hanford Atomic Products Operations, Report HW-78435, 240 pages.

Hoek van Dijke, A.J., R. Orth, A.J. Teuling, M. Herold, M. Schlerf, Martin M. Migliavacca, M. Machwitz, T.C. Van Hateren, X. Yu and K. Mallick, 2023. Comparing forest and grassland drought responses inferred from eddy covariance and Earth observation. Agric. Forest Meteorol. 341, 109635.

Holmes, N.S, and L. Morawska, 2006. A review of dispersion modelling and its application to the dispersion of particles: An overview of different dispersion models available. Atmospheric Environment, 40(30), 5902-5928. Doi: 10.1016/j.atmosenv.2006.06.003.

Hood C, Carruthers D, O'Neill J, Jackson R, Jinks D, Seaton M, Mickech J, Stocker J, Strickland S, Bedwell P and Wellings J,2024: Investigating the impact of applying different grid resolutions of NWP data in atmospheric dispersion modelling. Atmospheric Dispersion Modelling Liaison Committee, ADMLC-R15 Report. https://admlc.com/wp-content/uploads/2024/01/d5.2-finalreport-jan2024.pdf

Hoogerbrugge, R., M. Braam, K. Siteur, C. Jacobs, S. Hazelhorst, G. Stefess, E. van der Swaluw, R. Wichink Kruit, J. Wesseling and A. van Pul, 2023: Uncertainty in the determined nitrogen deposition in the Netherlands. Status report 2023. *RIVM report 2022-0085,* RIVM, Bilthoven.

Kooi, E. G. Thorkelsdottir, P. Meijer, J. Stocker, W. Lefebvre, A. Vigier, A.-S. Lansø and R. Wichink Kruit, 2025a. Differences in calculations of concentration and deposition of ammonia and nitrogen oxides at local scale. A comparison of eight atmospheric transport models. RIVM report 2025-0047, RIVM, Utrecht. DOI 10.21945/RIVM-2025-0047.

Kooi, E., G. Thorkelsdottir, P. Meijer, C. Jacobs, R. Wichink Kruit, J. Stocker, W. Lefebvre, A. Vigier, A.-S. Lansø and M. Krol, 2025b. Validation of operational models for concentration and deposition modelling of reactive nitrogen at local scale. RIVM report 2025-0050, RIVM, Utrecht. DOI 10.21945/RIVM-2025- 0050 (in preparation).

Leelőssy, Á., F. Molnár, F. Izsák, Á. Havasi, I. Lagzi, R. Mészáros, 2014. Dispersion modeling of air pollutants in the atmosphere: a review. Cent. Eur. J. Geosci., 6, 257-278, doi: 10.2478/s13533-012-0188-6.

Leelőssy, Á., I. Lagzi, A. Kovács and R. Mészáros, 2018. A review of numerical models to predict the atmospheric dispersion of radionuclides. Journal of Environmental Radioactivity,182, 20-33, doi: 10.1016/j.jenvrad.2017.11.009.

Massad, R. S., Nemitz, E., & Sutton, M. A., 2010. Review and parameterisation of bi-directional ammonia exchange between vegetation and the atmosphere. Atmospheric Chemistry and Physics, 10, 10359-10386, doi: 10.5194/acp-10-10359-201.

Meijer, E. and Van Loon, E. , 2024. Een ondergrens in de berekening van stikstof-depositiebijdragen voor vergunningverlening. TNO Publiek R11334, https://publications.tno.nl/publication/34642815/Qg8TI104/TNO-2024-R11334.pdf (In Dutch).

Noordhof Atlasproducties, 2021. De Bosatlas van weer en klimaat. Noordhof Atlasproducties, Groningen. 120 pp. (In Dutch)

Norton, J., 2015. An introduction to sensitivity assessment of simulation models. Environ. Modell. Softw., 69, 166-174, doi: 10.1016/j.envsoft.2015.03.020.

Olesen, H.R., Berkowicz, R.B, Løfstrøm, P., 2007. OML: Review of model formulation. National Environmental Research Institute, Denmark. 130pp. -NERI Technical Report No. 609, http://www.dmu.dk/Pub/FR609.

Pandey, G., A. Venkatram and S. Arunachalam, 2023: Evaluating AERMOD with measurements from a major U.S. airport located on a shoreline. Atm. Environ., 294, 119506, doi: 10.1016/j.atmosenv.2022.119506.

Price, C.S., Tickle, G.A., Attree, M.W., Lad, C.S., Carruthers, D.J., 2016. High Level Review of the Sensitivity of Dispersion Model Predictions to Individual Source Term Parameters. ADMLC report ADMLC/2016/1. Available from admlc.com/wp-content/uploads/2014/05/admlc_source_term_sensitivity_report_final.pdf

Projectgroep Revisie Nationaal Model, 2002. Het Nieuwe National Model. Model voor de verspreiding van luchtverontreiniging uit bronnen over korte afstanden. Rapportage over het onderzoek Revisie Nationaal Model en de besluitvorming daarover in de begeleidingscommissie (In Dutch). Revised version 2002. TNO Report R 98/306, TNO, Apeldoorn. Available from www.infomil.nl.

Roest, R., W. van der Maas, A. van Pul, P. Romeijn, A. Bleeker, S. Hazelhorst, R. Wichink Kruit and M. Wilmot, 2021. Verkenning afstandsgrens project-specifieke depositieberekeningen RIVM-briefrapport 2021-0115, DOI 10.21945/RIVM-2021-0115

Rutledge-Jonker, S., Braam, M., Hoogerbrugge, R., Wichink Kruit, R., Nemitz, E., Twigg, M., et al., 2023. Ammonia deposition measured with Conditional Time-Averaged Gradient (COTAG) systems in the Netherlands. Methodological advances and results for 2012–2020. RIVM report 2022-0202, RIVM, Bilthoven. Doi: 10.21945/rivm-2022-0202.

Sander, R., (2023). Compilation of Henry's law constants (version 5.0.0) for water as solvent. Atmos. Chem. Phys., 23, 10901-12440, doi:10.5194/acp-23-10901-2023Schrader, F. and Brümmer, C., 2014. Land use specific ammonia deposition velocities: a review of recent studies (2004-2013). Water Air Soil Pollut, 225(10): 2114. https://doi.org/10.1007/s11270-014-2114-7

Sauter, F., Sterk, M., Van Der Swaluw, E., Wichink Kruit, R., De Vries, W. and Van Pul, A., 2023. The OPS-Model. Description of OPS 5.1.1.0. RIVM, Bilthoven, www.rivm.nl.

Schulman L. L., Strimaitis D. G., Scire J. S., 2000. Development and evaluation of the PRIME plume rise and building downwash model, J. Air Waste Manage. Assoc., 50, 378–390.

Simpson, D., Benedictow, A., Berge, H., Bergström, R., Emberson, L. D., Fagerli, H., Flechard, C. R., Hayman, G. D., Gauss, M., Jonson, J. E., Jenkin, M. E., Nyíri, A., Richter, C., Semeena, V. S., Tsyro, S., Tuovinen, J.-P., Valdebenito, Á., and Wind, P. (2012). The EMEP MSC-W chemical transport model – technical description, Atmos. Chem. Phys., 12, 7825–7865. https://doi.org/10.5194/acp-12-7825-2012

Snoun, H., Krichen, M., & Chérif, H., 2023. A comprehensive review of Gaussian atmospheric dispersion models: current usage and future perspectives. Euro-Mediterranean Journal for Environmental Integration, 8, 219-242. Doi: 10.1007/s41207-023-00354-6.

Stocker, J., Ellis, A., Smith, S., Carruthers, D., Venkatram, A., Dale, W. and Attree, M., 2016. A review of the limitations and uncertainties of modelling pollutant dispersion from non-point sources. Report for the UK Atmospheric Dispersion Modelling Liaison Committee.

Stull, R.B., 1988: An introduction to boundary layer meteorology. Kluwer, Dordrecht.

Thunis, P., Georgieva, E., and Pederzoli, A., 2012. A tool to evaluate air quality model performances in regulatory applications. Environmental modelling & software, 38, 220-230.

U.S. EPA, 2023. AERMOD Model Evaluation. EPA report EPA-454/B-23-011, available from https://gaftp.epa.gov/Air/aqmg/SCRAM/models/preferred/aermod/aermod_med.pdf.

Uusitalo, L., Lehikoinen, A., Helle, I. and Myrberg, K., 2015. An overview of methods to evaluate uncertainty of deterministic models in decision support. Environ. Modell. Softw. 63, 24-31. Doi: 10.1016/j.envsoft.2014.09.017.

Van der Swaluw, E., de Vries, W., Sauter, F., Aben, J., Velders, G. and van Pul, A., 2017. High-resolution modelling of air pollution and deposition over the Netherlands with plume, grid and hybrid modelling. Atmospheric Environment, 155, 140-153.

Van der Swaluw, E., de Vries, W., Sauter, F., Kruit, R. W., Vieno, M., Fagerli, H., and van Pul, A., 2021. Trend analysis of reduced nitrogen components over the Netherlands with the EMEP4NL and OPS model. Atmospheric Environment, 248, 118183.

Vivanco, M.G., Bessagnet, B., Cuvelier, C., Theobald, M.R., Tsyro, S., Pirovano, G., Aulinger, A., Bieser, J., Calori, G., Ciarelli, G., Manders, A., Mircea, M., Aksoyoglu, S., Briganti, G., Cappelletti, A., Colette, A., Couvidat, F., D'Isidoro, M., Kranenburg, R., Meleux, F., Menut, L., Pay, M.T., Rouïl, L., Silibello, C., Thunis, P., Ung, A., 2017. Joint analysis of deposition fluxes and atmospheric concentrations of inorganic nitrogen and sulphur compounds predicted by six chemistry transport models in the frame of the EURODELTAIII project. *Atmospheric Environment*, **151**, 152 – 175.

Walker, J.T., Bell, M.D., Schwede, D., Cole, A., Beachley, G., Lear, G. and Wu, Z. 2019. Aspects of uncertainty in total reactive nitrogen deposition estimates for North American critical load applications. Sci. Total Environ. 690, 1005-1018, doi: 10.1016/j.scitotenv.2019.06.3.

Yao, L., Kong, S., Nemitz, E., Vieno, M., Cheng, Y., Zheng, H., et al., 2024. Improving below-cloud scavenging coefficients of sulfate, nitrate, and ammonium in PM2.5 and implications for numerical simulation and air pollution control. Journal of Geophysical Research: Atmospheres, 129, e2023JD039487. https://doi.org/10.1029/2023JD039487

# Appendix 1 Uncertainty in the mixing layer height, $z_i$, estimated from ERA5 reanalysis ensembles

## Background

Planetary boundary layer height (PBLH) estimates are available from ERA5 reanalysis data (Hersbach et al., 2020), which can be obtained from the Copernicus Climate Data Store (CDS; https://cds.climate.copernicus.eu). Part of the reanalysis is a (limited) uncertainty estimate, which is obtained as a by-product of the ERA5 Ensemble Data Assimilation system (EDA). For each out of ten ensemble members, the initial state of the weather model (in this case ECMWF's IFS[1]) is somewhat perturbed, within realistic bounds. Results of EDA are available 3-hourly, at a horizontal resolution of 0.5°, among which 3-hourly PBLH estimates from all individual members, along with the ensemble mean and their 'spread'. For the purpose of deriving uncertainty in mixing layer height, $z_i$, we assume that PBLH represents $z_i$.

The spread of the ensemble represents the standard deviation of the estimate. According to ECMWF's documentation (https:/confluence.ecmwf.int/display/CKB/ERA5%3A+uncertainty+estimation), this spread can be considered a representation of the model uncertainty due to (random) errors in atmospheric measurements and sea water temperature as well as to random errors in parameter values. It is stated that "as long as these uncertainties are properly described and there are no additional sources of uncertainty, then the EDA will properly describe the reanalysis uncertainties." Although the 'spread' does not fully represent all errors, it is also stated that "comparison of uncertainties provides excellent information on when and where the reanalysis products are more or less accurate."

Here, we take the ratio of the spread to the ensemble mean to represent a first-order estimate of the coefficient of variation (CV; standard deviation divided by the mean) of the PBLH, and hence $z_i$, at a given time and location. We assume that the uncertainty information contained in this CV suits our present purpose of deriving a first-order estimate of $z_i$ uncertainty.

## Data and analysis

PBLH data from the ERA5 ensemble, representing the grid box at De Bilt (Netherlands, 52.1°N, 5.2°E) and eight bordering grid boxes, were downloaded from the CDS. Ensemble mean and spread of PBLH were obtained for the years 2015-2022. The CV was computed as the ratio of PBLH spread to PBLH ensemble mean.

We first examined the mean diurnal variation of the PBLH and the CV for the year 2015, using their spatial averages over the nine grid boxes (Figure A1.1). Temporal averaging then reveals that the mean PBLH is lowest at 3 UTC and highest at 12 UTC. The error bars give the average of ± 1 standard deviation (SD, calculated from the ensemble). On *average*, the SD appears to be fairly constant (43-47 m). Therefore, the CV shows a clear diurnal course, with maximum values of about 13%

[1] ECMWF = European Centre for Medium-Range Weather Forecasts; IFS = Integrated Forecasting System

around 3 UTC and minimum values of about 6% around 12 UTC. This somewhat unexpected behaviour of the CV is probably due to the nature of the present uncertainty estimate from ERA5 (see above).
On the basis of these results, we analysed the ensemble mean and spread for the years 2015-2022, at 3 UTC and 12 UTC, focusing on the grid box for De Bilt only. For these hours, which may be expected to be representative for a low stable boundary layer and a high unstable boundary layer, respectively, we computed the mean, median, 0.90 and 0.95 quantiles of PBLH, SD and CV. Results in Table A1 show that at both 3 and 12 UTC, about 95% of the CV values remains within 25%. This result, *along with estimates from scientific literature*, is used to construct our $z_i$ uncertainty distribution, i.e. a lognormal distribution with $\mu = 0$ and $\sigma = 0.24$ (see Sections 3.1.3 and 3.1.7).

*Figure A1.1 Mean diurnal variation of the PBL Height (black dotted; left axis) near De Bilt (NL) and the relative standard deviation (CV) (orange dashed; right axis). Error bars are ± 1 standard deviation from the ensemble (10 members).*

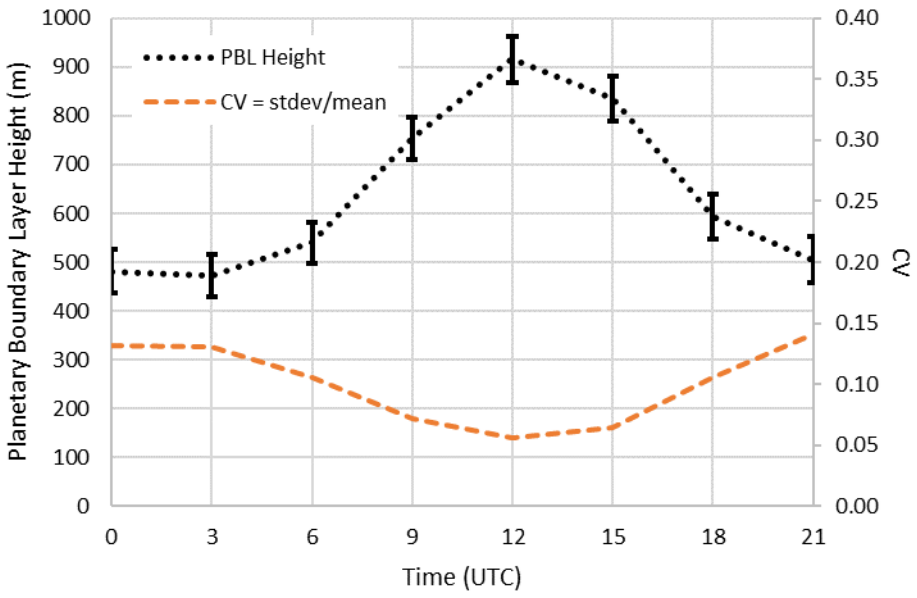


*Table A1 Average boundary layer height, standard deviation from the ensemble members and coefficient of variation near De Bilt (NL) from the ERA5 reanalysis. PBLH and SD are in meters.*

| | **PBLH (03 UTC)** | **SD (03 UTC)** | **CV (03 UTC)** | **PBLH (12 UTC)** | **SD (12 UTC)** | **CV (12 UTC)** |
|---|---|---|---|---|---|---|
| **Mean** | 369 | 24.8 | 0.096 | 942 | 78.3 | 0.092 |
| **Median** | 257 | 19.1 | 0.070 | 936 | 57.5 | 0.064 |
| **0.90 quantile** | 861 | 50.8 | 0.184 | 1486 | 165.6 | 0.178 |
| **0.95 quantile** | 1038 | 64.5 | 0.249 | 1648 | 211.2 | 0.245 |

# Appendix 2 Uncertainty distribution for chemical conversion rate, $k_{chem}$

Uncertainty in $k_{chem}$ is estimated from a comparison between observed and modelled $NH_4^+$ concentrations, at three LML stations run by RIVM (www.luchtmeetnet.nl). Used concentration values are listed in Table A2. The table shows yearly averages (2015-2021) at stations 444 (De Zilk), 538 (Wieringerwerf), and 929 (Valthermond). The differences between the modelled and observed value (Deviation) are *assumed* to be due entirely to $k_{chem}$ uncertainty. The standard deviation of the differences between modelled and observed values (highlighted in the table) is ~40% of the mean observed value. See the main text for further information and discussion.

*Table A2 Measured and modelled NH4+ concentrations and deviation of the model outcomes from the measurements.*

| | | **Concentrations (µg m$^{-3}$)** | | |
|---|---|---|---|---|
| **Year** | **Location** | **Observed** | **Modelled** | **Deviation** |
| 2015 | De Zilk | 1.06 | 1.06 | 0.00 |
| 2016 | De Zilk | 0.96 | 1.35 | 0.39 |
| 2017 | De Zilk | 0.98 | 1.40 | 0.42 |
| 2018 | De Zilk | 1.18 | 1.88 | 0.70 |
| 2019 | De Zilk | 0.95 | 1.25 | 0.30 |
| 2020 | De Zilk | 0.64 | 1.67 | 1.03 |
| 2021 | De Zilk | 0.70 | 1.69 | 0.99 |
| 2015 | Wieringerwerf | 1.35 | 1.11 | -0.24 |
| 2016 | Wieringerwerf | 1.35 | 1.35 | -0.01 |
| 2017 | Wieringerwerf | 1.15 | 1.36 | 0.20 |
| 2018 | Wieringerwerf | 1.31 | 1.87 | 0.56 |
| 2019 | Wieringerwerf | 0.89 | 1.24 | 0.35 |
| 2020 | Wieringerwerf | 0.67 | 1.60 | 0.93 |
| 2021 | Wieringerwerf | 0.71 | 1.71 | 1.01 |
| 2015 | Valthermond | 1.52 | 1.27 | -0.25 |
| 2016 | Valthermond | 1.34 | 1.56 | 0.22 |
| 2017 | Valthermond | 1.35 | 1.57 | 0.22 |
| 2018 | Valthermond | 1.23 | 1.98 | 0.75 |
| 2019 | Valthermond | 1.03 | 1.42 | 0.39 |
| 2020 | Valthermond | 0.65 | 1.65 | 1.01 |
| | *Average* | 1.05 | 1.50 | 0.45 |
| | *Standard deviation* | 0.28 | 0.26 | **0.41** |

# Appendix 3 Effect of variation in land use

The sensitivity of the model to a given parameter is determined by perturbing the parameter value and comparing the results to those of the default setting.
A given perturbation in deposition velocity also affects concentrations in the atmosphere due to changes in the amount of depleted material. These concentration changes tend to compensate the initial effect on deposition. A higher deposition velocity leads to lower concentrations which in turn cause a decreased deposition and vice versa.
A simple example is shown in Figure A3.1. In this example, a perturbation factor ($1+\varepsilon_g$) is used with values of $\varepsilon_g$=-0.5 and $\varepsilon_g$=0.5, respectively. For $\varepsilon_g$ the label g is applied to emphasise that grass is the dominant land use in the Netherlands. For a given deposition flux $F=V_dC$, it is easy to show that over homogeneous terrain, the concentration in a mixing layer with height H follows $C=C_o \exp(-kt)$, with time constant $k=V_d/H$. In addition, time (t) and distance (d) are related by d=ut, where u is wind speed.
Using this exponential relation, the ratio between the reference calculation and a perturbed calculation then scales with equation (1):

$$\frac{conc\left((1+e_g)V_d,d\right)}{conc(V_d,d)} = e^{-V_d\varepsilon_g d/H} \qquad \text{eq.(1)}$$

$$\frac{dep\left((1+e_g)V_d,d\right)}{dep(V_d,d)} = (1+\varepsilon_g)e^{-V_d\varepsilon_g d/H} \qquad \text{eq.(2)}$$

d = distance between source and receptor
$V_d$ = deposition velocity
H = mixing layer height
$\varepsilon_g$ = perturbation of $V_d$.

Effects of the aforementioned atmospheric feedback are visible in the changing curves of concentration (left) and deposition (right) with distance in Figure A3.1.

*Figure A3.1 Concentration (left-hand side) and deposition as functions of the distance for the reference value of the deposition velocity and the two perturbations described in the main text. Here e1 equals $\varepsilon_g$. All results are relative to the reference value.*

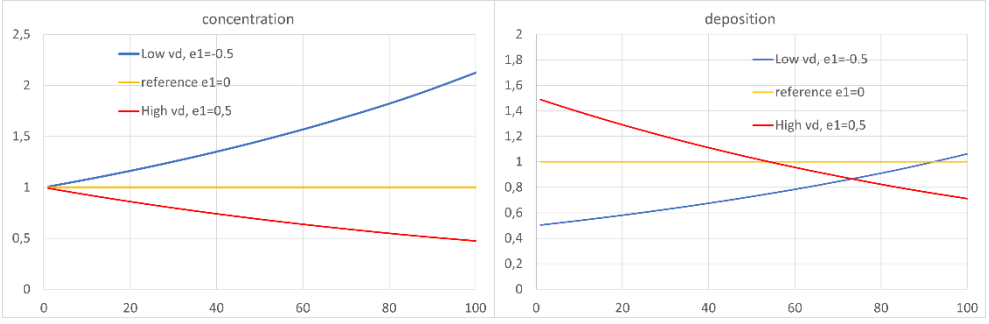

For practical reasons, in the present setup of the uncertainty assessment, the same perturbation factor is applied to each deposition velocity between source and receptor, irrespective of land use type. However, one could argue that the uncertainty in $V_d$ differs between land use types. In that case, different perturbation factors should be applied. This would interfere with the compensation (feedback) mechanism. Notably, if one type of land use needs a different perturbation than another, more dominant type of land use, compensation can be overestimated when applying one and the same perturbation factor. In other words, uncertainty due to $V_d$ might be underestimated. To study this potential underestimation, some straightforward calculations have been made, based on simple assumptions.

We perform calculations for a landscape consisting of one dominant land use type and one minority land use type, in a mix relevant for the Netherlands. The dominant land use in the Netherlands is grassland. As the second land use type we take forest, for the time being without making any distinction between deciduous and needleleaf forest. We take a land use mix of 80% grassland and 20% forest. The forest fraction is distributed across the grassland homogeneously. So there are many small forest patches instead of a single big one.

A graphical illustration is provided in Figure A3.2. The top panel shows the single land use situation, 100% grass (1). A positive perturbation of the deposition velocity (2a), leads to higher deposition, close to the source (3). Very close to the source, the effect of deposition on concentration is negligible. However, enhanced deposition leads to more depletion, and the concentration drops faster with distance from the source than in the reference situation (4). This reduces deposition (5), which may ultimately result in full compensation (6) and even lower deposition than in the reference cases beyond the compensation distance (i.e. the distance at which the deposition becomes equal to that in the reference case).

The bottom panel of Figure A3.2 illustrates the study with mixed terrain, 80% grass and 20% forest (1). Again the deposition velocity of grass is perturbed to a higher value (2a). For the purpose of illustration, we focus on a presumably unrealistic extreme situation with a perturbation of the deposition velocity of forest towards values *lower* than in the reference case (2b). Initially, near the source, the deposition over grassland is higher than in the reference case (3a), the one over forest is lower (3b). Due to the dominance of grass, the concentration is lower than the refence for increasing distances (4). However, because of the reduced deposition over forest, the decrease with distance is less than in the homogeneous case (4 bottom panel versus 4 top panel). Hence, the compensation of deposition over grass also becomes (slightly) less effective (5 bottom panel versus 5 top panel). However, for forest, compensation is absent, and we see enhancement of the initial effect with distance from the source (6). This is because of the dominant effect of grass, due to which the concentration continues to decrease over forest as well. Hence, deposition over forest continues to decrease with distance. Later, we will argue that the difference in the perturbations of deposition velocity (2a versus 2b) is likely to be less extreme than assumed in this illustration.

*Figure A3.2 Illustration of the difference in feedback between homogeneous land use (1) and a mixed grass and forest terrain (2). See text for the explanation of the steps/numbers in the figures.*

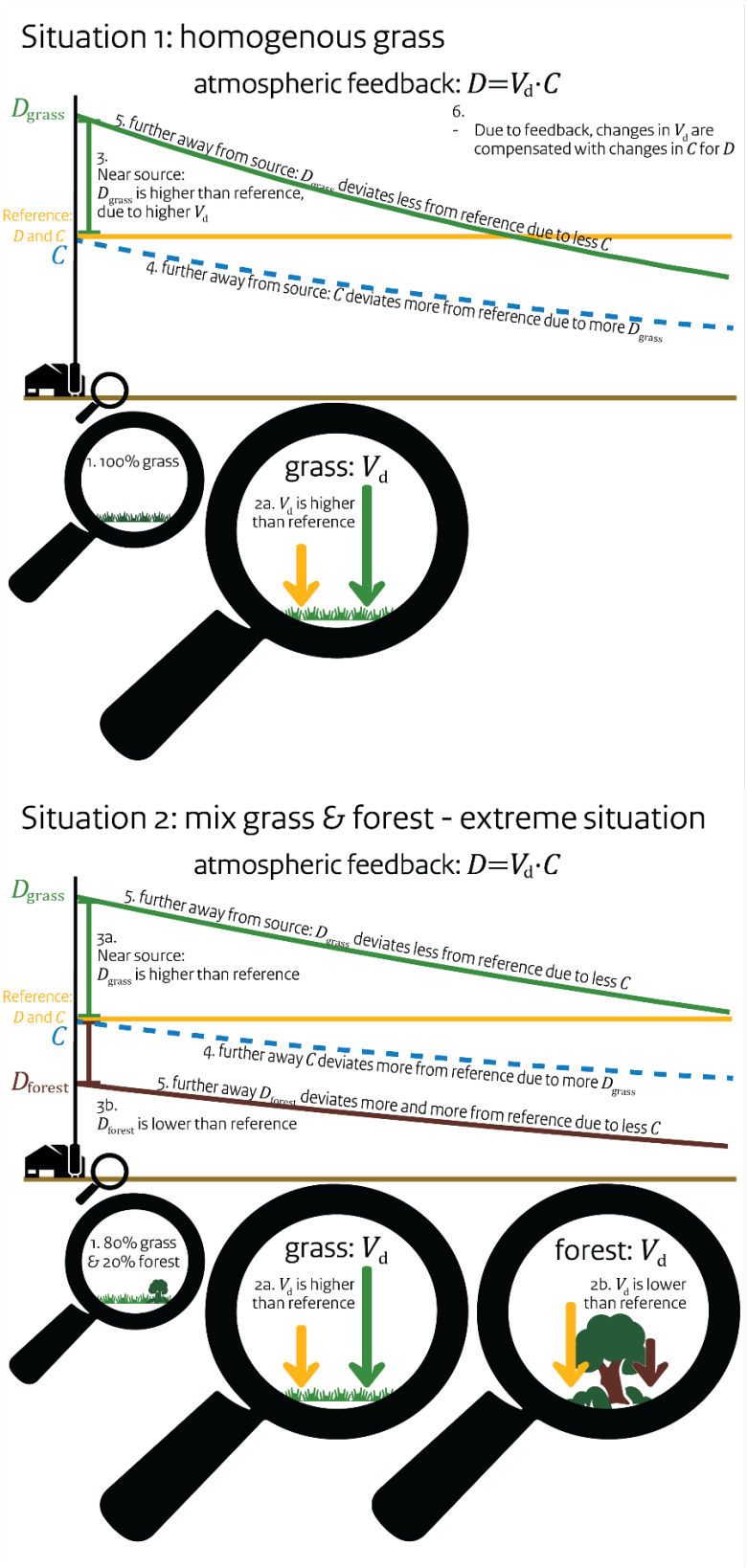

Mathematically, we again assume a perturbation factor (1+ $\varepsilon_g$) for the dominant land use, which is grassland. The reference $V_d$ of forest is estimated as 1.2 times the reference $V_d$ of grass. The perturbation of $V_d$ of forest (1+ $\varepsilon_f$) in this particular calculation may now differ from the perturbation of $V_d$ of grass (1+ $\varepsilon_g$). However, for different ecosystems, the inherent uncertainties in $V_d$ estimates seem to be within a similar order of magnitude (Schrader and Brümmer, 2014). Furthermore, the process leading to deposition on grass and forest shows considerable similarities regarding large-scale eco-physiological drivers, notably to light, temperature, humidity, soil moisture, and $CO_2$. Uncertainties due to, for example, drought, temperature extremes, and cloudiness, may be expected to induce $V_d$ uncertainties with a similar sign because of similar plant-physiological responses. Hence, extreme differences in perturbation are expected to be unlikely. Therefore, the domain of likely perturbations is assumed to be: $\varepsilon_f$ / $\varepsilon_g$ =[0.5-1.5].
The ratio between the modelled concentration relative to the reference calculation now reads:

$$\frac{conc((1+\varepsilon_g)V_d,(1+\varepsilon_f)V_d,R,\dots)}{conc(V_d,R,\dots)} = e^{-(1-R_l)\mathrm{a}\,V_d\varepsilon_g\mathrm{d}-R_l\mathrm{a}\,R_{Vd}V_d\varepsilon_f\mathrm{d}} \qquad \text{eq.(3)}$$

$R_l$ = ratio of land surface area covered with forest and covered with grass = 0.2
$R_{Vd}$ = ratio of $V_d$ of forest and $V_d$ of grass = 1.2.

Figure A3.3 shows the results of the perturbations of $\varepsilon_g$ of -0.5 (labelled low) and +0.5 (labelled high) for the concentration on the majority land use (grass). The solid line shows the default result for identical perturbation for forest and grass ($\varepsilon_f$ / $\varepsilon_g$ = 1). Figure A3.3 also shows a smaller perturbation for the minority land use (labelled forest) compared to the majority land use (labelled grass), using $\varepsilon_f$ / $\varepsilon_g$ = 0.5. The default is nearly the same as the concentration shown in Figure A3.1. The subtle difference is caused by a small difference in the effective average deposition velocity between forest and grass.

*Figure A3.3 Concentration relative to the reference calculation as a function of the distance from the source. Two types of land use are studied. Two perturbations of the deposition velocity, $\varepsilon_g$ (-0.5 and +0.5) and a perturbation of the $\varepsilon_f$ / $\varepsilon_g$ ratio (0.5) are applied. The perturbation on forest is less than the perturbation on grass.*

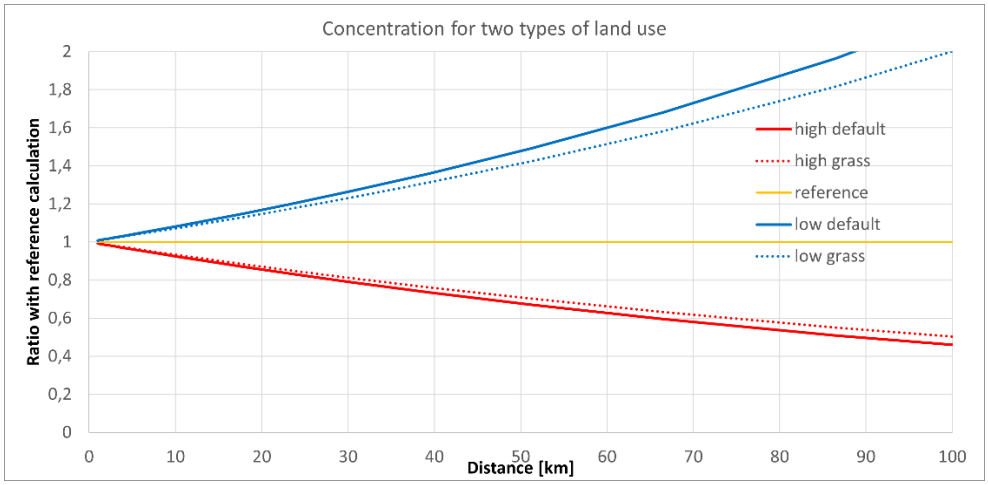

In Figure A3.4, the depositions are calculated for the same set of perturbations. So a smaller perturbation for the minority land use (labelled forest) is compared to the majority land use (labelled grass), using $\varepsilon_f / \varepsilon_g = 0.5$. Using the concentration from Figure A3.3, the deposition on grass and forest are both shown. Since both the deposition on grass and on forest are driven by the same concentration, the lines are similar but shifted.

*Figure A3.4 Deposition relative to the reference calculation as a function of the distance from the source. Two types of land use are studied. Two perturbations of the deposition velocity, $\varepsilon_g$ (-0.5 and +0.5) and a perturbation of the $\varepsilon_f / \varepsilon_g$ ratio (0.5) are applied.*

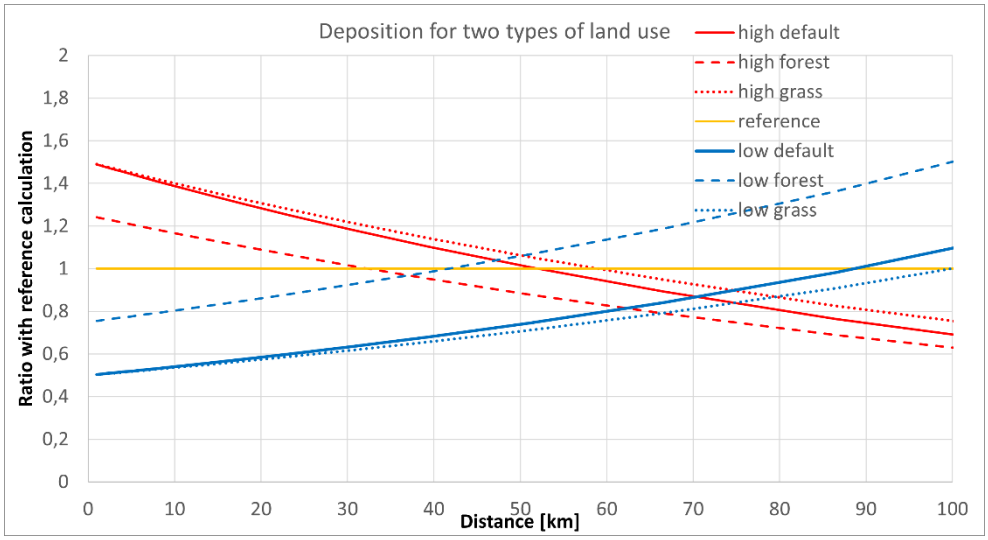


In Figure A3.5, results are shown for a larger perturbation for the minority land use, with $\varepsilon_f / \varepsilon_g = 1.5$. For the sake of comparison, the default deposition is also calculated.

*Figure A3.5 Deposition relative to the reference calculation. Two types of land use are studied. Two perturbations of the deposition velocity, $\varepsilon_g / \varepsilon_g$ (-0.5 and +0.5) and a perturbation of the $\varepsilon_f / \varepsilon_g$ ratio (1.5) are applied.*

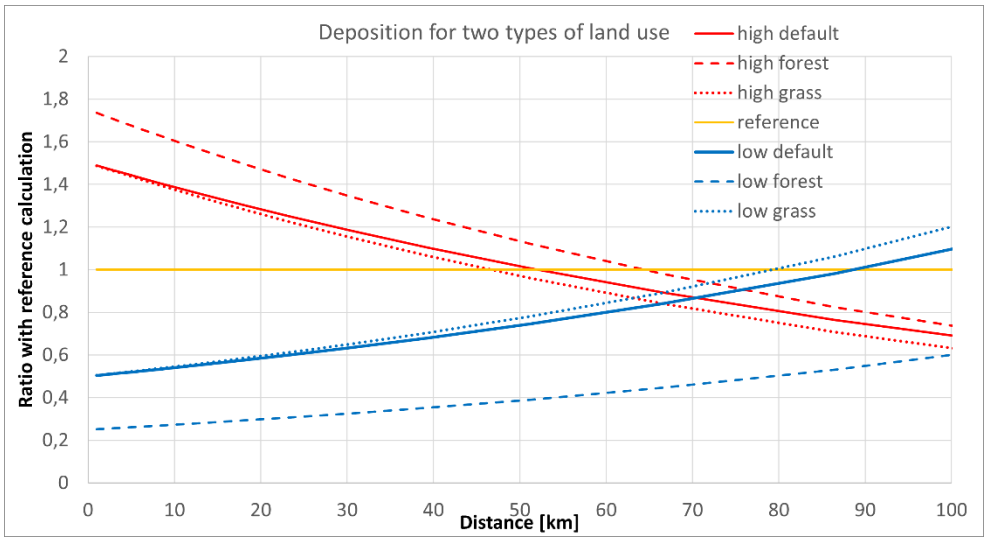

The effect of choosing the differing perturbations on the deposition over the dominant land use, grass, can be evaluated by comparing the dotted lines to the solid line. Across much of the distance range, in case of the smaller perturbation for forest (Figure A3.4), the deviations over grassland due to the perturbation are slightly larger than the default deviations. By contrast, in case of larger perturbations for forest (Figure A3.5), the deviations become smaller, at least up to 80 km from the source in the present calculations. So we see that a smaller deposition over grass becomes somewhat larger by choosing the larger perturbation for forest, and vice versa. This can be explained by the changes in the compensation. If $V_d$ decreases, the deposition decreases, and more mass remains within the atmosphere. This compensates the effect of $V_d$ on the deposition flux. If $V_d$ over forest decreases even more than it does over grass, more mass remains in the atmosphere than in the default case. Hence, the compensation over grass is stronger and we see enhanced fluxes in comparison to the default case. The reverse is true if $V_d$ increases.
The effect on the minority land use, forest, can be evaluated by comparing the dashed lines to the solid lines. For the smaller perturbation for forest (Figure A3.4), the deviation is smaller than the default deviation. For the larger perturbation for forest (Figure A3.5), the deviation of the dashed line is larger than the default deviation. As expected, the influence on the sensitivity on the minority land use type is larger than on the dominant land use type. For the forest we basically see the effect of the extra or reduced $V_d$ change over the forest patches. In comparison to the two situations studied in Figure A3.4 and Figure A3.5, both stronger and weaker deviations than the default calculation may occur. To study the importance of the effect of ratio $\varepsilon_f$ / $\varepsilon_g$ on the estimated deviation from the reference value, the results of the previous calculation are also plotted for several fixed distances from the source, but as a function of ratio $\varepsilon_f$ / $\varepsilon_g$.

*Figure A3.6 Relative deviation of the calculated deposition with respect to the reference calculation as a function of $\varepsilon_f$ / $\varepsilon_g$ (e2/e1 in the figure). Results are shown at 4 distances from the source (1 (upper left), 10 (upper right), 30 (lower left) and 50 km (lower right)). The solid lines show the deviation obtained for the same value for $\varepsilon_g$ and $\varepsilon_f$ ($\varepsilon_f$ / $\varepsilon_g$ =1). The dotted lines show the deviation from the reference for the dominant land use (grass). The dashed lines show the deviation for the minority land use (forest). The assumed distribution of $\varepsilon_f$ / $\varepsilon_g$ value is also shown (brown curve on top of the x-axis).*

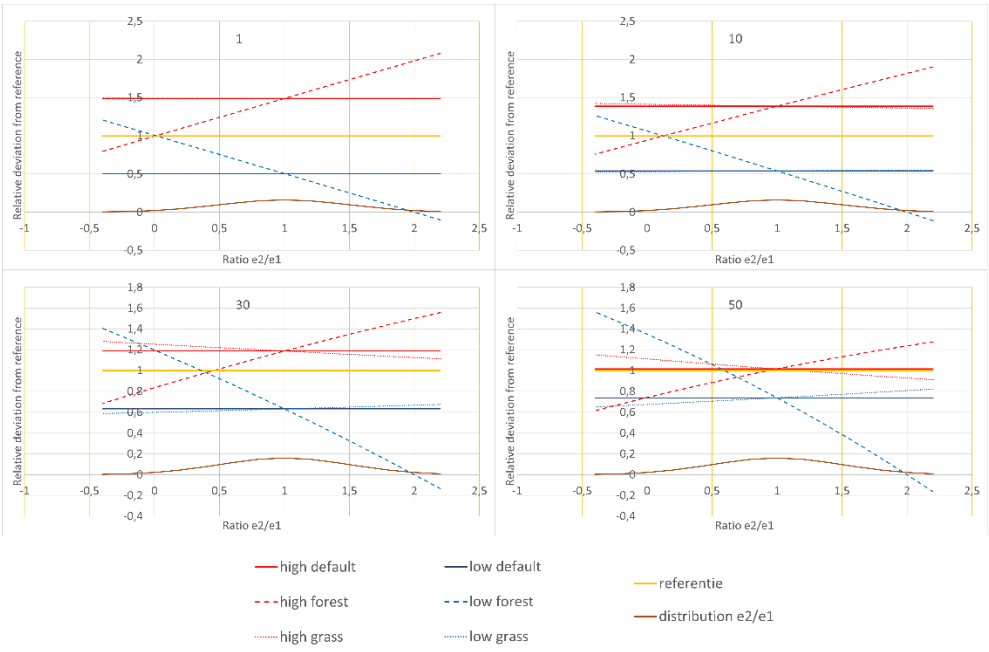


Figure A3.6 highlights the results for four distances. The default result, the solid lines, show the contribution to the uncertainty as estimated in the analyses of Chapter 4. The difference between the solid lines and the dashed and dotted lines show the potential increase or decrease of the deviation with respect to the default. Obviously, for $\varepsilon_f$ / $\varepsilon_g$ = 1, the default value is obtained.
For short distances (1 km, upper-left panel) the effect of compensation is small. Therefore, the effect of different perturbations is quite straightforward: $\varepsilon_f$ / $\varepsilon_g$ < 1 give smaller deviations and $\varepsilon_f$ / $\varepsilon_g$ >1 give larger deviations with respect to the reference calculation.
For greater distances, the dependences change slightly. For example, consider the results for a decrease of the grassland $V_d$ at the distance of 30 km (lower-left panel). For $\varepsilon_f$ / $\varepsilon_g$ =0 (i.e. no $V_d$ change of forest), the blue dashed line is not on the reference (here: x=0, y=1). The concentration remains larger due to the decreased $V_d$ over the dominant vegetation, and over the forest, this is fully translated into extra deposition because $V_d$ has not changed for the forest patches. Hence, due to the compensation, the deposition is higher than the reference. However, the deviation is still smaller than the default deviations. Therefore, no underestimation of sensitivities is to be expected. It can be seen that for $\varepsilon_f$ / $\varepsilon_g$ values larger than 1 (i.e. $V_d$ of forest changes more than $V_d$ of grassland) the relative changes become larger than in the default case (the dashed lines reach beyond the solid lines). Here underestimation of sensitivities occurs.

If $\varepsilon_f$ / $\varepsilon_g$ values follow a normal distribution around the value of one, under- and overestimation of sensitivities are equally likely. In that case, a serious general underestimation of sensitivity is not to be expected. This is further corroborated, in some statistical detail, by weighing the sensitivities from Figure A3.5 by an *assumed* normal distribution of $\varepsilon_f$ / $\varepsilon_g$ values given by f($\varepsilon_f$/$\varepsilon_g$)=N(average=1,stdev=0.5). We examine the ratio of the deviations and the reference value, R($\varepsilon_f$ / $\varepsilon_g$) as presented in Figure A3.5 (from the blue and red curves). The reference value is 1 by definition (yellow curve). The weighted estimated variance of the deviation from the reference value is then calculated as:

$$Var(\varepsilon_f \neq \varepsilon_g) = \int_{-\infty}^{\infty} f\left(\frac{\varepsilon_f}{\varepsilon_g}\right)(R\left(\frac{\varepsilon_f}{\varepsilon_g}\right) - 1)^2 d(\frac{\varepsilon_f}{\varepsilon_g}) \qquad \text{eq.(4)}$$

To evaluate the impact of $\varepsilon_f$ / $\varepsilon_g$ on this variance, we compare it to the variance for $\varepsilon_f$ / $\varepsilon_g$. This default deviation is also shown in Figure A3.5 as the solid lines.

$$Var(\varepsilon_f = \varepsilon_g) = (R(1) - 1)^2 \qquad \text{eq.(5)}$$

The square roots of these variances are interpreted as standard deviations of sensitivities, with respect to the reference calculation. These standard deviations are shown for some characteristic situations in Table A3 (the colours match the colours in Figure A3.5). The standard deviations of sensitivities for the weighted sensitivity of two land use type perturbations decreases with increasing distances from the source. However, the decrease is less effective than for the default, single-perturbation situation. For two combinations (100 km blue and 50 km red), the default nearly coincides with the reference. These combinations can also be recognised in Figure A3.4, since the default crosses the reference. This extremely low sensitivity, (the perturbation nearly yields the reference result) cannot be matched by the weighted two perturbation sensitivities. Presumably, the impact on the overall uncertainty in all parameters is small since the particular perfect match between perturbation and reference concerns only one of the parameters. Also, uncertainties in general add up as variances (squared standard deviations), which reduces the impact of relative differences in low numbers.

*Table A3 Standard deviation of sensitivity with respect to reference. The weighted two perturbation results for forest are compared to the default single perturbation results.*

| | Low | | High | |
|---|---|---|---|---|
| Distance | Default $\varepsilon_f=\varepsilon_g$ | Weighted $\varepsilon_f/\varepsilon_g=N(1,0.5)$ | Default $\varepsilon_f=\varepsilon_g$ | Weighted $\varepsilon_f/\varepsilon_g=N(1,0.5)$ |
| 1 | 0.50 | 0.55 | 0.49 | 0.54 |
| 10 | 0.45 | 0.53 | 0.39 | 0.44 |
| 30 | 0.37 | 0.47 | 0.19 | 0.24 |
| 50 | 0.26 | 0.43 | 0.02 | 0.12 |
| 100 | 0.09 | 0.44 | 0.31 | 0.32 |

On the basis of the results in Table A3, the additional sensitivity caused by the difference in perturbations is also estimated. The result is shown in Table A4. The average of the low and high perturbation is calculated via the average variance (square of the standard deviation).

*Table A4 Standard deviation of additional sensitivity.*

| | low | high | average |
|---|---|---|---|
| Distance | default | default | |
| 1 | 23% | 23% | 23% |
| 10 | 28% | 20% | 24% |
| 30 | 29% | 15% | 23% |
| 50 | 34% | 12% | 26% |
| 100 | 43% | 8% | 31% |

*Figure A3.7 Sensitivity of deposition calculations from the selected livestock farm configuration. The schematic sensitivity calculated from a homogeneous perturbation is shown in blue. The green line shows the sensitivity including the additional part due to a potential difference in perturbation for minority land use. The uncertainties in both curves are illustrated by colour intensities based on the estimated probability.*

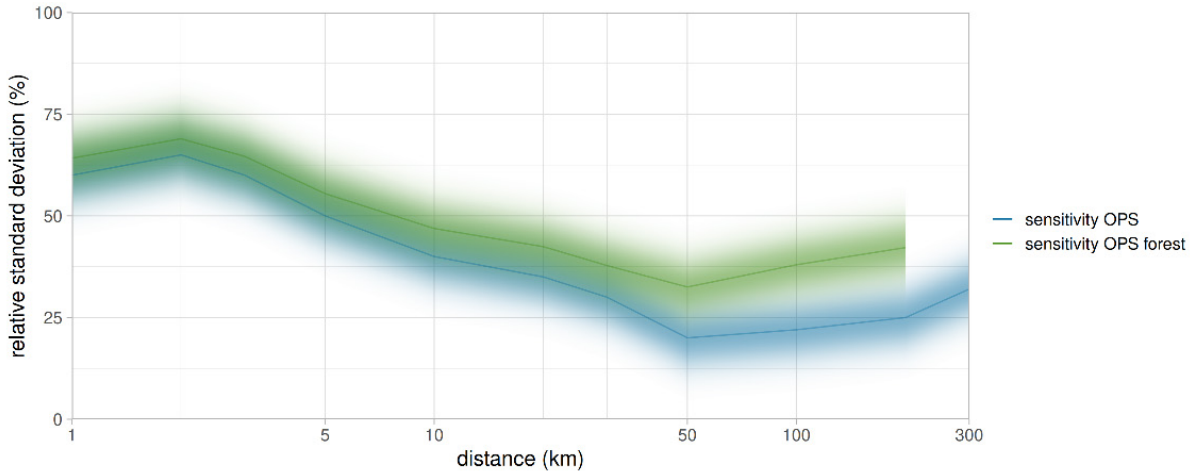


The effect of the additional uncertainty
The uncertainty due to differences in perturbation are shown in Figure A3.7. The uncertainties in both curves are illustrated by colour intensities, which are based on the estimated probability of the particular deviation. The standard deviation of the uncertainty of the sensitivity on the 10 parameters is estimated (blue line), based on the difference between the 12 spokes, as at least 5%.

## Conclusion

In general, the sensitivity to perturbation of the deposition velocity for minority types of land use is underestimated by the assumed equal perturbation for all types of land use. For the majority of combinations of distances and perturbations examined with respect to the sensitivity found for all parameters, the underestimation is relatively small. At a distance of around 100 km, the optimal compensation for the sensitivity to perturbations of the deposition velocity is found. The efficiency of this optimal compensation is reduced, as could expected, when differences in perturbations in various land types are considered.
The statistical evaluation on differences in perturbations of deposition velocities shows a small impact on the general sensitivities. However, larger sensitivities on a particular spot, with an unfavourable combination of conditions, might occur.

Published by:

**National Institute for Public Health and the Enviroment, RIVM**
P.O. Box 1 | 3720 BA Bilthoven
The Netherlands
www.rivm.nl/en

May 2025

Committed to
health and sustainability